

POLITECNICO DI TORINO

Collegio di Ingegneria Chimica e dei Materiali

**Corso di Laurea Magistrale
in Ingegneria Chimica e dei Processi Sostenibili**

Tesi di Laurea Magistrale

Bubble formation and fluid dynamics near the sparger of gas-liquid reactors.



Relatori

Prof. Antonio Buffo
Prof. Daniele Marchisio
Prof. Marco Vanni

Candidato

Paola Alejandra Martinez Acevedo

December 2018

Acknowledgement

First at all, if I must thank someone for giving me the chance to study (because not all people have it) I would have to thank God who never failed me, never, even once. He gave me wonderful parents, Sally and Wilfredo who since I was a little child, they raised me and give me moral values, ethics principles and they taught me that if I want something, I had to get it by myself and working hard. Furthermore, they taught me that there is not a short road to have success but getting a degree was a long and difficult one but secure.

So, God through them gave me the chance to start my studies with an extra effort from my mom, Sally who decided to remain by my side and not to work for study with me, help me and guide me. I am sure that it was thank to her sacrifice that i developed more abilities to study, organize me and learn whatever was the topic in front of me.

Thanks, to my sister Pierina, for being always one step in front of me, your road helped me to avoid some stones and take better decisions in life. Additionally, thank you because you helped me in some difficult times.

Thanks to my country, Venezuela which gave me many opportunities, specially to be a professional.

During my pass by the Universidad Central of Venezuela, there are some special people which deserve to be mentioned. Thank to Pedro Diaz for guide me and help me always, since I know you, I will always remember the time you told me "**do not be afraid, do it!**" in a world of people which are repeating you always "**you can't do it and it is too difficult**". To Daniela Vivanco, for showed me that I can have a true friend without no mask and thank you for the support and friendship. To Giovanina Ragusa, thank you because you always believed in me, and you behaved like a mother with me, thank you for all the opportunities. To Luis, Charbel, Manuel and Fabian you were also my friends and you helped me to study and to enjoy the University life.

In Politecnico the Torino there were many angels which helped me and taught me interested things. Thank you, Hana Tfaili, for being there always in the best moments and in the difficult ones, so, always. Your best quality is offering your help without wait anything by return. Thanks, God, because you gave me wonderful friends in a new country, new life in which I was completely alone, thanks for Dalton, my brother, Chinara, Flavia, Rosario, Lucien, Antonio, Lucio and Mustafa. Thank you for all the moments shared.

Thank you, Lorenali, Diana and Andrea because you were like my family since I arrived in Turin.

A special thanks goes to the Stifano Family, specially to Mario, Estela, Mario A. and Ernesto for receive me like part of your family. To Floriana Sansone, for helped me without knowing me and without expect nothing from me. To Ernesto Stifano, thanks for the support and for being always for me.

Thank to Javier Monguilo because you always offered your help specially with this thesis project and the road would have been more difficult without your help.

Finally, thank to professors Alberto Godio and Daniele Marchisio, my academic advisors in Politecnico di Torino, thank you for your time and kindness. Thank to my thesis tutors, Marco Vanni, Antonio Buffo and Daniele Marchisio for the opportunity to work with you and your time.

Contents

Contents

Riassunto

- 0.1 Introduzione
- 0.2 Obiettivi e metodi
- 0.3 Modello a due Stage
- 0.4 Modello di Scambio Termico
- 0.5 Risultati
- 0.6 Conclusioni

1. Introduction	1
1.1 Slurry reactors	1
1.1.1 Bubble Column Slurry Reactor	1
1.1.2 Stirred Tank Slurry Reactor	2
1.1.3 Flow regimes	2
1.2 Bubble Formation process	3
1.3 Literature review	4
1.3.1 Bubble formation and detachment models	4
1.3.2 Bubble formation models in high pressure conditions	6
1.3.3 Transition from bubbling to jetting regime	7
1.4 Objectives and thesis purpose	10
1.5 Methods	11
2. Research background	12
2.1 Bubble Fluid dynamics	12
2.1.1 Gravitational Force	12
2.1.1.1 Acceleration due to gravity, g	12
2.1.2 Gas Momentum	12
2.1.3 Inertia	12
2.1.4 Pressure difference	13
2.1.4 Flow through the orifice	13
2.1.5 Drag Force	14
2.1.5.1 Flow around submerged objects	14
2.1.6 Buoyancy Force	14
2.1.7 Surface Tension Force	14
2.2 Mass Transfer	15
2.2.1 Fick's Law of binary diffusion	15
2.2.2 Transient Mass Balance	15

2.2.3 Mass transfer coefficient	16
2.2.3.1 Higbie Theory	17
2.2.4 Raoult's Law	18
2.2.5 Normal boiling point	19
2.2.6 Vapor Pressure	19
2.3.6.1 Antoine's Equation	19
2.2.5 Ideal Gas Law	19
2.3 Heat Transfer	20
2.3.1 The First Law of Thermodynamics	20
2.3.2 Enthalpy Energy	21
2.3.2.1 Heat Capacity	21
2.3.2.2 Sensible Heat	22
2.3.2.3 Latent Heat	23
2.3.3 Heat transfer coefficient	23
2.3.3.1 Sherwood and Nusselt analogy	23
3. Modeling	25
3.1 Bubble Formation	25
3.1.1 First Stage	25
3.1.2 Second Stage	29
3.1.3 Sensitivity Analysis	33
3.2 Momentum, Heat and Mass Transfer Model	36
3.2.1 Bubble rising velocity	37
3.2.2 Mass transfer	39
3.2.3 Diameter differential equation	41
3.1.4 Heat transfer	41
4. Implementation and numerical details	45
4.1 MATLAB Algorithms	45
4.1.1 Bisection Model	45
4.1.2 ode45 Solver	48
4.1.3 System of ODEs	51
5. Results and discussion	53
5.1 Bubble formation model sensitivity analysis	53
5.1.1 First Stage	53
5.1.1.1 Adding terms to Original Model 1	54
5.1.1.2 Surface Tension effect	55

5.1.1.3 Gas density effect	56
5.1.1.4 Liquid density effect	56
5.1.1.5 Effect of hole diameter	57
5.1.2 Second Stage	58
5.2 Bubble formation Model validation	59
5.3 Transition to jetting regime	61
5.4 Combined Momentum, Heat and Mass transfer model	65
5.4.1 Effect of hole diameter	68
5.4.2 Effect of Vapor pressure	70
5.4.3 Effect of drag coefficient	73
6. Conclusions	75
Bibliography	77
Appendix	82
A	82
B	85
C	87
D	89
E	91

RIASSUNTO

01.Introduzione

Le colonne a bolle tipo “slurry” sono dei contenitori verticale che contengono sistemi multifase, costituiti da una miscela liquida avente uno o più componenti di interesse e piccole particelle solide sospese mediante la risalita di bolle provenienti da un distributore di gas situato sul fondo del reattore. Inoltre, esiste un altro tipo di reattore, il reattore agitato tipo “slurry” che è simile ma contiene un agitatore meccanico al suo interno per mantenere le particelle catalitiche sospese e quasi sempre viene utilizzato in modalità “batch”. Entrambi i reattori sono mostrati in Fig.1.

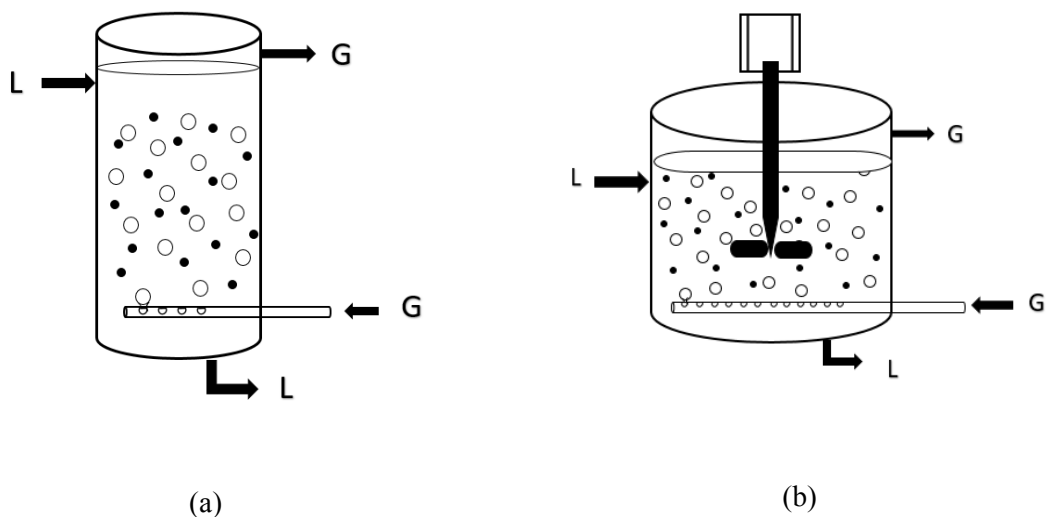


Fig. 1: (a) Colonne a bolle tipo “slurry” (b) Reattore agitato tipo “slurry”.

Diversi regimi fluidodinamici sono possibili nelle colonne a bolle in base alla velocità superficiale del gas.

A basse velocità superficiali si trova il regime omogeneo mostrato nella figura 2.a. In questo regime le bolle si disperdono uniformemente nel liquido, sono quasi sferiche e hanno dimensioni piccole e simili.

Il regime eterogeneo si manifesta quando la velocità del gas superficiale viene ulteriormente aumentata e le bolle si aggregano e formano bolle più grandi che risalgono più velocemente di quelle più piccole. Questo regime è caratterizzato dalla presenza di bolle piccole e grandi contemporaneamente ed è rappresentato in Fig. 2.b.

Infine, è stato identificato il regime di flusso tipo “Slug” in colonne di scala di laboratorio ad alta velocità superficiale del gas in cui le bolle grandi e allungate sono stabilizzate dalla parete della colonna e si muovono verso l'alto all'interno della colonna. Quest'ultimo modello di flusso è mostrato in Fig.2 (c).

Questi reattori sono comunemente utilizzati nelle industrie chimiche, biochimiche e petrolchimiche. Alcuni processi in cui questo tipo di reattori sono coinvolti sono la produzione di carburanti rinnovabili, chiamati Biodiesel. La trasformazione di oli pesanti e residui di petrolio attraverso il processo di cracking e idrogenazione, chiamato "hydrocracking", a

temperature elevate, da $350\text{ }^{\circ}\text{C}$ a $500\text{ }^{\circ}\text{C}$ e pressioni tra 7 e 25 MPa è una delle applicazioni commerciali più importanti delle colonne a bolle, come anche la conversione del carbone solido in combustibili liquidi, denominata liquefazione del carbone. Anche nuove alternative nel campo ambientale sono state trovate, ad esempio alcuni microrganismi che degradano il petrolio sono stati coltivati con successo in questi reattori. Inoltre, la rimozione di composti organici volatili (VOC) da acque reflue o aria di scarico attraverso emulsioni di petrolio e acqua viene effettuata in colonne a bolle. Infine, esiste un processo molto importante per la sintesi di paraffine pesanti, chiamato Fischer Tropsch, e viene effettuato in colonne a bolle liquide in condizioni di alta pressione per produrre combustibili liquidi da gas. Questo ultimo processo viene anche realizzato nei reattori agitati.

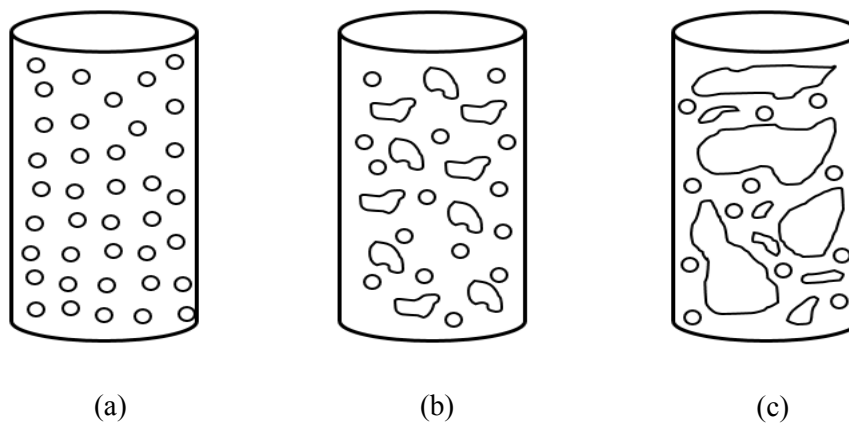


Fig. 2: Regimi di flussi trovati reattori gas-liquido: (a) Regime Omogeneo (b) Regime eterogeneo (c) Regime di flusso tipo Slug.

02. Obiettivi e Metodi.

Nei reattori a colonne a bolle, il gas viene introdotto da un distributore di gas situato nella parte inferiore della colonna. I distributori di gas (sparger) sono composti da tubi perforati e disposti in diverse geometrie per produrre bolle di gas. Il processo di formazione di bolle e risalita attraverso il reattore consente ai differenti reagenti all'interno delle diverse fasi di entrare in contatto e interagire per eseguire la reazione desiderata. Quindi, quantificare l'area interfacciale tra il gas e il liquido è importante poiché è determinante nel valutare il calore trasferito e la velocità di trasferimento di massa, processi che influenzano l'efficienza del reattore. Per caratterizzare il movimento della bolla nel reattore è importante ottenere prima una dimensione iniziale della bolla mediante la comprensione del fenomeno dalla nascita di bolle dal foro allo sparger fino al suo tempo di distacco. Inoltre, è importante considerare un incremento o decremento posteriore della dimensione della bolla a causa dell'evaporazione di alcuni componenti nella miscela liquida attraverso un processo di trasferimento di calore tra la bolla e la miscela liquida.

Nel presente lavoro viene sviluppato un modello, a due stadi per la formazione di una singola bolla fino al suo distacco, basato su un equilibrio di forze esercitate sulla bolla vicino alla regione dello sparger e verrà effettuata un'analisi di sensibilità, variando diversi parametri, ad esempio, verrà valutato l'effetto della pressione del sistema sul bilancio di forze e sulla taglia della bolla al momento del distacco.

Verranno valutati due diversi sistemi con il modello. Per prima cosa verrà considerato un sistema aria-acqua, successivamente un sistema costituito da una fase liquida oleosa con gas idrogeno. Entrambi i sistemi sono stati valutati in diverse condizioni di temperatura e pressione. Poiché il modello sarà valutato con una portata di gas elevata, verrà esaminata una vasta letteratura sui regimi di “bubbling” e di “jetting”, in modo da identificare un criterio per descrivere la transizione da un regime all’altro variando diverse condizioni operative e sistemi, compresi i sistemi ad alta pressione. In seguito, verrà descritto ciascun termine del bilancio di forze per la determinazione della dimensione della bolla. Infine, è stato sviluppato un modello combinato di quantità di moto, calore e trasferimento di massa dopo il tempo di distacco per determinare una dimensione finale della bolla nella regione dello sparger, principalmente per valutare l’effetto di evaporazione del liquido attorno alla bolla a seguito dell’iniezione di gas “caldi”.

Tutti i modelli sviluppati vengono risolti numericamente attraverso diversi script di MATLAB e facendo uso di diversi algoritmi numerici.

03. Modello di formazione della bolla.

Primo stadio di formazione della bolla.

Il primo stadio rappresenta la formazione iniziale della bolla attraverso il foro che ha un raggio caratteristico individuato con la terminologia " r_H ". Inizialmente, all’istante " t_0 ", si crea una specie di bolla di emisfero con una successiva espansione fino al momento in cui si formerà una bolla sferica e la base della bolla è ancora completamente collegata all'area del foro, come illustrato in Fig. 3. Questo stadio di formazione finisce proprio all’istante, " t_d ", in cui la base della bolla comincia a sollevarsi rispetto all’altezza del foro e una specie di collo si forma collegando la base della bolla al foro. È stato impostato un asse in direzione verticale identificato con il simbolo “y” e con origine nella base del foro come si vede nella Fig.3.

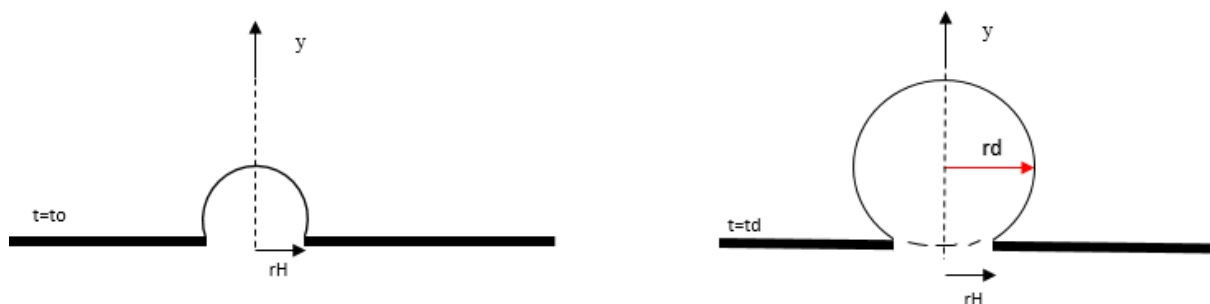


Fig. 3: Schema del primo stadio di formazione della bolla.

Il primo stadio è assunto soltanto di espansione, cioè, solo un cambio di raggio della bolla con il tempo. Inoltre, è stato assunto che la bolla formata in questo stadio sia formata istantaneamente, ossia, in un tempo molto piccolo.

Il raggio ottenuto alla fine di questo stadio è stato chiamato " r_d " e questo coincide con la posizione del centro di massa della bolla nell’ asse epsilon, “y” verticale impostato previamente.

Per la determinazione del raggio nel primo stadio viene impiegato un bilancio delle forze che influenzano l'espansione della bolla. Le forze che vengono considerate per questo stadio sono le forze di galleggiamento, gravità, differenza di pressione fra la bolla e liquido, tensione superficiale, inerzia e trascinamento.

Dopo tutti i passaggi matematici è stata trovata la seguente equazione in funzione del raggio della bolla; questa è una equazione non lineare, e viene risolta attraverso metodi numerici e in questo caso è stato utilizzato il metodo della Bisezione. Da questa equazione viene trovato il raggio alla fine del primo stadio di formazione, r_d .

$$\frac{4\pi}{3}r^3\rho_l g + \frac{G^2\rho_g}{\pi r_H^2} + \frac{1}{C_0^2}\frac{G^2\rho_g}{\pi r_H^2} = \frac{(\rho_g+\alpha\rho_L)G^2}{12\pi r^2} + \frac{4\pi}{3}r^3\rho_g g + 2\pi\sigma r_H + \frac{1}{2}C_D\pi r^2\rho_L\left(\frac{G}{4\pi r^2}\right)^2$$

I termini a sinistra sono quelli che spingono la bolla in alto e quelli a destra quelli che ritengono la bolla giù. Il primo termine a sinistra rappresenta la forza di galleggiamento dove "r" è il raggio della bolla, " ρ_l " è la densità del liquido e "g" è la accelerazione di gravità. Dopo, il secondo termine a sinistra è la forza di momento di gas, dove "G" è la portata di gas attraverso il foro, " ρ_g " è la densità del gas e " r_H " è il raggio del foro. L'ultimo termine a sinistra rappresenta la differenza di pressione fra la bolla e il liquido dove " C_0 " è un coefficiente di scarico che dipende della geometria del foro e della velocità del gas attraverso il foro. Il primo termine a destra rappresenta la forza d'inerzia, dove si ha conto della massa della bolla e una massa virtuale di liquido attraverso il parametro " α " chiamato coefficiente di massa aggregata. Il secondo termine a destra rappresenta il peso della bolla; il terzo a destra termine equivale alla tensione interfacciale gas-liquido, dove il seno dell'angolo di contatto sparisce perché in questo stage è ipotizzato che bolla si forma istantaneamente e che l'angolo sia pari a 90°. L'ultimo termine descrive la forza di trascinamento caratterizzata per un coefficiente di trascinamento, " C_D ". La equazione del coefficiente di trascinamento, " C_D ", utilizzata nel primo stadio di formazione della bolla è la seguente,

$$C_D = \frac{18.5}{Re_B^{0.6}}$$

Utilizzando questo coefficiente di trascinamento la equazione del primo stadio scritta prima viene chiamata Modello di Drag.

Comunque, per il modello combinato di moto e trasferimento di calore e materia spiegato dopo viene utilizzato una equazione per il coefficiente di trascinamento diversa,

$$C_D = \max\left[\frac{24}{Re_B}\left(1 + 0.15Re_B^{0.687}\right), \frac{8}{3}\frac{Eo}{Eo+4}\right]$$

Se questa equazione di coefficiente di trascinamento viene inserita nel bilancio di forze del primo stadio scritta sopra il modello viene chiamato Modello di Drag 132.

Secondo Stadio di Formazione della bolla.

Il secondo stadio di formazione inizia esattamente nel momento in cui finisce il primo stadio, cioè, quando la base della bolla comincia ad alzarsi. In questo stadio la bolla continua ad espandersi perché è ancora collegata al foro tramite il collo, mentre si solleva. Questo collo di gas viene ridotto con l'innalzamento della bolla come mostrato nella Figura 4, fino al momento in cui il collo si rompe e la bolla viene rilasciata con un raggio " r_f " in un istante " t_f ".

Il momento in cui viene rilasciata la bolla è chiamato "tempo di distacco" e si verifica quando il collo del gas che collega la bolla al distributore di gas si chiude.

Il modello proposto per questo stadio è di nuovo basato sull'equilibrio delle forze che agiscono sulla bolla. Le stesse forze considerate nella prima fase saranno considerate di nuovo nel secondo stage. Inoltre, viene assunto che l'innalzamento della bolla sia sempre verticale e il centro di massa si muova nell'asse epsilon; il liquido viene anche assunto stagnante in questa sezione vicino allo sparger.

È necessario introdurre un criterio di distacco per determinare la dimensione finale della bolla alla fine del secondo stadio. È stata presa una teoria di distacco correlata alla lunghezza

del collo di gas che unisce la bolla allo sparger. La lunghezza del collo e anche correlata a la posizione del centro di massa della bolla mentre si innalza.

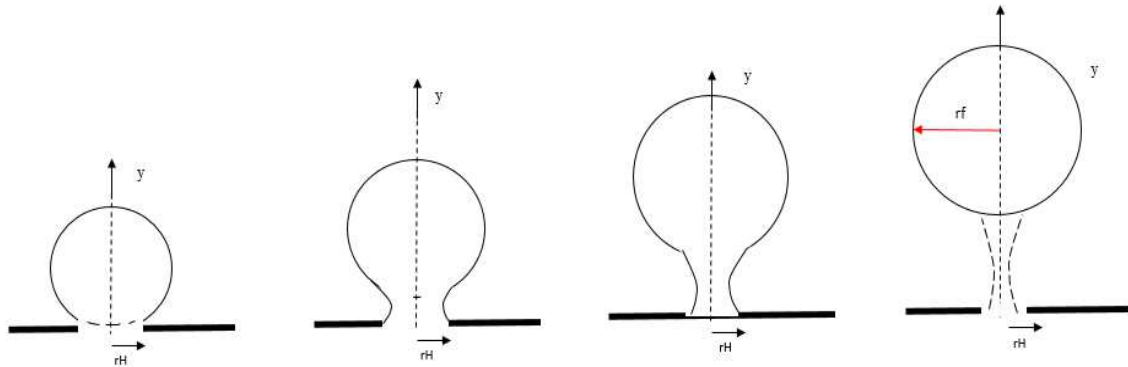


Fig.4: Secondo stadio di formazione della bolla.

In questo lavoro è stato impostato come criterio di distacco la lunghezza del collo uguale a due volte il raggio del foro, $2r_H$, cioè il diametro del foro.

La posizione del centro di massa al momento del distacco, y_f , sarà la somma della lunghezza del collo più il raggio finale della bolla “ r_f ” nell’istante finale “ t_f ” come mostrato in Figura 5.

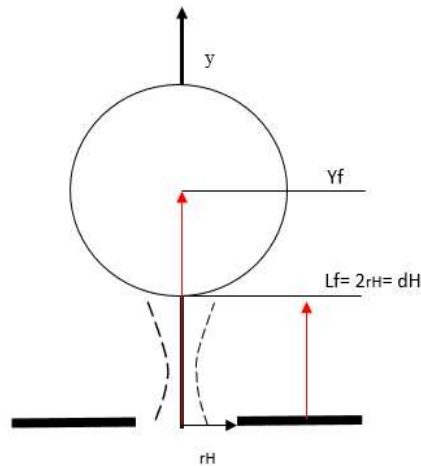


Fig.5: Criterio di distacco per la bolla.

La equazione risultante per questo modello è la seguente:

$$\frac{d^2y}{dt^2} = \frac{1}{(\rho_g + \alpha\rho_L)(Gt + \frac{4}{3}\pi r d^3)} \left[-(\rho_g + \alpha\rho_L)G \left(\frac{dy}{dt}\right) - \frac{1}{2}C_D\pi r^2\rho_L \left(\frac{dy}{dt}\right)^2 + \frac{4\rho_g G^2}{\pi d_h^2} \left(1 + \frac{1}{C_0^2}\right) + \left(Gt + \frac{4}{3}\pi r d^3\right)(\rho_L - \rho_g)g - \pi\sigma d_H \right]$$

Nella equazione sopra del lato sinistro c'è la accelerazione della bolla e del lato destro c'è una frazione in cui nel denominatore si trova la densità della bolla per il volume della bolla che considera il volume alla fine del primo stadio più il volume di gas che entra attraverso il collo. Tra parentesi quadre, ancora nel lato destro, si trova per primo un termine che è parte

della forza di inerzia, il secondo termine rappresenta la forza di trascinamento, caratterizzato per un coefficiente di trascinamento C_D , e la velocità della bolla, $\frac{dy}{dt}$, al quadro. Il terzo termine rappresenta la forza di momento di gas insieme alla forza di differenza di pressione tra la bolla e il liquido attorno. Il quarto termine a destra, fra parentesi quadre, rappresenta la differenza tra la forza di galleggiamento e la forza di gravità. Per ultimo, nel lato destro, si trova il termine di tensione superficiale che grazie alla presenza del collo si può dire che l'angolo di contatto fra gas e il liquido è 90° e il seno di questo angolo è uguale a 1.

La equazione sopra che rappresenta la accelerazione della bolla può essere scritta come la derivata prima della velocità e la velocità può essere scritta come la derivata prima della posizione come segue,

$$U_b = \frac{dy}{dt}$$

$$\frac{dU_b}{dt} = \frac{1}{(\rho_g + \alpha\rho_L)(Gt + \frac{4}{3}\pi r_d^3)} \left[-(\rho_g + \alpha\rho_L)G \left(\frac{dy}{dt}\right) - \frac{1}{2}C_D\pi r^2\rho_L \left(\frac{dy}{dt}\right)^2 + \frac{4\rho_g G^2}{\pi d_h^2} \left(1 + \frac{1}{C_0^2}\right) + (Gt + \frac{4}{3}\pi r_d^3)(\rho_L - \rho_g)g - \pi\sigma d_H \right]$$

Per la equazione di variazione di velocità, specificata sopra, il coefficiente di trascinamento, " C_D ", utilizzato è il seguente,

$$C_D = \frac{18.5}{Re_B^{0.6}}$$

Comunque, per il modello combinato di moto e trasferimento di calore e materia spiegato dopo viene utilizzato una equazione per il coefficiente di trascinamento diversa,

$$C_D = \max\left[\frac{24}{Re_B} \left(1 + 0.15Re_B^{0.687}\right), \frac{8}{3} \frac{Eo}{Eo+4}\right]$$

Dopo l'inserimento di questa equazione nella equazione della variazione della velocità è possibile ottenere attraverso uno script in MATLAB, la posizione e la velocità della bolla al momento del distacco e queste due valori saranno parte delle condizioni iniziali da inserire nel modello combinato di moto e trasferimento de materia e calore della bolla dopo il distacco.

04. Modello di moto e scambio termico.

Per questa sezione è importante descrivere il sistema e l'obiettivo per lo sviluppo di questo modello. L'istante iniziale per il quale questa valutazione viene sviluppata è alla fine del secondo stadio, cioè il momento del distacco. Quindi, la bolla nel momento iniziale di questo modello avrà una certa posizione, diametro e velocità calcolata mediante il primo modello della bolla, al quale si aggiungerà due nuove variabili ovvero sia la temperatura della bolla e la concentrazione molare della sostanza che evapora. All'istante iniziale la temperatura della bolla sarà uguale alla temperatura del gas all'interno del distributore di gas mentre la concentrazione molare iniziale è pari a zero.

Il gas valutato in questo lavoro sarà costituito da un componente identificato come componente "G". Diversi tipi di gas possono essere facilmente valutati dal modello solo è necessario modificare le proprietà del gas all'interno del modello. Tuttavia, si presume che il gas proveniente dal distributore di gas e quello proveniente del liquido attorno alla bolla che evapora si comportino secondo la legge del gas ideale. Il sistema liquido è considerato una miscela di idrocarburi con componenti identificati dal simbolo "A" e "K" entrambi ad una

temperatura della massa liquida, T_L , che è inferiore alla temperatura del gas, T , all'interno della bolla nel momento iniziale; la temperatura del liquido è assunta costante.

Anche in questo secondo modello è stato considerato un liquido stagnante e la bolla si muoverà nella direzione verticale senza spostamento orizzontale; il suo centro di massa si troverà nuovamente sull'asse verticale "y" di ascensione. Inoltre, come detto in precedenza verrà modellato il processo di evaporazione del componente liquido "A" a causa della differenza di temperatura tra la fase liquida e gassosa e delle alte pressioni del sistema. Tuttavia, questo modello è limitato alla regione vicina alla regione dello sparger e non considera altri fenomeni che si hanno allontanandoci dal distributore di gas come il trasferimento di massa e di calore vicino a una particella solida (o catalizzatore) all'interno del reattore. Si trascurano inoltre i fenomeni di coalescenza o rottura delle bolle.

Il modello precedentemente descritto è illustrato con uno schema in Fig.6 dove la bolla si muove sull'asse verticale e c'è un flusso di calore, "q", uscente dalla bolla radialmente, la massa liquido contenente il componente "A" attorno alla bolla tende ad evaporare a causa del trasferimento di calore tra la bolla e il liquido. Quindi, la bolla cresce di dimensione mentre risale e si raffredda.

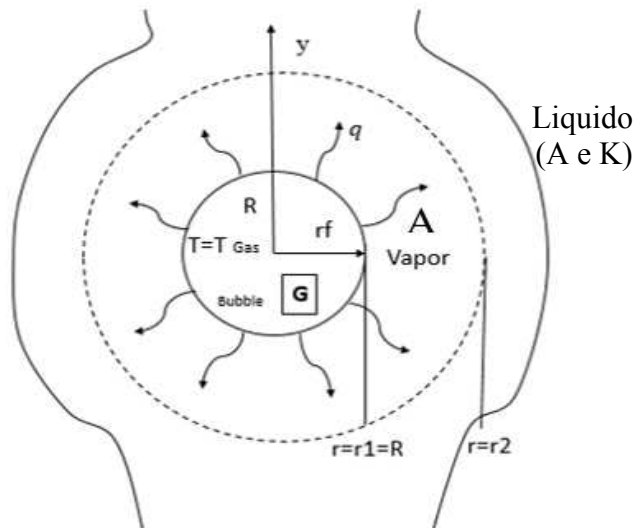


Fig.6: Modello di moto e scambio termico.

Qui sotto viene riportato il sistema di equazioni differenziali di primo ordine da risolvere e il loro ordine di implementazione è importante per la risoluzione del problema. Devono essere organizzati nel seguente ordine:

Innanzitutto, la equazione che esprime la velocità di trasferimento del componente "A" nella bolla:

$$\frac{dn_A}{dt} = \sqrt{\frac{4D_{AG} U_t(t)}{\pi L(t)}} (\pi L(t)^2) \left(C_{A,L} - \frac{n_A(t) R C_{tot}}{\frac{\pi}{6} L(t)^3} \frac{T(t)}{P_A(T)^{sat}} \right)$$

L'equazione scritta sopra e caratterizzata per un coefficiente di scambio rappresentato per la radice quadrata di una frazione, nel numeratore c'è il coefficiente di diffusività, D_{AG} , la velocità terminale della bolla U_t , e nel denominatore la costante "pi" per il diametro della bolla che varia nel tempo, $L(t)$. questo coefficiente di scambio è moltiplicato per la superficie di

scambio e per la forza spingente che in questo caso è data dalla differenza di concentrazione fra la concentrazione molare del componente “A” nel liquido, $C_{A,L}$ e la concentrazione del componente “A” all’interfaccia, trovata attraverso la legge di Raoult ed è rappresentata per la frazione che ha come denominatore i moli del componente “A” per la costante dei gas perfetti, “R”, per la concentrazione totale nel liquido C_{tot} , per la temperatura della bolla, $T(t)$; nel denominatore si trova il volume della bolla che varia nel tempo perché cambia il diametro, $L(t)$ e la tensione di vapore che dipende della temperatura ed è stata calcolata con la Equazione di Antoine.

Dopo, si trova il gradiente di temperatura che risulta del bilancio di entalpico fatto alla bolla giusto dopo il distacco,

$$\frac{dT}{dt} = \frac{1}{(n_A(t)\hat{C}_{p,A}^{vap} + n_G\hat{C}_{p,G})} \left[\sqrt{\frac{4\rho_L\hat{C}_p k U_t(t)}{\pi L(t)}} (\pi L(t)^2)(T_L - T(t)) + \frac{dn_A}{dt} \left\{ (\hat{C}_{p,A}^{liq} - \hat{C}_{p,A}^{vap})(T(t) - T_L) - \Delta\hat{H}_{vap}(T_L) \right\} \right]$$

In questa equazione, si trova una frazione dove nel denominatore si trova una somma, nel primo componente c’è il prodotto tra i moli del componente “A” che varia nel tempo e la capacità termica molare del vapore del componente “A”, $\hat{C}_{p,A}^{vap}$ e nel secondo termine c’è il prodotto tra i moli del componente “G” e la capacità termica molare del componente “G” in stato gassoso.

Tra parentesi quadre si trova nel primo la conduzione di calore attraverso la superficie della bolla caratterizzato per un coefficiente di scambio rappresentato per la radice quadrata, e una differenza di temperatura fra il liquido e la bolla; “k” è la conducibilità termica, \hat{C}_p e la capacità termica specifica del liquido, ρ_L , la densità del liquido, U_t , la velocità terminale della bolla e “L(t)” è il diametro della bolla che varia nel tempo. Dopo, nel secondo termine fra le parentesi quadre si trova la velocità di trasferimento del componente “A” per la differenza tra la capacità termica molare del liquido del componente “A”, $\hat{C}_{p,A}^{liq}$ e la capacità termica molare del vapore del componente “A”, $\hat{C}_{p,A}^{vap}$, per la differenza di temperatura; e un terzo termine che è il prodotto della la velocità di trasferimento del componente “A” e il calore latente di vaporizzazione a la temperatura di riferimento che è quella del liquido, $\Delta\hat{H}_{vap}(T_L)$.

La terza equazione è il cambio del diametro della bolla con il tempo descritta come segue:

$$\frac{dL}{dt} = \frac{2R}{P\pi L(t)^2} [(n_A(t) + n_G) \frac{dT}{dt} + T(t) \frac{dn_A}{dt}]$$

Questa equazione è ottenuta per mezzo de la legge dei gas perfetti, del lato sinistro si trova il cambio del diametro con il tempo e del lato destro si trova una frazione in cui il numeratore è due volte la costante dei gas perfetti, “R”, e nel denominatore si trova la costante “pi” per la pressione del sistema, “P” e per la dimensione della bolla che varia con il tempo al quadro. Dopo, tra parentesi quadre si trova nel primo termine la somma dei moli totali contenuti nella bolla, i moli del componente “A” che varia nel tempo, n_A , e i moli del componente “G”, n_G , per il gradiente di temperatura; il secondo termine tra parentesi quadre si trova la temperatura della bolla che varia con il tempo, $T(t)$, per la velocità di trasferimento dei moli di “A” alla bolla $\frac{dn_A}{dt}$.

Dopo di fare un bilancio di forze alla bolla che ascende liberamente, si ottiene l’ultima equazione di variazione della velocità però viene aggiunta prima la equazione della variazione della posizione come segue:

$$\frac{dy}{dt} = U_t$$

$$\frac{dU_t}{dt} = \frac{1}{(m_b + \frac{\pi}{6} L^3 \alpha \rho_L)} \left[\frac{\pi}{6} L^3 \rho_L g - (m_b)g - \frac{dy}{dt} \left[\frac{dn_A}{dt} M_A + \alpha \rho_L \frac{\pi}{2} L^2 \frac{dL}{dt} \right] - \frac{\pi}{4} L^2 C_D \frac{\rho_L}{2} \left(\frac{dy}{dt} \right)^2 \right]$$

Nella equazione sopra a sinistra si trova la variazione della velocità con il tempo e del lato destro si trova una frazione che ha come denominatore la massa totale della bolla, che ha conto del componente “A” che evapora e la massa virtuale della bolla attraverso un coefficiente “ α ” uguale a 11/16. Tra parentesi quadre si trova in questo ordine, la forza di galleggiamento, il peso della bolla, dove m_b , è la massa della bolla, dopo una parte della forza di inerzia, dove M_A e il peso molecolare del componente “A” e per ultimo la forza di trascinamento.

Il coefficiente di trascinamento, C_D , più appropriato per il modello di formazione delle bolle e questo modello che considera il moto più il trasferimento di massa e di calore dopo il distacco viene descritto nella seguente equazione,

$$C_D = \max\left[\frac{24}{Re_B} \left(1 + 0.15 Re_B^{0.687}\right), \frac{8}{3} \frac{Eo}{Eo+4}\right]$$

05. Risultati.

Validazione del Modello della formazione della bolla.

Utilizzando un sistema costituito da acqua nella fase liquida ed aria nella la fase gassosa per cui le proprietà necessarie da inserire nel modello della formazione della bolla, primo e secondo stadio sono state fissate, è stato possibile fare un confronto del modello della formazione della bolla sopra specificato con data sperimentale trovata in letteratura.

In Fig.7 si mostrano i risultati del modello di formazione della bolla per due condizioni operative di pressione diverse, 1MPa e 6 MPa per un diametro del foro uguale a 1.18mm.

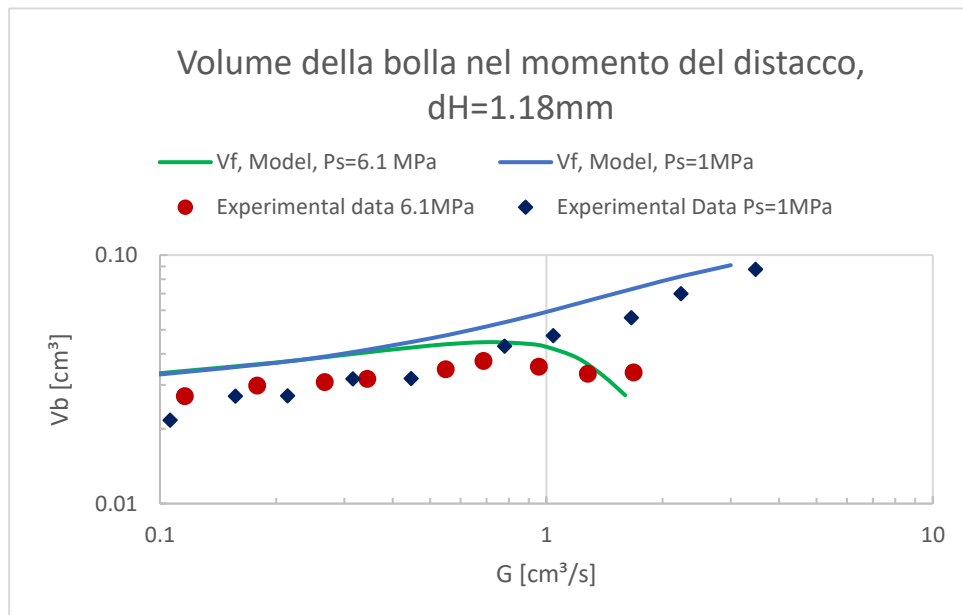


Fig.7: Volume della bolla nel momento del distacco, confronto modello e data sperimentale.

Nella figura 7 è possibile osservare l'effetto della pressione sul volume della bolla al momento del distacco per il modello e per la data sperimentale. Prima, si vede che il modello rappresentato per le linee continue e la data sperimentale vanno d'accordo e seguono le stesse tendenze per ogni valore di pressione valutato. Dopo, si vede che a bassa pressione e con l'aumento della portata di gas i volumi delle bolle tendono ad aumentare. Lo contrario accade per alta pressione, i volumi delle bolle aumentano fino a un massimo con la portata di gas e dopo si vede una tendenza a diminuire. È stato anche fatto un'analisi di questo tipo per la pressione atmosferica come si vede in Fig.8.

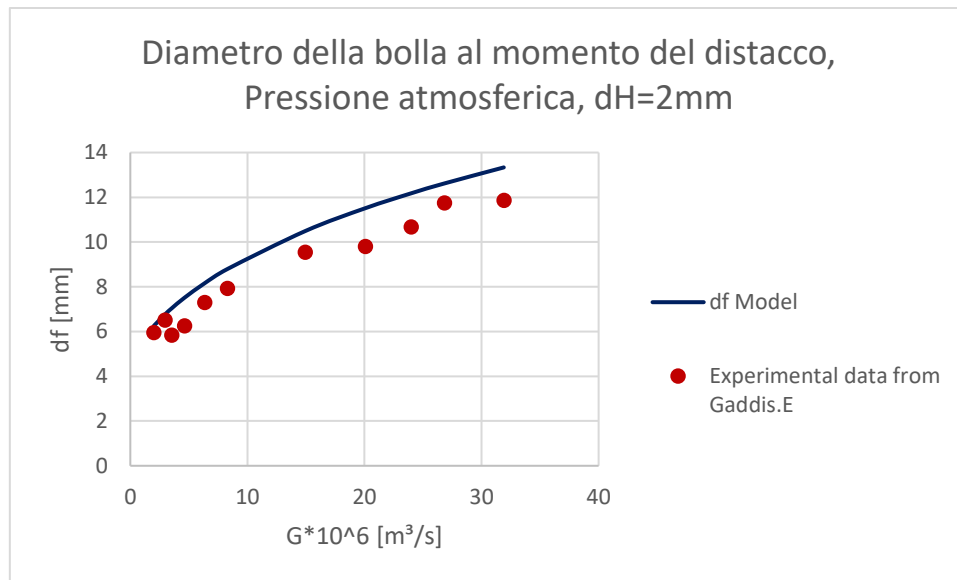


Fig.8: Diametro della bolla nel momento del distacco.

Anche nella Fig. 8 si vede che il modello della formazione della bolla va de accordo con la data sperimentale e in questo caso la deviazione media del modello rispetto alla data sperimentale è 12%. Anche con questa figura è possibile verificare una tendenza della dimensione della bolla ad aumentare con la portata di gas a bassa pressione. La differenza fra il modello e la data sperimentale può essere attribuita alle assunzioni fatte per costruire il modello della formazione della bolla, come la forma sferica e il criterio utilizzato per il distacco.

Transizione al regime di “jetting”.

È parte della validazione del modello di formazione della bolla lo studio dei regimi fluidodinamici che potrebbero comparire vicino allo sparger secondo la portata di gas impostata al foro. Nella Fig.9 si mostrano tre possibile regimi a trovare se la portata di gas uscente del foro viene incrementata.

Per valutare la transizione di regime è stato adottato la definizione del numero adimensionale chiamato numero di Weber che viene valutato come segue,

$$W_e = \frac{16\rho_g G^2}{\pi^2 d_h^3 \sigma}$$

Dove ρ_g , è la densità del gas valutata per attraverso la legge dei gas perfetti per avere conto delle condizioni operative, pressione e temperatura. “G”, è la portata di gas attraverso il foro, d_h , è il diametro del foro e σ , è la tensione interfacciale, e sarà valutata con una espressione che dipende della pressione.

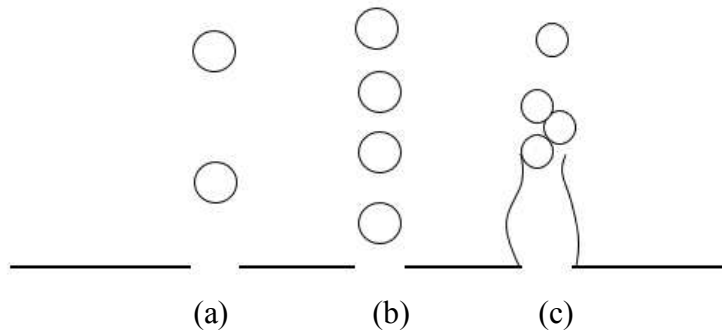


Fig.9: Regimi fluidodinamici trovati vicino lo sparger. (a) Regime omogeneo, (b) Regime a catena di bolle e (c) Regime di “*Jetting*”.

Il criterio dove si utilizza il numero di Weber per evidenziare la transizione dal regime omogeneo al regime di “*jetting*” e basato nel principio che quando la forza gas momento che rappresenta l’uscita della portata di gas attraverso il foro, supera la forza di tensione superficiale non viene formata più una bolla sferica se non un jet di gas. Secondo data trovata in letteratura il numero di Weber uguale a 4 è stato riconosciuto per la presenza di “*jetting*” nel sistema; in alcuni casi e anche stato trovato il fenomeno di “*jetting*” per numeri di Weber fra 1 e 2.

In questo lavoro il numero di Weber uguale a 4 e a 1 è stato trasformato in una portata di gas critica che delimita la zona dove sicuro esiste il fenomeno di “*jetting*” ($We \geq 4$), una zona di transizione dove potrebbero o non esistere *jetting* ($1 > We > 4$) e una zona dove non accade il fenomeno di *jetting* ($We < 1$) e il modello della formazione della bolla presentato in questo lavoro e valido. Le portate di gas critiche e le zone appena descritte vengono riportate in grafici portata di gas critica versus pressione; queste due condizioni operative sono di solito impostate nei reattori colonne a bolle.

Nella Fig.10 è possibile osservare due grafici per diversi valori di tensione interfacciale, 14 mN/m e 20 mN/m,

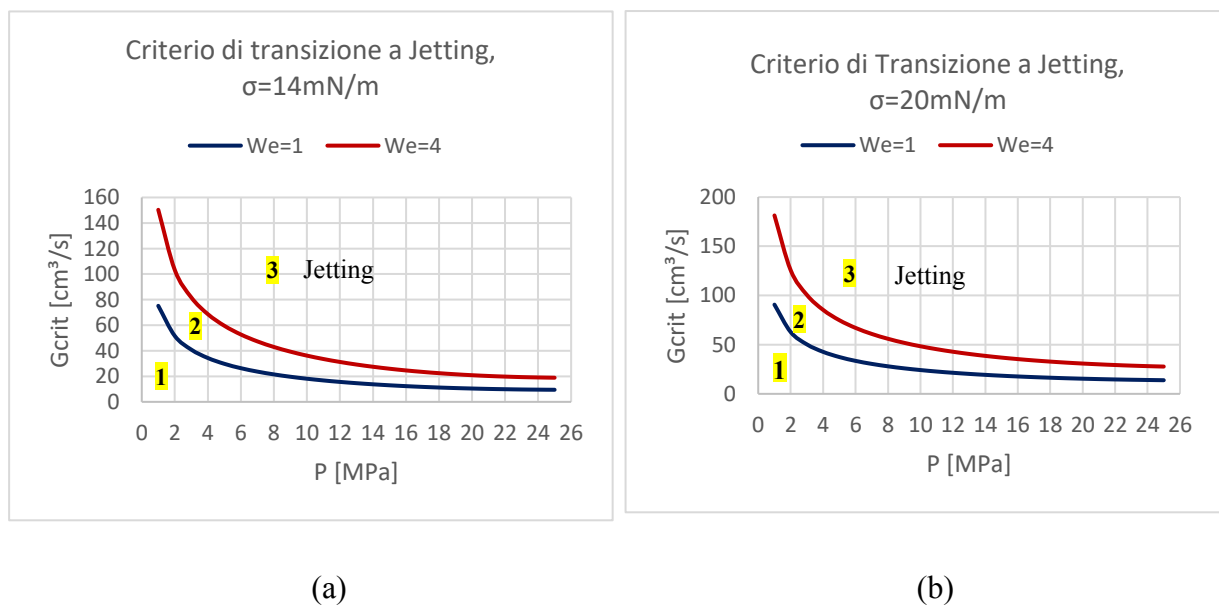


Fig.10: Criterio di transizione al regime “*Jetting*”: (a) $\sigma=14\text{mN/m}$ e (b) $\sigma=20\text{mN/m}$.

Nella figura 10 è possibile identificare le tre zone sopra descritte, la sezione 3 di “*jetting*” che si trova sopra la linea rossa che identifica il numero di Weber uguale a 4, sotto la linea blu si trova la sezione 1 dove esiste il regime omogeneo ed è valido il modello della formazione della bolla presentato in questo lavoro. Inoltre, nella figura 10 si trova la sezione 2 che identifica una zona chiamata di transizione dove potrebbe o no accadere il fenomeno di “*jetting*”. La figura 10 mostra anche l’effetto di aumentare la tensione superficiale che è quello di aumentare i valori di portata di gas critica per cui il regime di “*jetting*” accade.

È stato fatto questo stesso studio per diversi diametri del foro ed è stato trovato che diminuendo il diametro del foro si riducono i valori di portata de gas critica per avere regime omogeneo e di “*jetting*”.

Modello di moto e scambio termico.

In questo parte è stato utilizzato una miscela d’idrocarburi composta da Eptano come componente leggero ed Eicosane come componente più pesante. Per il gas è stato utilizzato idrogeno. L’obiettivo principale di questa sezione è valutare la dimensione della bolla dopo il momento del distacco e la possibile crescita della bolla dovuto a un fenomeno di vaporizzazione del componente liquido più leggero attorno la bolla. Questa vaporizzazione è assunta possibile dovuto a che la bolla viene formata dal distributore di gas a una temperatura notevolmente più alta dalla temperatura del liquido dentro del reattore. Dal sistema di equazione differenziale di primo ordine impostato per le variabili, moli di componente “A”: Eptano che vaporizzano, T , temperatura della bolla, L , diametro finale della bolla dopo il distacco e posizione, y , e velocità di risalita (U_t) della bolla dopo il distacco sono stati trovati diversi grafici per ogni una di queste variabili con il tempo, come mostrano le Figure 11, 12 e 13.

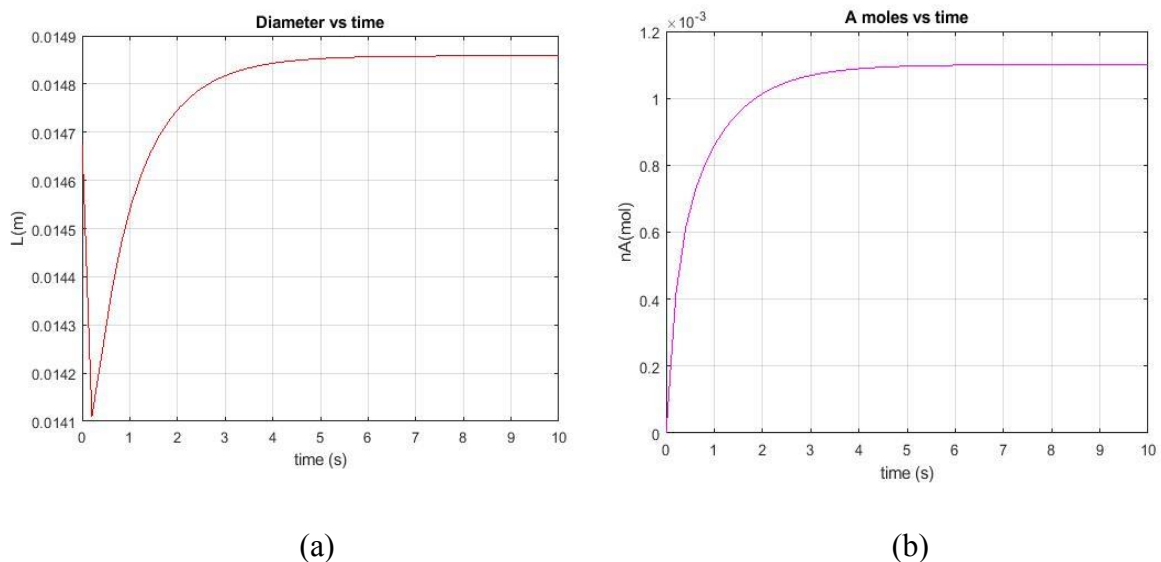


Fig.11: Risultati dei modello combinato moto, trasferimento di calore e materia:

(a) Diametro della bolla e (b) Moli di “A” vaporizzati dopo il distacco.

Dalla Fig. 11 (a) si può determinare il diametro della bolla stazionario dopo che accadono i processi di trasferimento di materia e calore e mentre la bolla si allontana dello sparger e risulta essere 1.25% più grande dalla bolla al momento del distacco; questo aumento di dimensione

viene considerato trascurabile. Nella Fig. 11 (b) si vedono come i moli di “A” vaporizzati aumentano nel tempo fino a un valore stazionario, questi moli fanno aumentare la dimensione della bolla, però essendo vaporizzata una quantità piccolissima del componente “A” alle condizioni di pressione e temperatura fissate per questo analisi la bolla si ingrandisce in una quantità considerata trascurabile come detto prima.

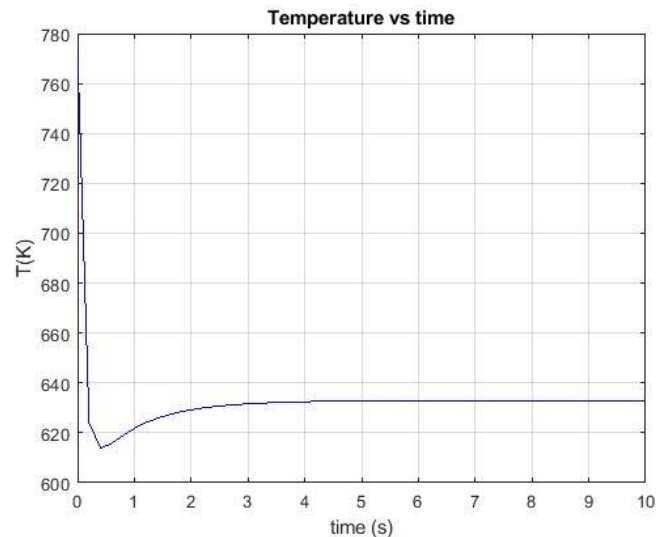


Fig.12: Risultato dei modello combinato moto, trasferimento di calore e materia:
Temperatura della bolla dopo il distacco.

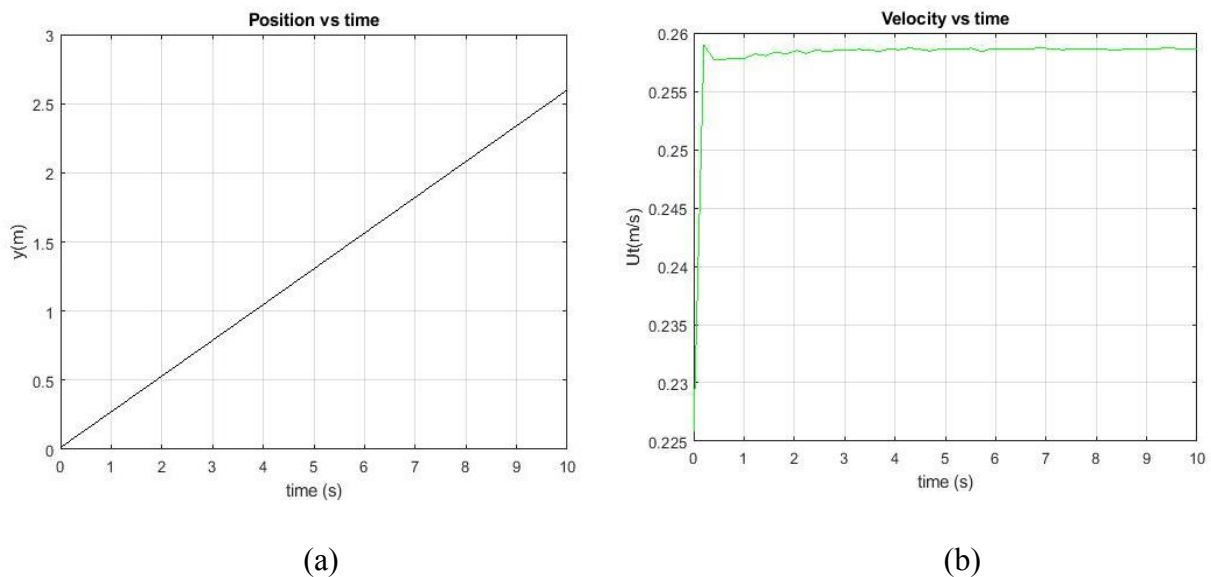


Fig.13: Risultati del modello combinato moto, trasferimento di calore e materia:
(a) Posizione della bolla e (b) Velocità di risalita della bolla dopo il distacco.

Nella fig.12 es possibile osservare una diminuzione della temperatura addirittura al di sotto della temperatura del liquido associata alla vaporizzazione del liquido e dopo la temperatura della bolla viene riportata alla temperatura del liquido. Il decremento repentino del diametro della bolla nei primi millisecondi di tempo si deve a questo raffreddamento iniziale.

Dopo in fig. 13 (b) si osserva il profilo di velocità della bolla dopo il distacco e si vede che dopo alcuni millisecondi la bolla acquisisce una velocità terminale pari a 0.256 m/s che è un valore ragionevole di risalita d'accordo ai dati trovati in letteratura.

Effetto della tensione di vapore.

Visto che il l'effetto di vaporizzazione dell'eptano dopo il distacco della bolla e per la presenza di un gradiente di temperatura fra la bolla e il liquido e trascurabile si è fatto un'analisi per valutare come influisce l'aumento della tensione di vapore sulla crescita della bolla per il fenomeno di vaporizzazione del componente "A". Una tensione di vapore maggiore si ha considerando liquidi più volatili come l'esano e il pentano. Invece di cambiare tutte le proprietà del componente liquido nel modello si ha inserito un coefficiente "k1" che moltiplica la tensione di vapore nella equazione di velocità di trasferimento del componente "A" per incrementare la tensione di vapore. I risultati di questo studio si trovano nella tabella numero 1.

Tabella 1: Effetto de la tensione di vapore sul volume della bolla dopo il distacco.

T[K]	Psat(T) C7H16[MPa]	k1*Psat(T) C7H16[MPa]	Vo 2nd Stage, [cm³]	Vf, combined Model, [cm³]	ΔV= Vf-Vo [cm³]
660	8.4574	1.892*Psat(T)	1.6554	2.226	0.571
654	8.056	2*Psat(T)	1.6554	2.352	0.697
633	6.7435	2.37*Psat(T)	1.6554	2.618	0.9626
628	6.4514	2.5*Psat(T)	1.6554	2.811	1.1556
624	6.0377	2.65*Psat(T)	1.6554	3.054	1.3986

Dalla tabella numero 1 si osservano i coefficienti "k1" utilizzati in questo esercizio per determinare l'effetto della tensione di vapore sul volume finale della bolla dopo il distacco. Con un coefficiente uguale a 1.892 l'incremento del volume finale della bolla allo stazionario è 34% maggiore in confronto con il diametro al momento del distacco. Incrementando il coefficiente k1 a 2 l'incremento in volume finale della bolla è 42%. Finalmente, con il coefficiente k1 più alto che è pari a 2.65 l'incremento finale della bolla in volume è pari a 84%. Tutti questi incrementi sono rilevanti e importanti rispetto a quello trovato per l'eptano che è stato uguale al 4% in volume rispetto al volume al momento del distacco.

In questa maniera è possibile dimostrare che l'effetto della tensione di vapore è rilevante per la crescita della bolla dopo il distacco dovuta alla vaporizzazione del componente liquido "A" più leggero.

Effetto del coefficiente di trascinamento.

Per questo modello combinato sono stati esaminati due espressioni di coefficienti di trascinamento diversi prima di ottenere i risultati finale rappresentati per i 5 grafici nelle Figure 11,12 e 13.

Le due equazioni di coefficienti di trascinamento ad analizzare sono le seguenti,

$$C_D = \frac{18.5}{Re_B^{0.6}}$$

$$C_D = \max\left[\frac{24}{Re_B} (1 + 0.15 Re_B^{0.687}), \frac{8}{3} \frac{Eo}{Eo+4}\right]$$

Nella Fig.14 vengono riportate i grafici di posizione e velocità della bolla dopo il distacco utilizzando la prima equazione per il coefficiente di trascinamento nel modello della formazione della bolla e dopo nel modello combinato.

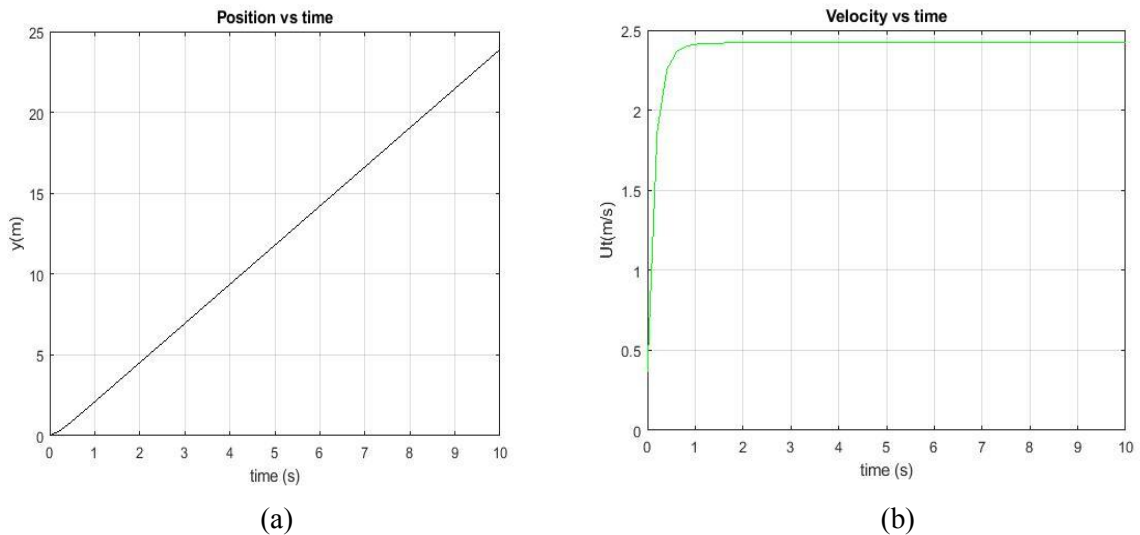


Fig.14: Risultati del modello combinato moto, trasferimento di calore e materia:

(a) Posizione della bolla e (b) Velocità di risalita della bolla dopo il distacco.
Prima equazione per il coefficiente di trascinamento.

Dopo nella Fig.15 vengono riportate i grafici di posizione e velocità della bolla dopo il distacco utilizzando la seconda equazione di coefficiente di trascinamento scritta sopra.

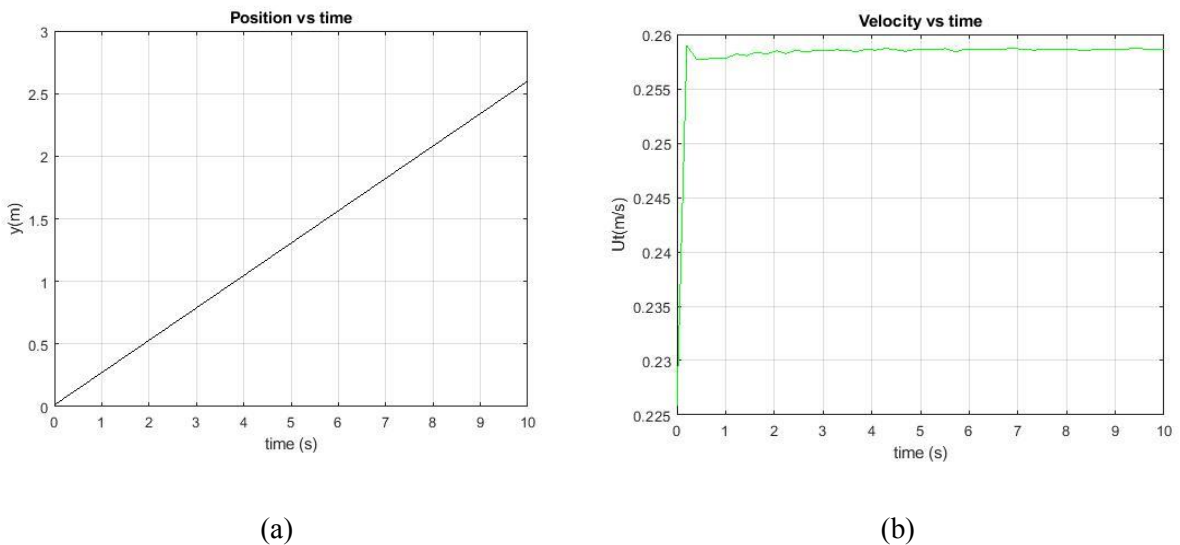


Fig.15: Risultati del modello combinato moto, trasferimento di calore e materia:

(b) Posizione della bolla e (b) Velocità di risalita della bolla dopo il distacco. Seconda Equazione di coefficiente di trascinamento.

Nella fig.14 si mostrano la posizione della bolla e la velocità di risalita terminale della bolla dopo il distacco. In 4 secondi che il tempo dove la bolla assume una dimensione e temperatura costante, secondo questi risultati, la bolla è salita nove metri e ha una velocità di risalita terminale di 2.4 m/s. Questi valori di posizione e velocità sono stati messi in confronto con dati sperimentali e sono molto elevati e fisicamente non sono ragionevoli.

Al contrario, in Fig. 15 sono mostrati i grafici di posizione della bolla e velocità terminale della bolla ottenuti con la seconda equazione di coefficiente di trascinamento scritta sopra. In 4 secondi la bolla è salita soltanto 1 metro e raggiunge in millisecondi una velocità terminale di 0.26 m/s che è abbastanza ragionevole in confronto con la data sperimentale. Per questo nel modello combinato viene preso come coefficienti di trascinamento la seguente espressione,

$$C_D = \max\left[\frac{24}{Re_B} (1 + 0.15 Re_B^{0.687}), \frac{8}{3} \frac{Eo}{Eo+4}\right]$$

Questa equazione di coefficiente di trascinamento è considerata la più idonea a utilizzare nel modello combinato di moto e trasferimento di materia e calore spiegato sopra.

06. Conclusioni.

Essendo l'obiettivo principale di questo lavoro determinare la dimensione della bolla vicino il distributore di gas, specificamente nel momento del distacco e dopo il distacco per il subseguente scambio di materia e calore fra la bolla calda e liquido meno caldo dentro il reattore vengono presentate le principali conclusioni alla fine di questo lavoro:

Il modello di formazione della bolla presentato in questo lavoro e che stato diviso in due stadi e stato validato con successo con un sistema acqua-aria a diverse condizioni di pressione. Il modello ha una deviazione media rispetto alla data sperimentale uguale a 12%. Questa differenza può essere attribuita a due assunzioni principali del modello come la forma sferica e il criterio di distacco della bolla.

È stato anche realizzato un'analisi di sensitività per capire come il modello reagisce a certi cambi nelle proprietà dei fluidi come la densità del liquido e del gas e alle condizioni operative del sistema del sistema, con la portata di gas nel foro e la pressione. È stato trovato che un aumento nella densità del liquido fa aumentare la dimensione della bolla perché il peso della colonna di liquido è maggiore e la bolla rimane più tempo attaccata al foro. Dopo la pressione del sistema affetta notevolmente la densità del gas e un incremento nella pressione causa un incremento nella densità del gas che risulta in bolle di dimensione minore. Inoltre, la densità di gas è proporzionale ai termini che spingono la bolla e si creano bolle più piccole.

È stato adottato un criterio di transizione al regime di "Jetting" tramite il numero adimensionale Weber. Il modello di formazione della bolla viene considerato valido nella regione di portata di gas critica e pressione del sistema sotto la linea che rappresenta un numero di Weber pari ad 1, questa zona è quella dove si trova il regime di omogeneo di formazione di bolle. L'incremento della tensione interfacciale e la dimensione del foro hanno un effetto sul numero di Weber permettendo di avere regime omogeneo per valore più elevati di portata di gas.

La dimensione della bolla è stata valutata anche dopo il distacco per un sistema liquido costituita da una miscela liquida d'idrocarburi, e il gas idrogeno come fase gassosa a elevata pressione e temperatura. Il componente liquido considerato vaporizzare è stato l'eptano e la bolla è aumentata 3.5% in volume rispetto al volume della bolla nel momento del distacco; questo aumento in volume è considerato trascurabile. Comunque, dopo un'analisi sulla tensione di vapore del componente che evapora è stato trovato che se il componente che evapora è un componente più volatile dell'eptano come l'esano o il pentano e la tensione di vapore aumenta il doppio rispetto a quella dell'eptano l'incremento in volume della bolla è del 42% dopo il distacco, questo incremento in volume della bolla rispetto a quello del momento del distacco è considerato importante.

Finalmente è stato fatto uno studio del coefficiente di trascinamento che influisce notevolmente nella modellazione della posizione e velocità terminale della bolla dopo il distacco ed è stata trovata una equazione che modella idoneamente il cambio di posizione e la velocità terminale di risalita della bolla dopo il distacco.

Chapter 1

Introduction

1.1 Slurry Reactors

1.1.1 Bubble Column Slurry Reactor

The bubble column reactor is a vertical vessel which contains different phases, constituted by a liquid mixture having one or more components of interest and small suspended solids particles by means of the rising of bubbles coming from a gas distributor located at the bottom of the reactor [1]. A sketch of the reactor is shown in Fig.1.1 a.

The reactor works as a contactor between the different phases to reach the conversion of some components of interest by means of a reaction mostly under high pressure and temperature conditions. Besides, the bubble column reactor is usually cooled or heated through internal heat exchanges to reach the desire temperature [2]. The reactor is considered convenient in term of energy consumption because the absence of mechanical parts inside it.

Having advantages as low power consumption and high heat and mass transfer efficiency these reactors are commonly utilized in chemical, biochemical and petrochemical industries. Some processes in which this kind of reactors are involved are the production of renewable fuels, such as Biodiesel by means of the transesterification reaction [3, 4]. The upgrade of heavy oils and petroleum residues through the cracking and hydrogenation process, hydrocracking, at elevated temperature, from 350°C up to 500°C and pressures between 7 and 25MPa, [5]; this last operation is one of the most important commercial applications of bubble columns [6]. The conversion of solid coal into liquid fuels, referred as Coal liquefaction, is also a process performed by this kind of slurry reactors at high pressure and temperature conditions [7].

New alternatives were found in the environmental field, for instance, some oil-degrading microorganisms were successfully cultivated in these reactors. Additionally, the removal of Volatile Organic Compounds (VOC) from waste water or exhaust air through emulsions of oil and water is done in bubble columns [8]. Besides, flue-gas desulfurization (FGD) and particulate removal [6].

A very important process for the synthesis of heavy paraffins, called Fischer Tropsch is carried out in slurry bubble column reactors under high pressure conditions [9]. Furthermore, through this process have been manufactured liquids fuels from gas, mainly methane [10].

Since hydrogen can substitute combustions engine systems, different technologies have been developed for its production. A singular procedure for hydrogen manufacture is the methane pyrolysis or methane cracking which is also executed in bubble columns reactors [11].

1.1.2 Stirred Tank Slurry Reactor

It is a mechanically agitated reactor, consisting in a cylindrical vessel containing a liquid-solid suspension as shown in Fig.1.1 (b). Gas enters at the bottom by means of a gas sparger in form of bubbles and it is recovered at top before going out of the system. Liquid phase can be

treated in continuous or batch mode while the gaseous phase is treated in a continuous manner. Liquid batch mode operation is preferred for the treatment of relatively small quantities. Continuous agitation guarantees a constant temperature and concentration throughout the reactor. Besides, the reactor is characterized by an excellent heat transfer performance, especially if internals are adopted [12]. Catalysts for this reactor are often small particles, which provide high performance, although its separation could cause some difficulties.

Important processes are carried out in this kind of reactors. In the petrochemical industry is possible to highlight the Fischer-Tropsch process to produce diverse synthetic hydrocarbon fuels [13]. In the production of biofuels, the catalytic cracking processes of residual fat, oils and grease (FOG) contained in wastewater streams is used to manufacture liquid fuels and heavy diesel-like fuels [14]. Besides, slurry stirred tanks have been used for the reduction of NO_x emission in diesel engines through diesel auto-oxidation [15]. In oil field degradation, these reactors have treated soil polluted with petroleum hydrocarbons with natural-rubber processing sludge [16].

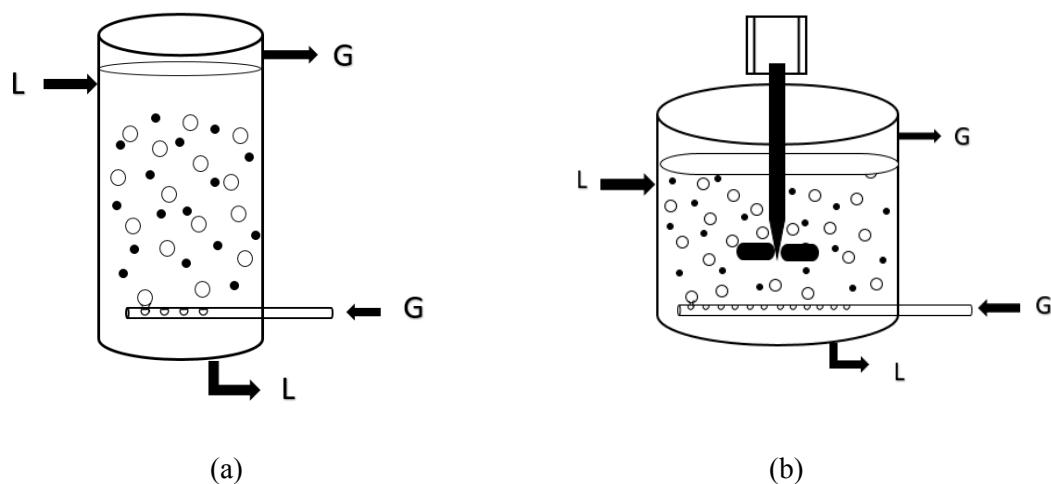


Fig. 1.1: (a) Slurry Bubble Column Reactor schematization and (b) Agitated Slurry Reactor.

1.1.3 Flow Regime

The flow regime inside a bubble column determines important properties, for instance, the hydrodynamics, holdup (volume fraction) of distinct phases, gas-liquid interfacial areas and overall mass and heat transfer [17]. Different flow regimes were found in bubble columns according to the superficial gas velocity, and a graphical representation of different regimes are reported in Fig.2 [18].

At very low superficial gas velocities, the homogeneous bubble regime or bubbly flow regime is found, [19], as shown in Fig. 2.a. In this regime bubbles are uniformly dispersed in the liquid, they are almost spherical and have small and similar size; besides, coalescence does not occur, too often.

The heterogeneous or Churn-turbulent regimes is originated when the superficial gas velocity is further increased through the reactor and bubbles coalesce, forming bigger bubbles which rise faster than smaller ones. This regime is characterized by the presence of small and big bubbles simultaneously, as is represented in Fig. 2.b. The presence of larger bubbles

represents a larger mass transfer coefficient, but the interfacial area gas-liquid is decreased, so the conversion in heterogeneous regime is reduced in comparison with bubbly regime [2].

Finally, it was identified the Slug flow regime in small columns, specially at laboratory scale at high superficial gas velocity in which large and elongated bubbles are stabilized by the column wall and move upwards inside the column [18]. This last flow pattern is shown in Fig.2. c.

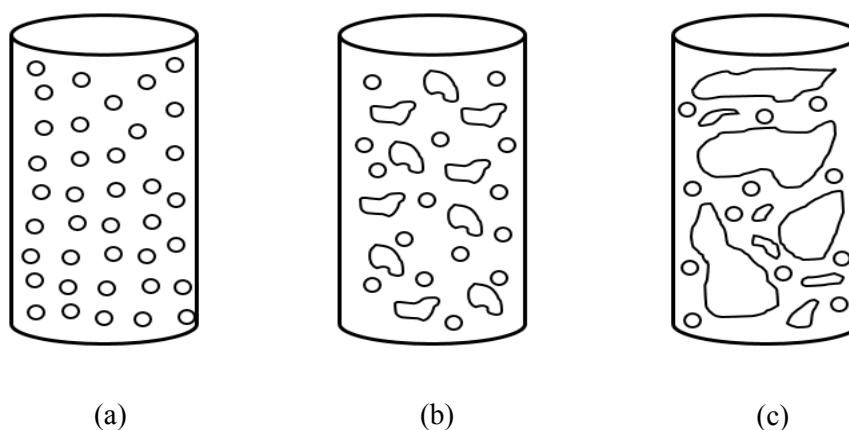


Fig. 1.2: Flow regimes in gas-liquid reactors: (a) Homogeneous regime (b) Heterogeneous regime (c) Slug flow regime.

1.2 Bubble Formation process

Inside bubble columns the liquid mixture could be placed in batch mode, it could flow in the same direction of gas phase, that is, co-current or counterflow respect the gas phase. In contrast, gas is introduced by a gas distributor located at the bottom. The gas distributors (or spargers) are usually made by perforated tubes and arranged in different geometries to produce gas bubbles. The process of bubble formation and rising through the reactor allows the different reactants inside the different phases get in contact and interact to carry out the desired reaction.

So, quantify the interfacial area between the gas and liquid has been an important issue since it is proportional to heat and mass transfer rates and influences the reactor efficiency. In order to obtain a final bubble characterization through the reactor it is important to obtain first an initial bubble size by means of the understanding of bubble formation phenomenon from the opening at the sparger to its detachment time. Furthermore, it is relevant to consider a subsequent increment or decrement in size due to evaporation of some components in the liquid mixture through a possible heat transfer process.

Diverse models have been proposed in order to predict bubble size. Some researchers have developed models based on the balance of forces acting on the bubble from its creation until its release from the sparger [20, 21, 22, 23, 24]. Besides, different authors have developed different experiments to assess bubble formation and detachment process. However, most of these works are limited to low gas flow rates and to low pressure conditions. Just few experiments are settled at industrial conditions, so, high pressure and temperature and high gas flow rates at the orifice.

Bubble formation models are usually classified into spherical and non-spherical models; spherical models are divided into one or two stages and those assume spherical bubble shape.

Additionally, spherical models use an empirical criterion for detachment moment. In contrast, Non-spherical models work with a determined shape of bubble different from spherical one and they are classified by numerical calculation method [25].

In the present work is developed a spherical, two stage model for bubble formation until its detachment, based on a balance of forces exerted on the bubble near the sparger region and it will be evaluated in a wide range of high gas of flow rate. Furthermore, pressure have been considered in some aspects of the models, for example in fluid properties and through some terms inside the balance of forces.

Two different systems will be evaluated with this model. First an air-water system will be investigated and eventually an oily liquid phase with hydrogen gas. Both systems assessed in several conditions of temperature and pressure.

Since the model will be assessed at high gas flow rate, it will be reviewed an extensive literature about the bubbling regimes and transition from bubbling to jetting at different operating conditions and systems, including high pressure systems to determine a qualitative limit for the established model.

Afterward, it will be shown an assessment of each term importance inside the balance of forces for the determination of bubble dimension at the end of each stage. Besides, important fluid properties have been changed in a wide range to evaluate its impact on the final bubble size at detachment.

Finally, it has been developed a combined momentum, heat and mass transfer model after the detachment time to determine a final bubble dimension in the region of the sparger.

1.3 Literature review

1.3.1 Bubble formation and detachment models

The first article reviewed for this thesis project was published in 1991 by Nicholas W. Geary and Richard G. Rice [26] . They presented a simple bubble formation model separated in two stages with the main objective to predict the bubble dimension from rigid and flexible spargers in bubble columns. The first stage was considered for expansion and second stage took in account both bubble growing and rising with a formation of a neck which connected the bubble and the gas distributor. The method used to develop the bubble formation model in this work was through a fundamental balance of forces in the system.

They emphasized that different flow regimes exist according the gas flow rate. In consequence, the model designed by them was tested and compared with the literature data of Kumar and Kuloor (1970) in a limited range of gas flow rate. The range of volumetric flow rate was changed from 2 cm³/s to 80 cm³/s, and the hole diameter was assessed between 0.36 mm and 5.945 mm.

Furthermore, Geary and Rice argued about the time of detachment, that is, when bubble releases from the sparger. The important parameter here to be measured was the length of the gas neck which connects the bubble with the sparger. The neck length was arbitrarily assumed in this work as twice of the hole sparger radius.

Secondly, other two important articles were considered in this thesis project and both were written by the same authors, Changjun L., Bin L., Shengwei T., and Enze M.,[27,23].

The first article [27] shows a model for bubble formation for different gas flow patterns

into a cross-flowing liquid phase. They considered four type of gas flow patterns, type I, when the bubble rises upward with a horizontal liquid flow, type II, when bubbles is pulled downward and the liquid stream have horizontal flow direction, type III, for horizontal bubbling in an upward liquid flow and Type IV, when the liquid falls and bubbling is horizontal. For each gas flow pattern a force balance was written according to the gas and liquid direction. Furthermore, in this work it was considered a spheroidal shape due the liquid cross flow effect. They set the moment of detachment at the time that the distance from the bubble center to the orifice center exceeds the sum of the major diameter of the spheroid and the orifice diameter.

After that, they tested each flow pattern model and compared them with literature data except for type II. In the case of Type I in which bubbling is upward and the liquid flow is horizontal it was got a 7% deviation from the literature data referenced as Marshall, S.H., 1993. Subsequently, it was shown the effect of increasing the hole diameter on the bubble size at detachment for each flow pattern. Finally, in this work the fluid properties were varied for each gas pattern model to understand its effect on bubble size and they concluded that operating parameters as gas velocity, liquid velocity and sparger hole diameter have a bigger impact on bubble size than the physical properties of both liquid and gas.

In the second paper,[23], the main aim of these authors was to develop a bubble formation model based on a balance of forces and analyze the effect of this forces acting on the emergent bubble with time. Furthermore, a horizontal liquid cross flow was taken into account during the bubble formation. The detachment time is considered when the distance between the bubble center and center of the orifice exceeds the sum of the bubble diameter (assumed as a sphere) and the orifice diameter. The forces counted in the balance were buoyancy, gravity, pressure force, shear lift force, gas momentum, surface tension, drag and inertia. The pressure force term took in consideration is based on the difference in pressure between the gas and the liquid phase; the gas is pushed into the liquid by this pressure difference at the orifice. Besides, geometrical parameter related to the orifices as its length, diameter and pressure drop. Regarding the bubble detachment results it was obtained for the water-air system a 16% deviation in comparison with literature data.

In 1986, an older work was published by Gaddis E.S and Vogelpohl A. [21]. The aim of this work was to determine the bubble detachment moment by means of two approaches. First approach utilizes the equation of motion in the detachment stage for a prearranged bubble geometry. The second approach utilizes an equation for bubble detachment volume as the sum of the volume of bubble at the end of an expansion stage and an extra volume equivalent to the bubble neck during the detachment time. It was developed a model based on the balance of forces for the expansion stage and then the excess for the neck was calculated through the determination of empirical parameters. The second approach was not further developed because it was found a great deviation from literature results.

However, the first approach was used with a fixed bubble geometry and with a different scheme from different authors; it takes in account a volume for the neck during the expansion stage. This work considers that the bubble expands because of the gas flow through an orifice, a constant volumetric flow rate and a quiescent liquid. The forces considered in this analysis were the buoyancy, gravity, momentum, surface tension, drag and inertia. The drag coefficient was set equal to $24/Re$ for small values of the Reynolds number. It was established a balance of forces at the moment of detachment and it was determined the bubble size iteratively.

In the pioneering work of Krishnamurthi S., Kumar R., and Kuloor N.R.,[28]. A bubble formation model was created to assess the bubble volume at detachment instant.

They created a two-stage model, a first stage where bubble expands until buoyancy becomes equal to the sum of surface tension and drag and a second stage, where the bubble

start to rise but it is still connected to the orifice and buoyancy overcomes the resisting forces. In the last step it is mentioned that for highly viscous liquids inertia effects are neglected. Additionally, this work divided the forces in two categories, upward and downward.

They suggested two possible mechanism for detachment, first one was that the bubble could rise faster than the expanding hemisphere left behind and second one, the bubble could detach at a distance that the expanding hemisphere and the free bubble can not coalesce.

Experiments were executed to verify the results coming from the model. Some experimental and operating parameters were the volumetric flow rate range assessed between 0.04 and 0.25 cm³/s, hole diameter between 2 and 3mm and some liquid viscosity values were 4.49 and 7.25 poises. Finally, the overall standard deviation obtained for the model results was 5.4%.

Finally, it was reviewed an article introduce by Zhang L., and Shoji M., in 2001 [29]. The non-linear theoretical model proposed by these authors seems to account the wake effect of the former bubbles, predict bubble behaviors and the bubble departing periods and sizes but in a low gas flow rate regime. The shape was assumed to be spherical and under constant flow conditions, it was present an overall force balance including buoyancy, gas momentum, surface tension, inertia, an original drag force and a drag force due to the wake of the earlier bubble. The model is separated as usual in an expansion stage and an elongation stage.

For detachment moment was taken the moment in which the neck connecting the bubble to the orifice pinched off. Referencing to the work of Kim, Kamatmani and Ostrach in 1994, this moment was supposed to be reached when the neck length becomes larger or at least equal than the orifice diameter. Overall, this method is useful with relatively low gas flow rate regime.

1.3.2 Bubble formation models on high pressure conditions

It is imperative to investigate the systems, that is, slurry reactors under high pressure and temperature because those are the real operating conditions for the majority of processes in the petrochemical industry.

The first article reviewed was written by D.-H Yoo, H. Tsuge, K. Terasaka and K. Mizutani in 1997, [22]. This article introduces a non-spherical bubble formation model and include the effect of the pressure in some fluid properties as well, surface tension and liquid viscosity. It was shown an equation for the change of pressure in the gas chamber together with an orifice equation. The model was solved through a numerical method. Two correlations were presented, referenced to different authors from this paper, in which the pressure of the system was considered for the calculation of the surface tension and the solid particle holdup was considered in the liquid viscosity.

Furthermore, an experimentation was done with a laboratory scale bubble column with a glycerol aqueous solution and a pressure variation from 0.1MPa to 8MPa. Several plots were shown, bubble volumes versus gas flow rate for different pressure values, for different solid particles holdup and different hole diameters. For system under 2MPa the impact of the pressure of the system was a reduction in bubble volume. However, the impact on the bubble for pressure system above 2MPa was smaller. For the highest value of pressure, 8MPa, they assessed the effect of hole diameter, bubble volume and gas flow rate. Overall, the effect of elevated pressure demonstrated in this article, through the model and experimentally, was a reduction on bubble volumes.

A second article studied was published by Luo X., G. Yang, Lee D.J., and Fan L., in 1998 [30]. The liquid system used in this work was a non-aqueous system and the maximum pressure

assessed was 17.3 MPa. This article proposes a two-stage spherical bubble formation to predict the initial bubble size in high pressure system. The method used was based on a balance of forces during each stage.

The experiments were carried out in a high pressure three-phase fluidized bed and the extreme condition evaluated in this work was at 21MPa and 180°C, that is, elevated pressure and temperature. Paratherm NF was utilized as liquid system with suspended solid particles.

Several plots for bubble size versus hole velocity varying the pressure in the system were presented as part of results. Through those plots the noticeable effect of pressure on bubble size is highlighted. Gas momentum inside the balance of forces was the most influencing term due to pressure, it was noticed a significant increment on it, although it was noticed also a considerable reduction on buoyancy term. This last balance on increment and reduction between upward and downward forces took the authors to conclude that pressure would have an insignificant effect under constant flow conditions. Finally, the analytical model results were written to be consistent with experimental results.

Next article to be mentioned in this literature review was proposed in 1999 by Tsao-Jen Lin and Liang-Shih Fan [31]. It was an experimental work in which it was used an organic fluid Paratherm NF in the liquid phase and nitrogen as gas phase; the most extreme operating condition was 15MPa and 180 °C. The results were obtained by means of visualization with high-speed camera. Heat transfer measurements were performed through a heat transfer probe.

They noted a reduction on bubble dimension and velocity as pressure was increased although the formation frequency behaved in the opposite way. Additionally, it is mentioned that pressure affects more significantly elevated nozzle gas velocity instead of lower ones. Furthermore, they observed that the transition velocity from bubbling to jetting regime decreased with the increment on pressure which is very important in the determination of a validity limit for models predicting bubble size, especially in systems at elevated pressure. Finally, they mentioned a notable increment in the heat transfer coefficient with high pressures.

An additional work to be reviewed was done by Soong Y., Harke F.W., Gamwo I.K., Schehl R.R and Zarochak M.F.[32]. The system consisted in Drakeol-10, an oily liquid system and nitrogen on the gas phase. The experimental work was done through a dual conductivity probe in a slurry bubble column. The maximum temperature and pressure assessed were 265°C and 1.36MPa, respectively. It was mentioned a significant change in properties at elevated temperature as surface tension, affecting the bubble size and resulting in smaller bubble dimension. The effect of the increment in pressure seems to cause a reduction in the bubble size in the column. This work, in contrast with previous articles, is referred to bubble size characteristic inside the column and in its overall hydrodynamics, not considering bubble formation objects.

1.3.3 Transition from bubbling to jetting regime

Gaddis E.S., and Vogelpohl A. et. al. (1986), [21], specified a limit for the validity of the model proposed to predict bubble diameters at formation. It is mentioned that there is a limit for the gas flow rate that identifies the transition from bubbling to jet regime, and therefore, the model suggested to evaluate the bubble diameter in bubbling regime is not valid anymore. The mechanism used to identify the transition from bubbling to jetting was based on the idea that spherical bubbles were not created if the gas momentum plus the pressure force exceeded the surface tension force and a jet would be developed at the nozzle. The result for this criterion was the definition of a critical dimensionless number, called Weber. A further consideration in

the criterion is to consider the contact angle between the gas and the liquid at the moment of the bubble formation.

The next study reviewed was presented by Camarasa E., Vial C., Pochin S., Wild G., Midoux N. and Bouillard J. in 1999, [33]. In this work it was presented three bubble formation regimes at the sparger depending on the gas flow rate. The regimes were “separated bubble formation”, “chain bubbling” and “jet regime” with a growing gas flow rate. Then, it is mentioned a criterion for the transition based on the dimensionless Reynolds number based on the orifice, Re_o . The transition was specified to occur for Re_o , between 2000 and 10000.

A similar approach was used by Chaumat H., Billet A. M. and Delmas H. [34]. They defined the same bubble formation regimes mentioned before, separated bubble formation, chain bubbling and jet regime. Using two different liquid systems, water and cyclohexane, it was recognized a transition from bubbling to jetting when the gas hole velocity was 22.1 m/s. For a gas hole velocity of 10 m/s bubbling regime was distinguished and it corresponds to an orifice Reynolds number of about 1000. Furthermore, it was shown a bubble size distribution for both liquid media (water and cyclohexane) with an increasing hole gas velocity. It was revealed through a comparison of size distribution for both medias that bubbles formed in cyclohexane are overall smaller than in water. This last result was the expected one according the smaller surface tension of cyclohexane.

Then, the work titled by Zhao Y.F and Irons G.A. [35] in 1990, discusses some theories in literature about bubbling to jetting regime transition and it expresses that the fundamental idea for the transition was based on the elongation of the bubbles with a growing gas flow rate through the orifice, that is, the linking of bubbles to form a jet. The work was aimed to model this phenomenon and give physical bases to the process. The analysis suggested that surface instability (gas-liquid) accelerates the onset on jetting and that phenomenon governs the transition regime. It was adopted from other authors the concept of jetting through the “linking” measure of jetting to compare the experimental results with literature results.

A special work was published by Qu C., Yu Y., and Zhang J.,[36], in which was performed a bubble dynamic study specialized in micro-sized orifices, that is, for hole diameters smaller than 0.3 millimeters. The article was aimed to analyze the bubbling regimes for this kind of orifices. The bubble formation examination was separated according the gas flow rate into “static” and “dynamic”. Bond, Bo, and Weber, We, dimensionless number were used in the bubble dynamics discussion. In the experimental set up, temperature and pressure were 25°C and 1atm, the gas flow rate varied between 0.167 and 25 ml/min and the hole diameter was assessed between 0.11 to 0.24mm with an air-water system. The bubble dynamic experimental study was supported with the help of a camera with 4.68 micro millimeters per pixel of resolution. Bubble detachment time was also measured experimentally. Weber number was useful to explain the bubble behavior at detachment time. Through some time versus Weber number plots, they observed a downward trend in detachment time with increasing Weber number. Furthermore, this dimensionless number is used to explain when the coalescence phenomenon occurs. Finally, it was designed a bubbling regime map based on experimental data. The vertical axis was represented by Weber and the horizontal one for the Bond number. In this map were identified 8 different regimes and it was also taken in account a bubble coalescence period and a bubble pairing period.

The next article examined was written by Sundar R. and Tan R.N.H. [37]. They developed a new mathematical model for capturing the transition from bubbling to jetting regime based on a force momentum balance in the liquid film around the gas core when jetting phenomenon starts. Then, model results were compared with results from the experimental analysis. An optical fiber probe was used in the experiments to estimate the time-averaged

volume fraction in the transition regime. Part of the results were presented through plots volume prediction versus air velocity showing the transition between the bubbling and jetting regime; the analysis was done for different hole diameters and liquid column heights.

Another article was written by Yang G.Q., Bing Du and Fan L.S., [38]. They mentioned the existence of three bubble flow regime for a gas injection in a submerged orifice: bubbling, transition regime (or sometimes called as doubling or coalesced regime) and jetting. In the transition regime coalescence between an detaches bubble and the emerging one occurs. The transition between bubbling and jetting is identified by a limit value of gas flow rate defined as “the onset velocity of gas jetting” by the writers. Some criteria mentioned in this article to estimate the onset of jetting at ambient conditions were related to the sonic velocity at the orifice. Other criteria were related to dimensionless numbers as orifice Reynolds numbers, Re_o , in which the transition occurs for a Re_o larger than 10000. Then, the Weber dimensionless number was also used as a criterion for predicting the transition. It is mentioned that for air-water system the critical Weber number for transition is equal to 2. Finally, there is an important highlight in this article and it is that pressure in the system as well gas density influence in a considerable way the bubbling to jetting transition. Furthermore, it was mentioned that the transition velocity tends to decrease with a higher pressure in both liquid and suspended liquids.

1.2 Aim of the Thesis

The main objective of this thesis project is to assess the dimension of a bubble forming from orifices in the gas distributors at the bottom of gas-liquid reactors in real operating conditions at the moment of detachment. Additionally, it aims to investigate how operating conditions as hole gas velocity, pressure, hole size and fluid properties affect the results. Finally, it aims to determine the subsequent bubble dimension just after the bubble is released when a combined momentum, heat and mass transfer between the gas and liquid occur.

Objectives:

1. Model the bubble formation in a first stage to obtain an initial bubble size.
2. Model a second stage for the continuous bubble expansion and lift process until detachment.
3. Investigate the transition from bubbling to jetting regime at normal and industrial conditions from literature.
4. Do a sensitivity analysis of some operating parameter and fluid properties over the bubble dimension.
5. Model the bubble momentum balance just after the detachment moment.
6. Model the bubble mass transfer just after the detachment moment.
7. Model the bubble heat transfer just after the detachment moment.
8. Solve the differential equation system developed for the combined momentum, heat and mass transfer model.

1.3 Methods

The bubble formation model deals with two complex equations both solved numerically with MATLAB. Then, these equations were modified in the sensitivity analysis and resolved again by means of MATLAB's solvers.

The last stage of this thesis project was to create a model including bubble motion, heat and mass transfer between the gas and the liquid phase just after the detachment time. The model outcome was a differential equation system solved in MATLAB.

Chapter 2

Research Background

2.1 Bubble Fluid Dynamics

Bubble fluid dynamics is determined by all the forces influencing the bubble formation and motion process. This section will introduce the most important force definitions to be considered in a bubble formation process.

2.1.1 Gravitational force

It is a pull force applied by the Earth on an object with a mass, m , near the Earth's surface. Its origin is based on the basic force of attraction between two objects. This force is also defined as weight of the object, W , as shown in Eq.2.1. The symbology used for this force is commonly, F_g . The field's direction is perpendicular to the level ground at every point on the Earth's surface. An object possessing a mass of 1.0 Kg have a gravitational force of about 9.8 N everywhere on Earth's surface [39]. Knowing the gravitational field strength, g , then,

$$W = m \cdot g \quad \text{Eq. (2.1)}$$

2.1.1 Acceleration due to gravity, g

It is the acceleration of an object defined by a mass m , during its free fall in the Earth's gravitational field and it is caused by its unbalanced weight force. The acceleration due gravity, g , has been determined experimentally with a value of 9.81 m/s² [40].

$$F = m \cdot a \quad \text{and} \quad a=g \quad \text{Eq. (2.2)}$$

2.1.2 Gas Momentum Force

It is the multiplication of the momentum flux through the orifice and the orifice area [41].

$$F_m = \frac{\pi d_o^2 \rho_g U_o^2}{4} \quad \text{Eq. (2.3)}$$

Then, U_o , denotes the velocity through the orifice, ρ_g is the gas density and d_o is the hole diameter. Finally, A_o is orifice area.

$$U_o = \frac{Q_g}{A_o} = \frac{Q}{\frac{\pi}{4} d_o^2} \quad \text{Eq. (2.4)}$$

2.1.3 Inertia

The inertia of matter is the predisposition of a mass to resist changes in its motion. Inertia makes an object difficult to start or stop its motion, hard to change its direction of motion or hard to accelerate. In contrast, the mass of an object, m , is the amount of matter on it and it depends on the number of atoms and its size [42].

2.1.4 Pressure difference

It is a force due to the difference on pressure between the fluids before and after the opening of a hole. The gas is coming from a chamber with pressure, p_g , and the liquid inside the reactor is exerted by a pressure, p_L [43].

$$F_p = \frac{\pi}{4} d_o^2 (p_g - p_L) \quad \text{Eq. (2.5)}$$

$$(p_g - p_L) = \frac{1}{C_o^2} \frac{16\rho_g Q_g^2}{\pi^2 d_o^4} \quad \text{Eq. (2.6)}$$

2.1.4.1 Flow through the orifice

Gas flow by means of an orifice could be assumed isothermal and incompressible. Hence, the orifice equation is presented below in Eq.2.7, which represents a quasi-steady state mechanical energy balance,

$$q_o = C_o A_o \left[\frac{p_g - p_L}{\rho_g} \right]^{0.5} \quad \text{Eq. (2.7)}$$

In Eq.2.7, p_g represents the pressure in the gas chamber before the orifice and p_L represents the bubble pressure. The discharge coefficient, C_o , is obtained through Eq.2.8 and it depends on the orifice geometry and flow properties. Then, K is an empirical constant found experimentally and L_o , is the orifice length. The discharge coefficient accounts for irreversible energy losses in the system. This coefficient varies according the Reynolds numbers and it is possible to determine it by means of experimental research done by Lichtarowicz, as shown in Fig.2.3. The results obtained by this author take in consideration wall friction loss and irreversibility due to flow separation [43].

$$\frac{1}{C_o^2} = K + \frac{32L_o}{Re d_o} \quad \text{Eq. (2.8)}$$

The Reynolds number, Re , is defined as the ratio of a convective term and a viscous dissipative term. It is characterized by a characteristic length and velocity, U_o and d_o (at the orifice) in the convective term and for the kinematic viscosity, ν_g , in the viscous dissipative term. It is a fundamental parameter which let identify the transition through different flow regimes, for instance, the transition from laminar to turbulent flow.

$$Re = \frac{4}{\pi} \frac{q_o}{d_o \nu_g} = \frac{U_o d_o}{\nu_g} \quad \text{Eq. (2.9)}$$

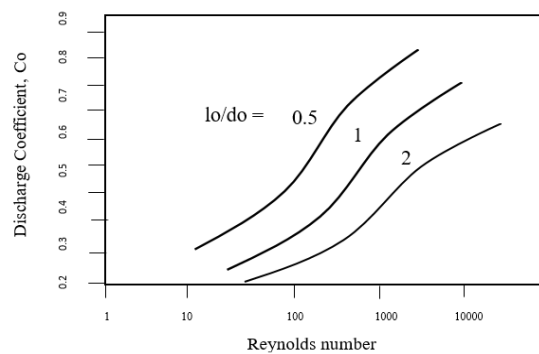


Fig. 2.3: Representation of Discharge coefficient vs. Reynolds graphic from [44] modified.

2.1.5 Buoyancy Force

According to Archimedes' principle, the vertical force of buoyancy on a completely or partially submerged object is equal to the weight of the displaced fluid. By fluid is meant gas or liquid. This buoyant force depends mainly on the displaced fluid density and the volume of the object immersed. B symbolizes the buoyancy force, W_f is the weight of the fluid that the object displaces and V_f is the volume of displaced fluid, so, it is equal to the volume of the immersed object [45].

$$B = W_f = V_f \rho g \quad \text{Eq. (2.10)}$$

2.1.6 Drag Force

It is the force exchanged between an object and a liquid flow. A general definition for this force is the product of a characteristic area, A , times a dimensionless coefficient called friction factor, f , and finally times a driving force, a characteristic kinetic energy, K , per unit volume [46] as shown below,

$$F_k = A \cdot K \cdot f \quad \text{Eq. (2.11)}$$

Each flow system is characterized by a characteristic area and a kinetic energy, then is possible to define a frictional coefficient, f .

2.1.5.1 Flow around submerged objects

For this system, the characteristic area is taken as a projection of the object into a plane perpendicular to the velocity of the approaching fluid; the characteristic driving force is defined as the approach velocity of the fluid at a large distance from the object, v_∞ .

For a flow around a sphere, f , is commonly named drag coefficient, C_D and it is determined by the measurement of the terminal velocity of a sphere falling through the fluid [46].

$$F_K = A \cdot K \cdot f = (\pi R^2) \left(\frac{1}{2} \rho v_\infty^2 \right) f \quad \text{Eq. (2.12)}$$

For the steady-state fall of a sphere in a fluid, the force F_K , is determined by a counterbalance between the gravitational force and the buoyancy force.

$$F_K = \frac{4}{3} \pi R^3 \rho_{sphere} g - \frac{4}{3} \pi R^3 \rho g \quad \text{Eq. (2.13)}$$

Then f , or C_D , is obtained matching the 2 equations expressed above,

$$C_D = \frac{8}{3} \frac{g R}{v_\infty^2} \frac{\rho_{sphere} - \rho}{\rho} \quad \text{Eq. (2.14)}$$

Where R , is the radius of the sphere, ρ , is the liquid density and ρ_{sphere} , is the sphere density.

2.1.7 Surface Tension Force

It is a uniform and isotropic force per unit length, acting on the contour line of a surface as shown in Eq.2.15. Additionally, it can be interpreted as the work required for the unit increase of surface area as show in Eq.2.16. Just because area extension processes are very close to reversible processes this last definition is valid even for no reversible processes.

$$\gamma = \frac{F_\gamma}{L} \left[\frac{N}{m} \right] \quad \text{Eq. (2.15)}$$

$$\gamma = \frac{dW_{rev}}{dA} \left[\frac{J}{m^2} \right] \quad \text{Eq. (2.16)}$$

2.2 Mass Transfer

An integral mass balance of a property “G” is written below in Eq. 2.17 and being $\hat{G} = \frac{G}{\text{unit mass}}$, then,

$$\frac{\partial \rho}{\partial t} + \nabla(\rho \bar{U}) + \nabla J_G = g_G \quad \text{Eq. (2.17)}$$

The first term in the left side of Eq. 2.17 represents the accumulation within the system. The second one represents the convective motion term, the third one represents the diffusive phenomenon and the only term to the right is the rate of generation or consumption, g_G .

For a single component the mass balance is reduced because there is no diffusion with a single component and the rate of generation is null.

It results in the Continuity Equation, in Eq. 2.18,

$$\frac{\partial \rho}{\partial t} + \nabla(\rho \bar{U}) = 0 \quad \text{Eq. (2.18)}$$

Last equation “describes the time rate of change of the fluid density at a fixed point in space”, [45]. The first term denotes the rate of increase of mass per unit volume and the second term is the net rate of mass addition per unit volume by convection.

2.2.1 Fick’s Law of binary diffusion

Diffusion has its origin on the individual motion of molecules inside the fluids, it is defined as “the molecular transport of one substance relative to another” [45]. In the case of binary diffusion, the Fick’s First Law let to define the mass flux of each component as shown in Eq. 2.19. Having two components, A and B, then

$$J_A = -D_{AB}(\nabla \rho_A) \quad \text{Eq. (2.19)}$$

where D_{AB} is the diffusivity of A-B system, ρ_A is the density of component “A” and J_A is the mass flow rate per unit area. This law is valid for any binary solid, liquid or gas solution [45].

2.2.2 Transient Mass Balance

Mass transfer is commonly a time dependent process in which the contact time between different phases is an important parameter. The non-stationary process is not considered in the film model. However, some authors have developed important theories which let evaluate this phenomenon. For instance, the penetration theory developed by R. Higbie in 1935.

In a multicomponent system, it is possible to write a microscopic and local mass balance, for the component α , as shown in Eq. 2.20 in terms of molar concentration,

$$\frac{\partial c_\alpha}{\partial t} + \nabla(C_\alpha \underline{U}^*) + \nabla J_\alpha^* = R_\alpha \quad \text{Eq. (2.20)}$$

The first term in the left side of Eq. 2.20 represents the accumulation term. The second term is a convective term, it considers the motion of the fluid by means a macroscopic fluid velocity. Then, the third term, represents molecular diffusion at for a binary and

multicomponent mixture can be substituted by the First Fick's Law. The last term symbolizes the molar rate of production or consumption of species α in a chemical reaction.

2.2.3 Mass transfer coefficient

The mass transfer coefficient is a proportionality constant for the molar or mass flux in a process of mass transfer when exist a driving force, as a concentration gradient of a component. The molar mass flux can be written as follows:

$$N_A = k_c A (C_{A0} - C_{Ab}) \quad \text{Eq. (2.21)}$$

where, N_A , is the molar flux of component A, K_c , is the mass transfer coefficient, A is a characteristic surface area when mass transfer occurs, C_{A0} , is the concentration of component A at the surface or interface and C_{Ab} , is the concentration of component A in the bulk stream [45]. This definition for mass transfer coefficient is similar in the case of conduction heat transfer processes when a temperature gradient exists.

The mass transfer coefficient definition and its determination have been explained by several theories as the Film model in stationary process and Higbie penetration model for some unsteady processes. To introduce these theories is necessary to introduce some dimensionless numbers as Schmidt, Sc and Sherwood, Sh numbers. Some of this dimensionless numbers have been found through the conversion of the main properties balance, as mass, momentum and energy balance equations in dimensionless equations.

When the Continuity equation or mass balance for a single component have been established and transformed into a dimensionless equation is possible to identified, the resulting dimensionless group,

$$\frac{1}{ReSc} = \frac{1}{Re} \frac{1}{\nu/D_{AB}} \quad \text{Eq. (2.22)}$$

The product of these last two dimensionless numbers generates a new dimensionless number called, Péclet number, Pe_{AB} . *“The Schmidt number is the ratio of momentum diffusivity to mass diffusivity and represents the relative ease of molecular momentum and mass transfer”* [45].

$$S_c = \frac{\nu}{D_{AB}} \quad \text{Eq. (2.23)}$$

where, ν , is the kinematic viscosity and D_{AB} denotes the mass diffusivity coefficient. Another important dimensionless number is called, Sherwood number, S_h , and it represents a dimensionless mass transfer coefficient and it is defined as,

$$S_h = \frac{k_c D}{D_{AB}} \quad \text{Eq. (2.24)}$$

where, D , represents a characteristic length, k_c , the mass transfer coefficient. The Sherwood number can be written in function of two important dimensionless numbers, Reynolds, Re , and Schmidt, S_c .

In general, it has been found a mathematical form for the Sherwood number,

$$S_h = \text{const.} (Re S_c)^a \quad \text{Eq. (2.25)}$$

It has been demonstrated that the coefficient, a , is $1/2$ -power for the gas-liquid system and to the $1/3$ -power for the liquid-solid system for creeping flow. Besides, if there is no flow around a solid sphere or even for a bubble system [45],

$$S_h = 2 \quad \text{Eq. (2.26)}$$

2.2.3.1 Higbie Penetration Theory

This theory works well for fluid-fluid interfaces, for instance, gas-liquid or liquid-liquid interface. For this kind of systems is assumed that the mass transfer surface is formed and renewed instantaneously, and transient diffusion of the components occurs. Some examples in which this theory have been applied with success are the gas absorption from rising bubbles into liquids and the absorption by wetted-wall columns [47].

The penetration model is based on in several assumptions,

- There are liquid blocks coming from the liquid bulk to a gas interphase or another phase and these remain attached a period of time, as show in Fig.2.4, during this time transient mass transfer process take places. Because these blocks are thought very small is supposed that diffusion phenomena are more important in comparison with the convective phenomena.
- At the gas-liquid interface is established thermodynamic equilibrium.
- All liquid blocks remain attached at the interface the same period of time [47].

If the more relevant phenomenon is the diffusive one the mass balance for the liquid component of interest, A, can be expressed as,

$$\frac{\partial C_A}{\partial t} = \mathcal{D} \frac{\partial^2 C_A}{\partial x^2} \quad \text{Eq. (2.27)}$$

The solution of the last equation gives the variation on component A concentration with space and time. And it can be solved with an initial condition and the following 2 boundary conditions, As initial condition,

$$t = 0, \quad C_A = C_{A,bulk} \quad \text{Eq. (2.28)}$$

Then, the boundary conditions are set as,

$$x = 0, \quad C_A = C_{A,i} \quad \text{Eq. (2.29)}$$

$$x \rightarrow \infty, \quad C_A = C_{A,bulk} \quad \text{Eq. (2.30)}$$

where, $C_{A,i}$, is "A" concentration at the interface and $C_{A,bulk}$, is "A" concentration at the liquid bulk.

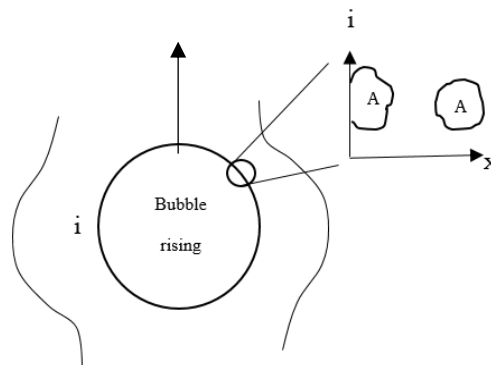


Fig. 2.4: Penetration theory scheme.

The solution for the mass balance equation is,

$$\frac{C_A(x,t) - C_{A,bulk}}{C_{A,i} - C_{A,bulk}} = 1 - \text{erf}\left[\frac{x}{\sqrt{4\mathcal{D}t}}\right] \quad \text{Eq. (2.31)}$$

where the erf(x) is the error function, defined as,

$$\operatorname{erf}[x] = \frac{2}{\sqrt{\pi}} \int_0^x \exp(-x^2) dx \quad \text{Eq. (2.32)}$$

Then, the instantaneous flux of component A is,

$$\bar{J}_A = -D \left. \frac{\partial C_A}{\partial x} \right|_{x=0} = -(C_{Ai} - C_A^{bulk}) \sqrt{\frac{D}{\pi}} t^{-1/2} \quad \text{Eq. (2.33)}$$

After some time, the driving force decreases. To calculate the total flux of component A for the period of time in which this remains attached, called the exposure time by some literature [45], it is necessary to do an average respect this exposure time, τ

$$\bar{J}_A = \frac{1}{\tau} \int_0^\tau -(C_{Ai} - C_A^{bulk}) \sqrt{\frac{D}{\pi}} t^{-1/2} dt \quad \text{Eq. (2.34)}$$

From this integral the result is,

$$\bar{J}_A = -(C_{Ai} - C_A^{bulk}) \sqrt{\frac{4D}{\tau\pi}} \quad \text{Eq. (2.35)}$$

The last expression evidence the mass transfer coefficient, K_c , obtained in the penetration theory,

$$K_c = \sqrt{\frac{4D}{\pi\tau}} \quad \text{Eq. (2.36)}$$

Then for a bubble rising through a liquid phase, the exposure time can be defined as,

$$\tau = \frac{d_b}{U_t} \quad \text{Eq. (2.37)}$$

where, d_b is the bubble size and U_t is the bubble terminal velocity.

2.2.4 Raoult's Law

Considering a system constituted by a liquid phase and a vapor phase, both containing of N chemical species, a condition of vapor/liquid equilibrium can be represented by having the chemical potential of vapor and liquid equal for each component:

$$\mu_i^v = \mu_i^l \quad (i = 1, 2, \dots, N) \quad \text{Eq. (2.38)}$$

If the vapor phase is an ideal gas and the liquid phase is an ideal solution, it is possible to substitute the chemical potential with expressions depending on Gibbs free energy as below,

$$\mu_i^{ig} = G_i^{ig} + RT \ln(y_i) \quad \text{Eq. (2.39)}$$

$$\mu_i^{id} = G_i + RT \ln(x_i) \quad \text{Eq. (2.40)}$$

Matching these last equations,

$$G_i^{ig} + RT \ln(y_i) = G_i + RT \ln(x_i) \quad \text{Eq. (2.41)}$$

Reorganizations gives,

$$RT \ln\left(\frac{y_i}{x_i}\right) = G_i^l(T, P) - G_i^{ig}(T, P) \quad \text{Eq. (2.42)}$$

Here, pure-species properties are assessed at equilibrium temperature, T and pressure, P . Assuming a negligible effect on pressure on G_i^l ,

$$G_i^l(T, P) = G_i^l(T, P_i^{sat}) \quad \text{Eq. (2.43)}$$

where P_i^{sat} is the saturation or vapor pressure of pure species i at temperature T . For pure i as an ideal gas and constant temperature,

$$dG_i^{ig} = V_i^{ig} dP \quad \text{Eq. (2.44)}$$

Integration at temperature T from P to P_i^{sat} yields,

$$G_i^{ig}(T, P_i^{sat}) - G_i^{ig}(T, P) = \int_P^{P_i^{sat}} \frac{RT}{P} dP = RT \ln\left(\frac{P_i^{sat}}{P}\right) \quad \text{Eq. (2.45)}$$

Combining, Eq 3.42, 3.43 and 3.45 results in,

$$RT \ln \left(\frac{y_i}{x_i} \right) = G_i^l(T, P) - G_i^{ig}(T, P_i^{sat}) - RT \ln \left(\frac{P_i^{sat}}{P} \right) \quad \text{Eq. (2.46)}$$

However, the first two terms at the right of last equation are equal at equilibrium conditions, T and P_i^{sat} and the last equation is reduced to the Raoult's Law [48],

$$y_i P = x_i P_i^{sat} \quad (i = 1, 2, \dots, N) \quad \text{Eq. (2.47)}$$

The terms in Raoult's Law are the following, y_i , is the mole fraction of species i in the vapor phase and P is total pressure. Then, x_i , is the liquid-phase mole fraction of species i and P_i^{sat} is its vapor pressure at temperature T .

2.2.5 Normal boiling point

It is defined as the temperature at which vapor pressure of a pure substance in a liquid phase reaches the atmospheric pressure, then it boils [49]. Besides, it is an indicator for the physical state of a chemical compound.

2.2.6 Vapor Pressure

It is the pressure that a vapor of a chemical component exerts in equilibrium with its liquid or solid phase [50]. It is a relative measure of the volatility of a chemical in its pure state [51]. The relation between vapor pressure and temperature is given by the Antoine equation.

2.2.6.1 Antoine's Equation

It is the oldest and simplest empirical equation describing vapor pressure. The change in boiling point with pressure may be calculated by this equation [52]. The equation contains the constants A , B , C , which must be obtained by fitting the equation to the experimental vapor pressure data of every hydrocarbon separately. The use of this equation for all hydrocarbons requires a large data bank for the equation coefficients [51].

$$\ln(P_i^{sat}) = A_i - \frac{B_i}{C_i + T} \quad \text{Eq. (2.48)}$$

Antoine equation has been derived from the Clausius-Clapeyron equation, which is the simplest representation of the vapor pressure-temperature relationship,

$$\frac{d(P_{vap})}{dT} = \frac{\Delta H_{vap}}{T(V_g - V_l)} \quad \text{Eq. (2.49)}$$

where, ΔH_{vap} , is the difference in enthalpy between the saturated liquid and the saturated vapor, or the heat of vaporization, T is the absolute temperature and $(V_g - V_l)$, is the difference between the molar volume of the saturated gas and the saturated liquid [53]: It can be extrapolated for small ranges in temperature, as long as one remains well below the critical temperature [54].

2.2.7 Ideal Gas Law

The ideal gas law was defined through the kinetic molecular theory and it was found by experimental observations. This theory deals with the motion of the molecules of gas. The assumptions of the kinetic molecular theory in order to establish the behavior of the ideal gas were:

-Gas particles are very small and far apart from each other. Most of the volume occupied by a gas consist of empty space.

-The molecules of gas are constantly moving in a random way.

-Gas molecules do not attract or repel each other.

-Gas molecules collide with each other and with the walls of the container, producing the pressure exerted by the gas.

-Collisions of gas molecules are perfectly elastic; no kinetic energy is lost during a collision.

Even when there are no gases following these 5 assumptions perfectly, real gases differ only slightly from the ideal gas behavior. The temperature is an indicator of the motion of this gas molecules [55].

An ideal gas follows a macroscopic behavior represents by Equation of state:

$$PV = nRT \quad \text{Eq. (2.50)}$$

where n denotes moles, P , pressure, V , volume, T , temperature and R , is the ideal gas constant and it is equal to $8.314 \text{ (Pa}\cdot\text{m}^3/\text{mol}\cdot\text{K)}$.

2.3 Heat Transfer

2.3.1 The First Law of Thermodynamics

A formal statement of the first law of the thermodynamics is the following:

“Although energy assumes many forms, the total quantity of energy is constant, and when energy disappears in one form it appears simultaneously in other forms”. [48].

The First Law of Thermodynamics in its most simple form is represented by the following equation:

$$\Delta(\text{energy of the system}) + \Delta(\text{energy of surroundings}) = 0 \quad \text{Eq. (2.51)}$$

$$\Delta(\text{energy of the system}) = \Delta U + \Delta(E_k) + \Delta E_p = \frac{dE_k}{dt} + \frac{dE_p}{dt} + \frac{dU}{dt} \quad \text{Eq. (2.52)}$$

When this Law is applied the space of influence is separated in two parts, the system and its surrounding. The system is taken as the limited zone where the process is developed and the rest out of this zone is called surroundings.

In the thermodynamic sense, heat and work refer to energy in transit across the boundary between the system and the surroundings but they are not ways to store energy. Energy can be just stored in form of kinetic, potential and internal energy forms. Heat and work are the mechanisms for energy transformation and transportation.

A closed system is the one which does not let the transfer of mass between the system and its surroundings, so, the mass is constant. For a closed system all energy passing across the boundaries is through the mechanism of heat and work. Hence, the total energy change of the surroundings equals the net energy transferred to or from it as heat and work [48].

So, for a closed system,

$$\Delta U + \Delta(E_k) + \Delta E_p = \Delta(\text{energy of surroundings}) = \pm Q \pm W \quad \text{Eq. (2.53)}$$

The sign convention for heat, Q , and work, W , is considered as follow,

“Heat given up by the system to the surroundings is counted negative whereas heat absorbed by the system from the surroundings is counted positive” [56].

For work, “The work done on the system by the surroundings is taken as positive whereas the work done on the surroundings by the system is taken as negative” [56].

After the sign convention is fixed, last equation, can be written as,

$$\Delta U + \Delta(E_k) + \Delta E_p = Q - W \quad \text{Eq. (2.54)}$$

Equation 2.54 states that total energy change of the system is equal to the heat added to the system minus the work done by the system [48].

Heat, Q , represents the energy transfer which cause a difference of temperature between the system and the surroundings. Work, like a mechanism of energy transfer can be divided in two parts as shaft work, W_s , when is present a mechanical part in motion in the system, for instance the work executed by a turbine, compressor or pump and Flow work, W_f , executed when system boundary move against pressure, for example, the expansion or compression of the system.

$$W = W_s + W_f \quad \text{Eq. (2.55)}$$

Eq.2.54, could be further reduced when kinetic and potential energy remain unchanged,

$$\Delta U = Q - W \quad \text{Eq. (2.56)}$$

However, Eq. 2.56 is valid for processes including finite changes in the system. Instead for differential changes is valid,

$$dU = dQ - dW \quad \text{Eq. (2.57)}$$

2.3.2 Enthalpy Energy

It is a function of state, related to the internal energy of a system and it is defined when a system increases its volume at constant temperature,

$$H = U + pV \quad \text{Eq. (2.58)}$$

Enthalpy characterizes the heat content of the system [56]. It is possible to obtain the heat change through the following equation,

$$Q = \int_1^2 dH = H_2 - H_1 = U_2 + pV_2 - (U_1 + pV_1) \quad \text{Eq. (2.59)}$$

2.3.2.1 Heat Capacity

It is related to the ability of an object to hold or release heat and its change in temperature when heat is transferred. It is possible to define two kinds of heat capacities which are both state functions. The first one is related to the Internal Energy and it is the heat capacity at constant volume,

$$C_v \equiv \left(\frac{\partial U}{\partial T} \right)_v \quad \text{Eq. (2.60)}$$

The second one is the heat capacity at constant pressure, related to the state function, Enthalpy [48],

$$C_p \equiv \left(\frac{\partial H}{\partial T}\right)_P \quad \text{Eq. (2.61)}$$

Then, these definitions can be useful when processes are carried out in a constant- volume and is possible to write,

$$dU = C_v dT \quad \text{Eq. (2.62)}$$

or in constant- pressure processes where,

$$dH = C_p dT \quad \text{Eq. (2.63)}$$

2.3.2.2 Sensible Heat

The heat transferred to a system which react with a change in temperature. No reaction or phase transition is causing the variation of the temperature in the system.

It is possible to denote the molar or specific enthalpy in terms of 2 state variables for a homogeneous substance of constant composition [48]. Then, enthalpy can be defined as function of temperature and pressure as below,

$$H = H(T, P) \quad \text{Eq. (2.64)}$$

Then its derivative must be in function of both variables,

$$dH = \left(\frac{\partial H}{\partial T}\right)_P dT + \left(\frac{\partial H}{\partial P}\right)_T dP \quad \text{Eq. (2.65)}$$

In this equation the first term was defined before as heat capacity at constant pressure, then,

$$dH = C_p dT + \left(\frac{\partial H}{\partial P}\right)_T dP \quad \text{Eq. (2.66)}$$

The second term could be canceled if the process is developed at constant pressure or when the enthalpy of the substance does not depend on pressure. Then, it is possible to write,

$$dH = C_p dT \quad \text{Eq. (2.67)}$$

and integrating the last equation,

$$\Delta H = \int_{T_1}^{T_2} C_p dT \quad \text{Eq. (2.68)}$$

For a mechanically reversible, constant-pressure, nonflow process, when there is no change potential and kinetic energy and no shaft work, the enthalpy change is equal to heat transferred to the system,

$$Q = \Delta H \quad \text{Eq. (2.69)}$$

The same analysis can be done for the case of molar or specific Internal Energy, so, it can be expressed also as function of temperature and molar or specific volume [48],

$$U = U(T, V) \quad \text{Eq. (2.70)}$$

its derivative becomes,

$$dU = \left(\frac{\partial U}{\partial T}\right)_V dT + \left(\frac{\partial U}{\partial V}\right)_T dV \quad \text{Eq. (2.71)}$$

The is first term is recognized as the heat capacity at constant volume and,

$$dU = C_v dT + \left(\frac{\partial U}{\partial V}\right)_T dV \quad \text{Eq. (2.72)}$$

The second term could be neglected for constant volume processes and when the internal energy does not depend on volume, which is the cases of ideal gases and incompressible fluids. In both cases,

$$dU = C_v dT \quad \text{Eq. (2.73)}$$

And,

$$\Delta U = \int_{T_1}^{T_2} C_v dT \quad \text{Eq. (2.74)}$$

In order to solve Equation 2.70 and 2.74 it is necessary to have a mathematical relationship between heat capacities and temperature.

2.3.2.3 Latent heat

It is the heat associated to a pure substance phase transition. A phase transition, for instance, evaporation or liquefaction, are processes carried out at constant temperature and pressure. The intensive state of a two-phase system characterized by a single component can be specified by one intensive property [48]. As a result, latent heat associated to a phase change is function on temperature only and it can be expressed through the Clapeyron thermodynamic equation:

$$\Delta H = T \Delta V \frac{dP^{sat}}{dT} \quad \text{Eq. (2.75)}$$

Here, ΔH , is the latent heat, ΔV , is the volume change accompanying the phase change and P^{sat} , is the vapor pressure. For a process of vaporization, ΔH , is called, Latent Heat of Vaporization [48].

2.3.3 Heat transfer coefficient

It is a proportionality factor defined in a flow system where there is a difference of temperature and it causes a heat flux across a characteristic interface area in the system. It characterizes the heat transfer efficiency in the system [45]. For example, the rate of heat flow through a solid interface can be written as,

$$Q = h A \Delta T \quad \text{Eq. (2.76)}$$

where Q is the heat flow into the fluid (J/hr), A is a characteristic area and ΔT , is the temperature difference. It is possible to estimate h just after the characteristic area and the temperature difference are established. h usually has units (W/m². K) or (kcal/ m².hr.C).

Then there are some dimensionless numbers related to the heat transfer coefficient, the Prandtl and the Nusselt dimensionless number.

Prandtl is similar to the Schmidt number for mass transfer, “*it represents the ratio of the momentum diffusivity to the thermal diffusivity*” [45],

$$Pr = \frac{\nu}{\alpha} \quad \text{Eq. (2.77)}$$

And the Nusselt number, or the dimensionless heat transfer coefficient number is defined as,

$$Nu = \frac{hD}{k} \quad \text{Eq. (2.78)}$$

where h symbolizes the heat transfer coefficient, D is a characteristic length and k , the thermal conductivity.

This dimensionless number can be written in function of other dimensionless number as the Prandtl and Reynolds numbers. Furthermore, for many common systems experimental relationships for the Nusselt number have been proposed in function of Re and Pr numbers which let evaluate the heat transfer coefficient.

In general, the Nusselt number is formulated as below,

$$Nu = cost. Pr^a Re^b \quad \text{Eq. (2.79)}$$

2.3.3.1 Sherwood and Nusselt analogy

The definition of mass and heat transfer coefficients and the different dimensionless groups appearing in the developing of these processes through mathematical models have shown several similarities contained in the equations.

These parallels, for instance between Prandtl and Schmidt number and between Nusselt and Sherwood dimensionless coefficients numbers, have let since many years ago, solve many mass transfer issues by means of solved heat transfer problems or vice versa [45]. Based on this concept was developed and analogy between mass and heat transfer.

This analogy is very important because sometimes mass and heat transfer processes can occur simultaneously, and its effect must be also assessed at the same time.

Chapter 3

Modeling

3.1 Bubble Formation

The slurry reactor is the general medium in which the considered bubble formation process is developed. The zone inside these reactors where this process really begins is the sparger zone. Spargers or gas distributors are basically perforated pipes located at the bottom of the reactor in which orifices represent the opening area for the gas entering in form of bubbles to the reactor. However, the zone of interest to be modeled in this thesis project is a zone of the sparger just above one of these orifices without take in account the presence of others holes around and the possible interaction between bubbles formed in the surrounding.

The model to be proposed in this work will be separated in two stage. Bubbles created by means of the orifice are assumed to have spherical shape. The methodology to determine the bubble dimension is similar to the work done by Geary and Rice et.al. [26].

3.1.1 First Stage

The first stage will represent the initial exit of the gas flow stream through the orifice being studied with a characteristic radius identified with the symbology, " r_H ". Initially, at time t_0 , it will be created a kind of hemisphere bubble cap up to the moment in which a perfect spherical bubble is formed but its base is still completely connected to the hole area as illustrated in Fig. 3.5. This stage will end just in the moment in which bubble base start rising at time, t_d .



Fig. 3.5: Model first stage scheme.

During the first stage the bubble increases its radius, that is, it only expands. Locating a vertical axis, " y ", with origin at the orifice base and passing through the bubble center of mass. The final radius at the end of this stage was called expansion radius, " r_d " and this time it coincides with the position of the bubble center of mass.

For the determination of the radius at the end of this stage is employed a balance of forces containing the forces which are considered to influence the bubble expansion. The forces considered in this work are presented below.

The Buoyancy Force is a force existing due to the submergence of the bubble in a liquid inside the reactor as mentioned in section 2.1.6. The bubble is replacing a volume of liquid and the force is equal to the weight of liquid replaced. The force can be written as in Eq.3.80,

$$F_b = V_b \rho_L g = \frac{4\pi}{3} r^3 \rho_L g \quad \text{Eq. (3.80)}$$

where, “ V_b ” is the bubble volume, ρ_L , is the liquid density and “ r ” is the bubble radius at time t . This buoyancy force is positive in the vertical direction, that is, with vertical axis, y .

Then, another force which pushes the bubble upward and causes its growing is commonly named “gas momentum force” and it can be written in function of the gas flow rate and hole area,

$$F_m = \frac{G^2 \rho_g}{\pi r_H^2} \quad \text{Eq. (3.81)}$$

where, G is the gas flow rate, ρ_g is the gas density.

The surface tension force is a force which retains the bubble attached to the orifice; it depends strongly on the fluids involve and on the molecular strength of the bonds. It is expressed as,

$$F_s = 2\pi\sigma r_H \sin\theta = 2\pi\sigma r_H \quad \text{Eq. (3.82)}$$

where, σ is the interfacial tension, in the case of an air-water system and θ is the contact angle between the phases and it will be considered in this work equal to 90° because it is assumed that the bubble formed in this first stage is created instantaneously, that is, very fast and it is a consequence of high gas flow rate and pressure.

A term in the force balance must take into account the difference of pressure between the gas phase coming from a gas chamber or a compressor and the liquid inside the reactor. This force depends strongly in the orifice geometry and pressure drop through it. It can be considered as a force which increases bubble expansion and it can be written as,

$$F_P = \pi r_h^2 (p_g - p_L) \quad \text{Eq. (3.83)}$$

The difference on pressure between the gas and the liquid can be calculated through equations developed in flow through orifices. According to [40] the difference of pressure can be calculated with Eq. 3.84

$$(p_g - p_L) = \frac{1}{C_0^2} \frac{16\rho_g G^2}{\pi^2 d_h^4} = \frac{1}{C_0^2} \frac{\rho_g G^2}{\pi^2 r_h^4} \quad \text{Eq. (3.84)}$$

where, d_h is the hole diameter and C_0 , is a discharge coefficient determined experimentally through the work done by Lichtarowicz [44].

Then, the bubble inertia force is a bubble resisting force to motion due to the mass of the bubble and it is written as,

$$F_I = \frac{d}{dt} ((\rho_g + \alpha\rho_L)V_b U_b) \quad \text{Eq. (3.85)}$$

where, U_b , is the bubble velocity and V_b is the bubble volume. Besides, this term takes in account the bubble mass and the virtual mass which is calculated through a coefficient called added mass coefficient α , which is found to have a value 11/16 in this kind of balance of forces [23].

The gravitational force is a negative force according the reference axis, “ y ” and for the gas bubble emerging from the orifice can be expressed as,

$$F_g = V_b \rho_g g \quad \text{Eq. (3.86)}$$

where g is the acceleration due to gravity. It will be considered a constant in this study equal to 9.81 m/s^2 .

Finally, the last force taken in account in the first stage was the drag force, which pulls the bubble downward, and it is expressed as,

$$F_D = \left(\frac{1}{2}\right) C_D A_b \rho_L (U_b)^2 \quad \text{Eq. (3.87)}$$

where, C_D , is the drag coefficient and it can be found to vary sometimes according dimensionless number bubble Reynolds number. First, bubble Reynolds number will be defined as,

$$Re = \frac{\rho_L U_b d}{\mu_L} \quad \text{Eq. (3.88)}$$

where d , is the bubble diameter and μ_L is the liquid viscosity.

Then, correlations for drag coefficient have been proposed by several authors in the case of bubble formation and those are expressed below,

$$C_D = \frac{18.5}{Re_B^{0.6}} \quad \text{for } 2 \leq Re_B \leq 500, \text{ according [23]} \quad \text{Eq. (3.89)}$$

$$C_D = \frac{10}{Re_B^{0.5}} \quad \text{for } 1 \leq Re_B \leq 500, \text{ according [57]} \quad \text{Eq. (3.90)}$$

$$C_D = 0.44 \quad \text{for and } Re_B > 500, \text{ according [23]} \quad \text{Eq. (3.91)}$$

$$C_D = \max\left[\frac{24}{Re_B} (1 + 0.15 Re_B^{0.687}), \frac{8}{3} \frac{Eo}{Eo+4}\right] \text{ according [58]} \quad \text{Eq. (3.92)}$$

Drag coefficients to be evaluated in this work will be Eq.3.89, Eq.3.90 and Eq.3.92. Eq.3.89 and Eq. 3.90 have been used before in works related to bubble size determination, [40,57]. In contrast Eq.3.92 have used in a work, [58], where bubbles are rising in contaminated water as liquid phase system; this system is considered similar to the liquid suspension inside the reactor and could be appropriate for the model.

At constant gas flow rate conditions, the bubble volume is

$$V_b = Gt \quad \text{Eq. (3.93)}$$

where G is the gas flow rate, V_b is the bubble volume and considering a spherical shape as written before,

$$\frac{4}{3} \pi r^3 = Gt \quad \text{Eq. (3.94)}$$

The derivative of Eq. 3.94 with time is,

$$\frac{dV}{dt} = 4\pi r^2 \frac{dr}{dt} = G \quad \text{Eq. (3.95)}$$

As the first stage is considered as an expansion stage, the bubble velocity, U_b , is associated to the change in radius with time,

$$U_b = \frac{dr}{dt} = \frac{G}{4\pi r^2} \quad \text{Eq. (3.96)}$$

Then, the bubble acceleration will be,

$$\frac{dU_b}{dt} = \frac{d}{dt} \left(\frac{G}{4\pi r^2} \right) = \frac{G}{4\pi} (-2)r^{-3} \frac{dr}{dt} = \frac{G}{4\pi} (-2)r^{-3} \frac{G}{4\pi r^2} = \frac{-2G^2}{(4\pi)^2 r^5} \quad \text{Eq. (3.97)}$$

The drag force which include the bubble velocity can be rearranged as,

$$F_D = \left(\frac{1}{2}\right) * C_D * \pi r_h^2 * \rho_L \left(\frac{G}{4\pi r^2}\right)^2 \quad \text{Eq. (3.98)}$$

Additionally, the inertia force is another force containing the bubble velocity,

$$F_I = \frac{d}{dt} ((\rho_g + \alpha\rho_L) \frac{4}{3} \pi r^3 \frac{G}{4\pi r^2}) \quad \text{Eq. (3.99)}$$

Eventually, it is possible to write the balance of forces of this first stage for the bubble formation. To the right side will be placed the forces which pull the bubble downward and to the left side of the balance will be located the forces which push the bubble upward,

$$F_b + F_m + F_P = F_I + F_g + F_S + F_D \quad \text{Eq. (3.100)}$$

that is, in a general form,

$$V_b \rho_L g + \frac{G^2 \rho_g}{\pi r_H^2} + \pi r_h^2 (p_g - p_L) = \frac{d}{dt} ((\rho_g + \alpha\rho_L) V_b U_b) + V_b \rho_g g + 2\pi\sigma r_H + \frac{1}{2} C_D \pi r^2 \rho_L (U_b)^2 \quad \text{Eq. (3.101)}$$

Eq. 3.101 can be further developed, for instance, the inertia and difference of pressure term,

$$V_b (\rho_L - \rho_g) g + \frac{G^2 \rho_g}{\pi r_H^2} + \frac{1}{c_0^2} \frac{\rho_g G^2}{\pi r_h^2} = (\rho_g + \alpha\rho_L) \left(\frac{dV}{dt} U_b + V_b \frac{dU_b}{dt} \right) + 2\pi\sigma r_H + \frac{1}{2} C_D \pi r^2 \rho_L \left(\frac{G}{4\pi r^2} \right)^2 \quad \text{Eq. (3.102)}$$

As in this stage was assumed that bubble just expands, the bubble velocity can be written as the change of the radius with time and can be correlated with the gas flow rate through the orifice as shown in Eq. 3.96.

Then, in Eq. 3.102, it is possible substitute the bubble velocity, U_b , in function of the gas flow rate, G and bubble radius, r .

$$V_b (\rho_L - \rho_g) g + \frac{G^2 \rho_g}{\pi r_H^2} \left(1 + \frac{1}{c_0^2}\right) = (\rho_g + \alpha\rho_L) \left(G * \frac{G}{4\pi r^2} + \frac{4\pi}{3} r^3 * \frac{-2G^2}{(4\pi)^2 r^5} \right) + 2\pi\sigma r_H + \frac{1}{2} C_D \pi r^2 \rho_L \left(\frac{G}{4\pi r^2} \right)^2 \quad \text{Eq. (3.103)}$$

It is possible to reorganize Eq. 3.103 to get a final equation in function of an only variable; this variable could be the bubble volume, the bubble diameter or the bubble radius.

$$\frac{4\pi}{3} r^3 (\rho_L - \rho_g) g + \frac{G^2 \rho_g}{\pi r_H^2} \left(1 + \frac{1}{c_0^2}\right) - 2\pi\sigma r_H - \frac{1}{2} C_D \pi r^2 \rho_L \left(\frac{G}{4\pi r^2} \right)^2 = \frac{(\rho_g + \alpha\rho_L) G^2}{12\pi r^2} \quad \text{Eq. (3.104)}$$

Eq. 3.104 was obtained changing the bubble volume and velocity in function of bubble radius. Besides, the second and third term to the left side of Eq. 3.104 are constants.

It is possible to obtain a solution for Eq. 3.104 taking the term in the right side and passing it to the left to obtain an equation function of one variable equal to zero.

$$\frac{4\pi}{3} r^3 (\rho_L - \rho_g) g + \frac{G^2 \rho_g}{\pi r_H^2} \left(1 + \frac{1}{c_0^2}\right) - 2\pi\sigma r_H - \frac{1}{2} C_D \pi r^2 \rho_L \left(\frac{G}{4\pi r^2} \right)^2 - \frac{(\rho_g + \alpha\rho_L) G^2}{12\pi r^2} = 0 \quad \text{Eq. (3.105)}$$

Eq.3.105 is a non-linear equation solved iteratively through the bisection numerical method to fine the value bubble radius for which this equation is equal to zero. The drag coefficient used for this first stage is the one presented in Eq.3.89. The methodology of determination of Eq. 3.105 will be explained in chapter 4. The bubble radius determined with Eq.3.105 is taken as the bubble radius at the end of the first stage, r_d , just expansion.

3.1.2 Second Stage

There is a moment during the bubble formation process in which the bubble expansion is maximum and the bubble base is completely connected to the sparger orifice, that is the end of the previous stage. Now a second stage starts, where the bubble continues to expand and additionally, it starts to lift. The bubble rises but still there is a connection between the bubble and the orifice, a kind of neck as shown in Figure 3.6. While bubble is growing and rising in the second stage the gas neck becomes thinner.

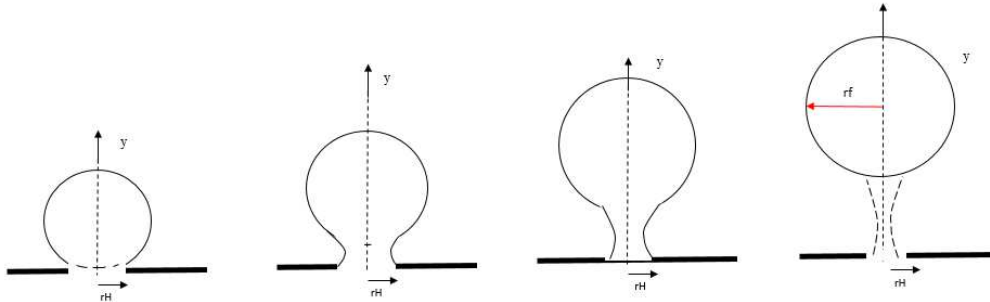


Fig.3.6: Second Stage scheme for the Bubble formation process.

The moment in which the bubble is released is called, “*detachment time*” and it occurs when the neck of gas connecting the bubble to the gas distributor closes.

The model proposed for this stage is again based on the balance of forces acting on the bubble in second stage. The same forces considered in the first stage will be considered in the second one. However, all the forces are required to be rewritten to take in account the new configuration, including the neck. Besides, it is essential to consider the simultaneous bubble growth and lifting.

Using the same vertical axis of first stage, y , it is assumed that while bubble is rising its center of mass is always positioned on this axis because there is no horizontal liquid flow which deviate the bubble in a horizontal direction at least in the sparger zone in which this work has been focused.

This second stage will start at the end of the first stage where the center of mass is located in the vertical axis exactly at a distance equal to the radius found in the first stage, r_d , as illustrated in Fig.3.7.

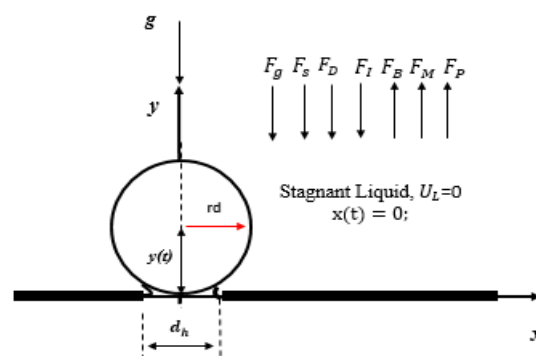


Fig.3.7: Bubble initial condition for the second stage.

The forces considered in this second stage will be exposed afterward. Now, the position of the center of mass will be indicated with the symbology “ y ” and it will vary with time. Then, the bubble velocity is expressed as,

$$U_b = \frac{dy}{dt} \quad \text{Eq. (3.106)}$$

and the bubble acceleration, “ a_b ” will be expressed as,

$$a_b = \frac{d^2y}{dt^2} = \frac{dU_b}{dt} \quad \text{Eq. (3.107)}$$

The bubble volume will depend on time and it will be expressed in function of the gas flow rate, “ G ”, and the initial bubble volume at the first stage, V_d , as in Eq.3.108,

$$V_b(t) = Gt + V_d = Gt + \frac{4}{3}\pi r_d^3 \quad \text{Eq. (3.108)}$$

where, V_d is the bubble volume at the end of the first stage characterized by a radius, r_d . Then the bubble volume in the second stage is characterized by a diameter, “ d ”,

$$d(t) = \left(\frac{6V_b}{\pi}\right)^{1/3} = \left[\frac{6}{\pi}\left(Gt + \frac{4}{3}\pi r_d^3\right)\right]^{1/3} \quad \text{Eq. (3.109)}$$

Now, it is possible to show the forces taken into account for the balance in this second stage in the vertical direction.

Buoyancy can be expressed as the weight of the liquid replaced by the bubble,

$$F_b = V_b \rho_L g = \left(Gt + \frac{4}{3}\pi r_d^3\right) \rho_L g \quad \text{Eq. (3.110)}$$

Gas momentum force is still present in this stage and it causes the bubble growing and lifting. It can be written as,

$$F_M = \frac{4\rho_g G^2}{\pi d_h^2} \quad \text{Eq. (3.111)}$$

where, d_h is the hole diameter.

Pressure force is the term considering again the difference of pressure between the gas and liquid phase,

$$F_P = \frac{\pi}{4} d_h^2 (p_g - p_L) = \frac{1}{c_0^2} \frac{4\rho_g G^2}{\pi d_h^2} \quad \text{Eq. (3.112)}$$

The surface tension is considered as,

$$F_S = \pi \sigma d_h \sin\theta \quad \text{Eq. (3.113)}$$

where, θ is the contact angle and it is assumed to be 90° because the existence of the bubble neck.

The drag force is considered to be,

$$F_D = \left(\frac{1}{2}\right) C_D A_b \rho_L (U_b)^2 = \frac{\pi}{4} d^2 C_D \frac{\rho_L}{2} \left(\frac{dy}{dt}\right)^2 \quad \text{Eq. (3.114)}$$

where C_D is the drag coefficient and it will be considered as in Eq.3.89.

Then, the inertia term is written as,

$$F_I = \frac{d}{dt} \left[(\rho_g + \alpha \rho_L) V_b \frac{dy}{dt} \right] \quad \text{Eq. (3.115)}$$

developing the derivative product in Eq.3.115 are produced two terms for the inertia force,

$$F_I = (\rho_g + \alpha\rho_L)G \frac{dy}{dt} + (\rho_g + \alpha\rho_L)V_b \frac{d^2y}{dt^2} \quad \text{Eq. (3.116)}$$

The last force to be set is the gravitational force as the weight of the bubbles,

$$F_g = V_b\rho_g g \quad \text{Eq. (3.117)}$$

Finally, the balance of forces can be set as,

$$F_b + F_m + F_P = F_I + F_g + F_s + F_D \quad \text{Eq. (3.118)}$$

and replacing each force by the expressions written before,

$$V_b\rho_L g + \frac{4\rho_g G^2}{\pi d_h^2} + \frac{\pi}{4} d_h^2 (p_g - p_L) = (\rho_g + \alpha\rho_L)G \frac{dy}{dt} + (\rho_g + \alpha\rho_L)V_b \frac{d^2y}{dt^2} + \frac{\pi}{4} d^2 C_D \frac{\rho_L}{2} \left(\frac{dy}{dt}\right)^2 + V_b\rho_g g + \pi d_h \quad \text{Eq. (3.119)}$$

by rearranging the terms is possible to obtain an equation for the bubble acceleration,

$$\frac{d^2y}{dt^2} = \frac{1}{(\rho_g + \alpha\rho_L)V_b} [V_b(\rho_L - \rho_g)g + \frac{4\rho_g G^2}{\pi d_h^2} + \frac{\pi}{4} d_h^2 \frac{1}{c_0^2} \frac{\rho_g G^2}{\pi^2 r_h^4} - (\rho_g + \alpha\rho_L)G \frac{dy}{dt} - \frac{\pi}{4} d^2 C_D \frac{\rho_L}{2} \left(\frac{dy}{dt}\right)^2 - \pi \sigma d_h] \quad \text{Eq. (3.120)}$$

Eq.3.120 can be ready for the calculations if bubble volume is substituted by Eq. 3.108, and the bubble diameter by Eq. 3.109 as,

$$\frac{d^2y}{dt^2} = \frac{1}{(\rho_g + \alpha\rho_L)(Gt + \frac{4}{3}\pi r_d^3)} \left[-(\rho_g + \alpha\rho_L)G \left(\frac{dy}{dt}\right) - \left(\frac{6}{\pi} \left(Gt + \frac{4}{3}\pi r_d^3\right)\right)^{2/3} \frac{\pi}{4} C_D \frac{\rho_L}{2} \left(\frac{dy}{dt}\right)^2 + \frac{4\rho_g G^2}{\pi d_h^2} \left(1 + \frac{1}{c_0^2}\right) + \left(Gt + \frac{4}{3}\pi r_d^3\right)(\rho_L - \rho_g)g - \pi \sigma d_h \right] \quad \text{Eq. (3.121)}$$

Eq. 3.121 is a time dependent second order differential equation.

Then, a system of first order differential equations is proposed to be solved with the fourth-order Runge-Kutta method. The first equation is the derivative of the bubble center of mass position as,

$$\frac{dy}{dt} = U_b \quad \text{Eq. (3.122)}$$

and the second equation is the derivative of the velocity, that is the acceleration,

$$\frac{dU_b}{dt} = \frac{1}{(\rho_g + \alpha\rho_L)(Gt + \frac{4}{3}\pi r_d^3)} \left[-(\rho_g + \alpha\rho_L)G \left(\frac{dy}{dt}\right) - \left(\frac{6}{\pi} \left(Gt + \frac{4}{3}\pi r_d^3\right)\right)^{2/3} \frac{\pi}{4} C_D \frac{\rho_L}{2} \left(\frac{dy}{dt}\right)^2 + \frac{4\rho_g G^2}{\pi d_h^2} \left(1 + \frac{1}{c_0^2}\right) + \left(Gt + \frac{4}{3}\pi r_d^3\right)(\rho_L - \rho_g)g - \pi \sigma d_H \right] \quad \text{Eq. (3.123)}$$

For the bubble formation model presented in this section, section 3.1.2, the drag coefficient, C_D , used in Eq.3.123 will be the one expressed in Eq.3.89. However, for the evaluation of bubble dimension after detachment as in section 3.2.1, Eq.123 will be used to obtain the initial conditions at the moment of detachment but using the drag coefficient, C_D in Eq.3.92.

For Eq. 3.122, the initial condition is,

$$t = 0, y(t = 0) = r_d = \text{first stage bubble radius} \quad \text{Eq. (3.124)}$$

Then for Eq. 3.123 the initial condition is,

$$t = 0, U_b(t = 0) = 0 \quad \text{Eq. (3.125)}$$

The result of the first order differential equation system proposed above is the variation of the position and the velocity with time. However, the aim of this second stage is to find the bubble dimension and velocity at the moment of detachment, that is, when the bubble releases from the gas distributor.

It is required to introduce a detachment criterion and according [57] the criterion is related to the length of the neck connecting the bubble to the sparger. Similar works [23, 57] argued about which is the length of the neck at the moment of detachment and it is mentioned that this length, measured in the vertical direction, could be once or twice the hole radius.

For this work the detachment criterion adopted is when the neck length is two times the hole radius, $2r_H$, as in the work developed by Geary and Rice et.al. [57]. Afterwards the criterion is set, it must be related to the system of differential equations obtained above.

The position of the center of mass, $y(t)$, is related to the length of the neck connecting the bubble to the gas distributor as shown in figure 3.8.

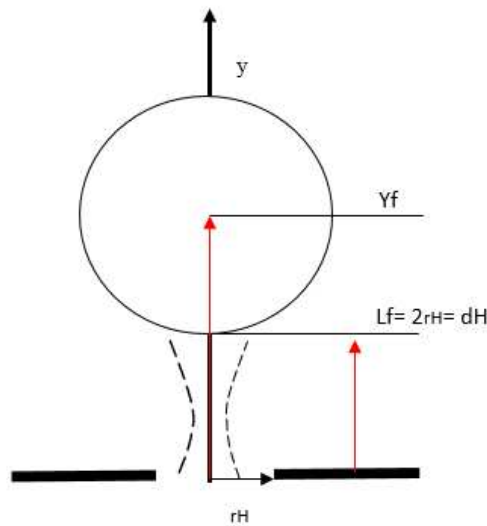


Fig.3.8: Detachment criterion scheme.

The final position of the center of mass at the detachment moment, “ y_f ”, is related to the neck length and to the final bubble radius, r_f , as,

$$y_f(t) = L_f + r_f(t) \quad \text{Eq. (3.126)}$$

where “ L_f ” is the neck length and “ r_f ” is the bubble final radius when the bubble is released from the sparger at detachment time, t_f .

Then, the detachment criterion is set as,

$$y_f(t) \geq 2r_H + r_f \quad \text{Eq. (3.127)}$$

So, the bubble will detach at the moment in which the length neck is twice the hole radius and the bubble has a final dimension equal to r_f .

3.1.3 Sensitivity Analysis

In this section the objective is to evaluate the influence of each term inside the balances of forces developed in the section 3.1.1 on the final bubble dimension.

The rationale of this section will consist to propose a simple but elementary balance of forces acting on the bubble during its formation for the first. Afterward, to these elementary balances of forces it will be added the rest of terms one by one to assess its impact in the model outcome.

For the second stage all the forces are taken in account because all these forces are considered important in this work.

In the First Stage will be considered as elementary forces: Buoyancy, Gas Momentum, Surface Tension, Drag and Inertia. The general balance of forces will be expressed as,

$$F_b + F_m = F_I + F_s + F_D \quad \text{Eq. (3.128)}$$

The main differences of Eq.3.128 with the balance of forces for the first stage in Eq.3.105 are gravitational force, that is, the bubble weight is not considered here, pressure difference term which means that the pressure drop through the hole is not considered, the drag force expression is changed as in Eq.3.90 and finally, the inertia term does not take in account the bubble mass as in Eq.3.129.

$$F_I = \frac{d}{dt}(\alpha\rho_L V_b U_b) \quad \text{Eq. (3.129)}$$

The elementary force in Eq.3.128 is the one proposed by N. Geary and R. Rice et al. [26]. However, this elementary force in this work will be assed at higher gas flow rate values and for industrial conditions of pressure and temperature. Furthermore, it will be used the elementary force proposed just for the first expansion stage.

Then, it is substituted the definition of each force as done in the first stage, the result is

$$V_b \rho_L g + \frac{G^2 \rho_g}{\pi r_H^2} = \frac{d}{dt}(\alpha\rho_L V_b U_b) + 2\pi\sigma r_H + F_D \quad \text{Eq. (3.130)}$$

The drag coefficient will set as in Eq.3.90 and the bubble velocity and volume are substituted by Eq. 3.96 and Eq. 3.94. Then the balance of forces result is,

$$\frac{4\pi}{3} r^3 \rho_L g + \frac{G^2 \rho_g}{\pi r_H^2} - 2\pi\sigma r_H - 5\pi \sqrt{\frac{\rho_L \mu}{2}} \left(\frac{G}{4\pi r}\right)^{3/2} = \alpha\rho_L \left(\frac{dV}{dt} U_b + V_b \frac{dU_b}{dt}\right) \quad \text{Eq. (3.131)}$$

Finally, rearranging the terms, passing all of them to the left side and leaving as only variable the bubble volume to be find, the equation becomes,

$$V_b \rho_L g + \frac{\rho_g}{\pi r_H^2} G^2 - 2\pi\sigma r_H - \frac{5}{4} \sqrt{\frac{\rho_L \mu}{6}} (G)^{3/2} \frac{1}{\sqrt{V_b}} - \frac{\alpha\rho_L}{12\pi} \left(\frac{4\pi}{3}\right)^{2/3} G^2 \left(\frac{1}{V_b}\right)^{2/3} = 0 \quad \text{Eq. (3.132)}$$

Eq. 3.132 represents a non-linear equation for the determination of the bubble volume at the end of the first stage, V_d , and it will be solved iteratively through the Bisection Method. Eq.3.132 will be identified in the next sections as “**Original Model 1**”.

Then, to the elementary force expressed in Equation 3.128, will be added now the bubble weight and the mass bubble will be taken in account in the inertia term, to obtain the following balance of forces

$$F_b + F_m = F_I + F_s + F_D + F_g \quad \text{Eq. (3.133)}$$

Then substituting the definition of each force as done in the first stage, the result is

$$V_b \rho_L g + \frac{G^2 \rho_g}{\pi r_H^2} = \frac{d}{dt} ((\rho_g + \alpha \rho_L) V_b U_b) + 2\pi \sigma r_H + F_D + V_b \rho_g g \quad \text{Eq. (3.134)}$$

The final balance of forces after the substitution of the drag force by Eq.3.90 is

$$V_b (\rho_L - \rho_g) g + \frac{\rho_g}{\pi r_H^2} G^2 - 2\pi \sigma r_H - \frac{5}{4} \sqrt{\frac{\rho_L \mu}{6}} (G)^{3/2} \frac{1}{\sqrt{V_b}} - \frac{(\alpha \rho_L + \rho_g)}{12\pi} \left(\frac{4\pi}{3}\right)^{2/3} G^2 \left(\frac{1}{V_b}\right)^{2/3} = 0 \quad \text{Eq. (3.135)}$$

Eq. 3.135 represents again a non-linear equation for the determination V_d , and it will be solved iteratively through the Bisection Method. Eq.3.135 will be identified in the next sections as “**Rhog Model**”.

Afterwards, it is added the pressure force to the balance of forces in Eq.3.133,

$$F_b + F_m + F_p = F_l + F_s + F_D + F_g \quad \text{Eq. (3.136)}$$

substituting the definitions of all the forces and the drag force in Eq.3.90

$$V_b \rho_L g + \frac{G^2 \rho_g}{\pi r_H^2} + \frac{\pi}{4} d_H^2 (p_g - p_L) = \frac{d}{dt} ((\rho_g + \alpha \rho_L) V_b U_b) + 2\pi \sigma r_H + 5\pi \sqrt{\frac{\rho_L \mu}{2}} \left(\frac{G}{4\pi r}\right)^{3/2} + V_b \rho_g g \quad \text{Eq. (3.137)}$$

Then, the final equation to be solved is

$$V_b (\rho_L - \rho_g) g - \frac{5}{4} \sqrt{\frac{\rho_L \mu}{6}} G^{3/2} (V_b)^{-1/2} - \frac{(\rho_g + \alpha \rho_L) G^2}{12\pi} \left(\frac{4\pi}{3}\right)^{2/3} (V_b)^{-2/3} + \frac{\rho_g G^2}{\pi r_H^2} \left(1 + \frac{1}{Co^2}\right) - 2\pi \sigma r_H = 0 \quad \text{Eq. (3.138)}$$

Eq.3.138 is again a non-linear equation used to calculate the bubble volume due to expansion in the first stage. Eq. 3.138 is solved by the Bisection Method and will be identified in the next sections as “**Pressure Model**”.

Additionally, in this sensitivity analysis can be assessed the effect of choosing different drag coefficient relationships.

For this evaluation will be used the balance containing all the forces proposed for Stage 1 in section 3.1.1 with different drag coefficient expressions. The drag coefficient to be evaluated will be Eq.3.89 and Eq.3.92 for fully contaminated liquid.

The balance of forces to be solved will be,

$$(\rho_L - \rho_g) g + \frac{G^2 \rho_g}{\pi r_H^2} - 2\pi \sigma r_H + \frac{\pi}{4} d_H^2 (p_g - p_L) - F_D = \frac{d}{dt} ((\rho_g + \alpha \rho_L) V_b U_b) \quad \text{Eq. (3.139)}$$

then, replacing the drag force with Eq. 3.89 and difference of pressure force,

$$\frac{4\pi}{3} r^3 (\rho_L - \rho_g) g + \frac{G^2 \rho_g}{\pi r_H^2} + \frac{1}{Co^2} \frac{G^2 \rho_g}{\pi r_H^2} - 2\pi \sigma r_H - (\mu_L)^{0.6} \frac{18.5}{23.2} \left(\frac{\rho_L}{\pi}\right)^{0.4} \left(\frac{G}{r}\right)^{1.4} = (\rho_g + \alpha \rho_L) \left(\frac{dV}{dt} U_b + V_b \frac{dU_b}{dt}\right) \quad \text{Eq. (3.140)}$$

After the proper arrangements, the non-linear equation to be solved is

$$V_b (\rho_L - \rho_g) g + \frac{G^2 \rho_g}{\pi r_H^2} \left(1 + \frac{1}{Co^2}\right) - 2\pi \sigma r_H - (\mu_L)^{0.6} \frac{18.5}{23.2} \left(\frac{4\pi}{3}\right)^{1.4} \left(\frac{\rho_L}{\pi}\right)^{0.4} V_b^{-1.4/3} (G)^{1.4} - \frac{(\rho_g + \alpha \rho_L) G^2}{12\pi} \left(\frac{4\pi}{3}\right)^{2/3} V_b^{-2/3} = 0 \quad \text{Eq. (3.141)}$$

Eq. 3.141 is solved iteratively through the Bisection method to obtain the bubble volume at the end of the first stage, V_d . Eq.3.141 will be identified in the next sections as “**Drag Model**”.

The second assessment for the drag force will be drag coefficient by [47],

$$C_D = \max\left[\frac{24}{Re_B} \left(1 + 0.15 Re_B^{0.687}\right), \frac{8}{3} \frac{Eo}{Eo+4}\right] \quad \text{Eq. (3.142)}$$

where, Re_B is the bubble Reynolds number, and E_o is the Eötvös number which is defined as,

$$E_o = \left[\frac{d^2 g (\rho_L - \rho_g)}{\sigma} \right] \quad \text{Eq. (3.143)}$$

where σ is the interfacial tension.

Then, the balance of forces will be,

$$V_b(\rho_L - \rho_g)g + \frac{G^2 \rho_g}{\pi r_H^2} - 2\pi\sigma r_H + \frac{\pi}{4} d_0^2 (p_g - p_L) - \left(\frac{\rho_L}{2}\right) \max\left[\frac{24}{Re_B} \left(1 + 0.15 Re_B^{0.687}\right), \frac{8}{3} \frac{E_o}{E_o + 4}\right] \pi r^2 \left(\frac{G}{4\pi r^2}\right)^2 = \frac{d}{dt} ((\rho_g + \alpha \rho_L) V_b U_b) \quad \text{Eq. (3.144)}$$

Eq.3.144 will result again in a non-linear equation solved by the Bisection Method with an outcome of the bubble volume or the equivalent bubble radius at the end of the first stage. The outcome of Eq.3.144 will be identified later as “**Drag Model 132**” and it will be used to obtain the results of the position of the bubble center of mass at the end of the first stage inside the combined model presented in the next section, section 3.2.

In conclusion Table 3.1 shows the specific equation numbers of each force used inside the balance of forces for each model in section 3.1.3.

Table 3.1: Models developed in section 3.1.3.

Model	F_b	F_m	F_p	F_I	F_D	F_S	F_g
Original Model 1	Eq.3.80	Eq.3.81	-	Eq.3.129	Eq.3.90	Eq.3.82	-
Rhog Model	Eq.3.80	Eq.3.81	-	Eq.3.85	Eq.3.90	Eq.3.82	Eq.3.86
Pressure Model	Eq.3.80	Eq.3.81	Eq.3.83 & Eq.3.84	Eq.3.85	Eq.3.90	Eq.3.82	Eq.3.86
Drag Model	Eq.3.80	Eq.3.81	Eq.3.83 & Eq.3.84	Eq.3.85	Eq.3.89	Eq.3.82	Eq.3.86
Drag Model 132	Eq.3.80	Eq.3.81	Eq.3.83 & Eq.3.84	Eq.3.85	Eq.3.92	Eq.3.82	Eq.3.86

3.2 Momentum, Heat and Mass Transfer Model

In this section the system described correspond to the bubble motion, heat and mass transfer after detachment. The initial instant for which this model is developed is at the end of the second stage established in section 3.1.2, that is, the detachment time. So, the bubble at the initial time of this model will have an initial position, diameter, velocity, temperature and molar concentration corresponding to the detachment time.

The system is constituted by a bubble rising freely with an initial temperature, T equal to the gas temperature inside the gas distributor. The gas assessed in this work will be constituted by component identified as component “G”. Different kind of gasses can easily be considered by the model by changing the gas properties inside the model. However, it is assumed that the gas coming from the gas distributor has a behavior according the ideal gas law.

The liquid system is considered a mixture of hydrocarbons with components identified by the symbol “A” and “K” both at a temperature of the liquid bulk, T_L , which is lower than the gas temperature, T , inside the bubble at the initial time. It was considered a stagnant liquid in this work as well in the previous section, so the bubble will rise in the vertical direction without horizontal displacement; its center of mass will be located again in the “y” axis specified in section 3.1.1 and 3.1.2 during the bubble rising.

Additionally, in this thesis project will be modeled a process of evaporation of the liquid component “A” due to the difference of temperature between the liquid and gas phase and the pressure system. A process of mass transfer for the component “A” due to a driving force will be studied.

However, this model is limited to the region near to the sparger region and it does not consider other phenomena going on far away from the gas distributor as the mass and heat transfer near a solid particle or catalyst inside the reactor. Bubble coalescence and breakup are also neglected.

The model previously described is illustrated with a scheme as shown in Fig.3.9 where the bubble is moving in the vertical direction and there is a heat flux, “ q ”, going out from the bubble radially toward the liquid bulk containing the component “A” which tends to evaporate due to the heat transfer carried out between the bubble and the liquid. Due to this phenomenon, the bubble grows.

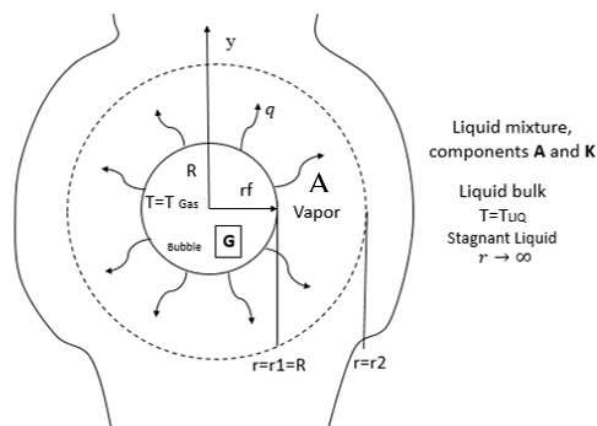


Fig.3.9: Momentum, Heat and Mass transfer model scheme.

3.2.1 Bubble rising velocity

Now, the bubble is already released from the gas distributor and it should not change anymore in size while it continues rising forward the top of the reactor. However, the bubble grows, it changes in size and the final dimension will be determined at the end of this section.

The bubble rising velocity is an important parameter to assess in this section. It will be evaluated through a similar analysis in section 1.3.2, that is, a balance of forces exerted on the bubble during the ascension.

During the ascension will be taken in account the buoyancy force, drag force, gravitational force and inertia force. As the bubble is not connected anymore to the gas distributor the gas momentum, surface tension and the pressure force disappear from the balance of forces. The bubble center of mass will rise on a vertical axis, “y” with origin in the orifice base as shown in Fig. 3.10.

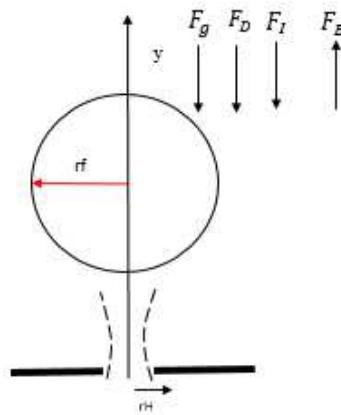


Fig.3.10: Bubble rising scheme just after detachment time.

The bubble just after detachment has a known center of mass position, diameter, velocity and composition because it just contains component “G”. This amount of component “G” is assumed to be constant,

$$m_G = n_G M_G \quad \text{Eq. (3.145)}$$

where n_G is the moles of G inside the bubble and M_G G molecular weight.

Nevertheless, the bubble will grow due to vaporization of the liquid component “A”. Then, its vapor will be considered part of the bubble and the total bubble mass, m_b , will be,

$$m_b = n_A M_A + n_G M_G \quad \text{Eq. (3.146)}$$

where n_A is the moles of component “A” inside the bubble and M_A , the molecular weight of “A”. The bubble volume will be characterized by a new diameter, L, which includes the vapor of the component A,

$$V_b = \frac{\pi}{6} L^3 \quad \text{Eq. (3.147)}$$

The bubble gas density is also considered to change according its new mass,

$$\rho_g = \frac{m_b}{V_b} = \frac{n_A M_A + n_G M_G}{\frac{\pi}{6} L^3} \quad \text{Eq. (3.148)}$$

where V_b is the bubble volume.

Inside the inertial term is considered a virtual mass, m_v , defined as,

$$m_v = \frac{\pi}{6} L^3 \alpha \rho_L \quad \text{Eq. (3.149)}$$

where, α is the added mass coefficient, defined as before as 11/16, [23].

A similar analysis to the one in section 3.1.2 for the bubble motion will be presented. The bubble center of mass will rise in the vertical “y” axis and the derivative of the position will be the bubble terminal velocity, U_t ,

$$U_t = \frac{dy}{dt} \quad \text{Eq. (3.150)}$$

As mentioned before during the bubble ascension, the buoyancy, drag, gravitational and inertia force will be taken in account in the balance,

$$F_b = F_l + F_g + F_D \quad \text{Eq. (3.151)}$$

After the substitution of each term in Eq. 3.151 by its definition,

$$V_b \rho_L g = \frac{d}{dt} \left[(m_b + m_v) \frac{dy}{dt} \right] + V_b \rho_g g + \frac{\pi}{4} L^2 C_D \frac{\rho_L}{2} \left(\frac{dy}{dt} \right)^2 \quad \text{Eq. (3.152)}$$

Then, for the drag coefficient, C_D , will be considered the Eq. 3.92. After some development for Eq. 3.152 is found,

$$\frac{\pi}{6} L^3 (\rho_L - \rho_g) g = (m_{bubble} + m_{virtual}) \frac{d^2 y}{dt^2} + \frac{dy}{dt} \frac{d(m_b + m_v)}{dt} + \frac{\pi}{4} L^2 C_D \frac{\rho_L}{2} \left(\frac{dy}{dt} \right)^2 \quad \text{Eq. (3.153)}$$

In equation 3.153 it is found the derivative of the bubble mas and the virtual mass,

$$\frac{d(m_b + m_v)}{dt} = \frac{dn_A}{dt} M_A + \alpha \rho_L \frac{\pi}{2} L^2 \frac{dL}{dt} \quad \text{Eq. (3.154)}$$

Eq.3.154 include the derivative of moles of component A, $\frac{dn_A}{dt}$, with time in the first term and in the second term is found the derivative of diameter respect to time, $\frac{dL}{dt}$.

Then, the momentum balance equation can be written as in Eq.3.155,

$$\frac{\pi}{6} L^3 \rho_L g - (m_b) g = (m_b + m_v) \frac{d^2 y}{dt^2} + \frac{dy}{dt} \left[\frac{dn_A}{dt} M_A + \alpha \rho_L \frac{\pi}{2} L^2 \frac{dL}{dt} \right] + \frac{\pi}{4} L^2 C_D \frac{\rho_L}{2} \left(\frac{dy}{dt} \right)^2 \quad \text{Eq. (3.155)}$$

Finally, it is possible to find and equation for the bubble acceleration,

$$\frac{d^2 y}{dt^2} = \frac{1}{(m_b + m_v)} \left[\frac{\pi}{6} L^3 \rho_L g - (m_b) g - \frac{dy}{dt} \left[\frac{dn_A}{dt} M_A + \alpha \rho_L \frac{\pi}{2} L^2 \frac{dL}{dt} \right] - \frac{\pi}{4} L^2 C_D \frac{\rho_L}{2} \left(\frac{dy}{dt} \right)^2 \right] \quad \text{Eq. (3.156)}$$

Eq. 3.156 is a second order differential equation, but it can be rewritten as a first order differential equation as,

$$\frac{dU_t}{dt} = \frac{1}{(m_b + m_v)} \left[\frac{\pi}{6} L^3 \rho_L g - (m_b) g - \frac{dy}{dt} \left[\frac{dn_A}{dt} M_A + \alpha \rho_L \frac{\pi}{2} L^2 \frac{dL}{dt} \right] - \frac{\pi}{4} L^2 C_D \frac{\rho_L}{2} \left(\frac{dy}{dt} \right)^2 \right] \quad \text{Eq.(3.157)}$$

and the bubble velocity can be written as,

$$\frac{dy}{dt} = U_t \quad \text{Eq. (3.158)}$$

Eq. 3.157 and Eq.3.158 must be solved simultaneously as part of a system of first order differential equation which contain also the derivative of moles of component A, $\frac{dn_A}{dt}$, the derivative of diameter respect to time, $\frac{dL}{dt}$ and the derivative of temperature respect to time, $\frac{dT}{dt}$. Actually, Eq. 3.157 depends on $\frac{dn_A}{dt}$ and $\frac{dL}{dt}$ so, these terms must be determined before of trying to solve the velocity and position derivative equation.

The initial condition for Eq.3.157 and Eq.3.158 is the result of the second stage of bubble formation process, that is, the bubble velocity and the position of the bubble center of mass at detachment moment. To obtain the bubble velocity and the position of the bubble center of mass at detachment moment will be use Eq. 3.105 with a drag coefficient in Eq.3.92 to model the first stage bubble expansion and the second stage is represented by the balance of forces in Eq. 3.159,

$$V_b \rho_L g + \frac{\pi}{4} d_h^2 \rho_g U_g^2 + \frac{\pi}{4} d_h^2 (p_g - p_L) = (\rho_g + \alpha \rho_L) G \frac{dy}{dt} + (\rho_g + \alpha \rho_L) V_b \frac{d^2 y}{dt^2} + \frac{\pi}{4} d^2 C_D \frac{\rho_L}{2} \left(\frac{dy}{dt} \right)^2 + V_b \rho_g g + \pi d_h \sigma \sin \theta \quad \text{Eq. (3.159)}$$

From Eq. 3.159 it is possible to obtain a bubble acceleration equation as done in the section 3.1.2. However, this time the drag coefficient, C_D , expression will be Eq.3.92 because is considered the most suitable for this combined model. The final result is presented in Eq.3.160,

$$\frac{d^2 y}{dt^2} = \frac{1}{(\rho_g + \alpha \rho_L) V_b} [V_b (\rho_L - \rho_g) g + \frac{\pi}{4} d_h^2 \rho_g U_g^2 + \frac{\pi}{4} d_h^2 (p_g - p_L) - (\rho_g + \alpha \rho_L) G \frac{dy}{dt} - \frac{\pi}{4} d^2 C_D \frac{\rho_L}{2} \left(\frac{dy}{dt} \right)^2 - \pi \sigma d_h \sin \theta] \quad \text{Eq. (3.160)}$$

Eq.3.160 is transformed in a first order differential equation as the derivative of the velocity as shown in Eq. 3.161. The contact angle, θ in the second stage is considered 90° because the presence of the gas neck connecting the hole and the bubble base.

$$\frac{dU_b}{dt} = \frac{1}{(\rho_g + \alpha \rho_L) V_b} [V_b (\rho_L - \rho_g) g + \frac{\pi}{4} d_h^2 \rho_g U_g^2 + \frac{\pi}{4} d_h^2 (p_g - p_L) - (\rho_g + \alpha \rho_L) G \frac{dy}{dt} - \frac{\pi}{4} d^2 C_D \frac{\rho_L}{2} \left(\frac{dy}{dt} \right)^2 - \pi \sigma d_h] \quad \text{Eq. (3.161)}$$

Eq. 3.161 is solved simultaneously with Eq. 3.162 as a system of first order differential equations to obtain the velocity and position of bubble at detachment moment,

$$\frac{dy}{dt} = U_b \quad \text{Eq. (3.162)}$$

Initial conditions for Eq. 3.161 and 3.162 are bubble velocity equal to zero and initial bubble center of mass position equal to the first stage bubble radius, r_d , obtained in Eq. 3.105 with drag coefficient in Eq.3.92. The results of Eq.3.161 and 3.162 will be the initial conditions of Eq.3.157 and 3.158.

3.2.2 Mass transfer

As mentioned before, there is a driving force in the system which generates a molecular motion of component "A" from the liquid to the gas phase in the liquid. The molar concentration of component "A", $C_{A,L}$, is maximum in the liquid bulk and minimum at the gas-liquid interface. This difference of concentration represents a driving force for the mass transfer process. The molar flux of component "A" can be expressed as:

$$\frac{dn_A}{dt} = k_L (\pi L^2) (C_{A,L} - C_{AL,i}) \quad \text{Eq. (3.163)}$$

where, k_L is mass transfer coefficient, considering the liquid resistance as the most important and neglecting the resistance in the gas side. Then, $C_{AL,i}$, is the molar concentration of component "A" at the gas-liquid interface and $C_{A,L}$, is total molar concentration of component "A" in the liquid phase.

The mass transfer coefficient is obtained through the Higbie's penetration theory,

$$k_L = \sqrt{\frac{4D_{AG}}{\pi t_e}} \quad \text{Eq. (3.164)}$$

where, \mathcal{D}_{AG} , is the binary diffusivity coefficient of component “A” in a medium constituted by component “G” and t_e , is the exposure time, namely, the time in which one block of liquid constituted by component “A” is attached to the gas-liquid interface and available to the mass transfer occur.

The exposure time for a bubble rising in a liquid can be calculated as,

$$t_e = \frac{L(t)}{U_t(t)} \quad \text{Eq. (3.165)}$$

Then, the molar concentration of component “A” at the gas-liquid interface, $C_{AL,i}$, can be found by means of the Raoult’s Law, assuming thermodynamic equilibrium at the vapor-liquid interface,

$$P_{A,i} = X_{A,i}P_A(T)^{sat} \quad \text{Eq. (3.166)}$$

where $P_A(T)^{sat}$ is the vapor pressure of component “A”, $X_{A,i}$ is the molar fraction of component “A” at the vapor-liquid interface, $P_{A,i}$ is the partial pressure of component “A” at the interface which can be consider equal to the partial of component “A”, P_A ; the vapor of component “A” will be treated as an ideal gas. Then is possible to write,

$$P_A = \frac{n_A RT(t)}{V} = \frac{n_A(t)RT(t)}{\frac{\pi}{6}L(t)^3} \quad \text{Eq. (3.167)}$$

The molar fraction of the component “A” at the vapor-liquid interface $X_{A,i}$ is related to the molar concentration of component “A” at the gas-liquid interface, $C_{AL,i}$ by

$$X_{A,i} = \frac{C_{AL,i}}{C_{tot}} \quad \text{Eq. (3.168)}$$

where C_{tot} is total molar concentration of the liquid mixture which can be found through the molar concentration of the components in the liquid mixture.

$C_{A,L}$, the total molar concentration of component “A” in the liquid phase, will be calculated as;

$$C_{A,L} = \frac{\rho_A}{M_A} \quad \text{Eq. (3.169)}$$

and C_{tot} , the total molar concentration of the liquid mixture, will be calculated as:

$$C_{tot} = \frac{C_{A,L} + C_{K,L}}{2} \quad \text{Eq. (3.170)}$$

where $C_{K,L}$, is the total molar concentration of the second component “K” in the liquid phase and it will be calculated as,

$$C_{K,L} = \frac{\rho_K}{M_K} \quad \text{Eq. (3.171)}$$

Eventually, it is possible to find an expression for, $C_{AL,i}$

$$C_{AL,i} = \frac{n_A(t)RT(t)}{\frac{\pi}{6}L(t)^3} \frac{C_{tot}}{P_A(T)^{sat}} \quad \text{Eq. (3.172)}$$

In Eq. 3.172 the vapor pressure, $P_A(T)^{sat}$, depends on the temperature and it will be expressed through the Equation of Antoine as follow,

$$P_A(T)^{sat} [bar] = 10^{(A - \frac{B}{C+T[K]})} \quad \text{Eq. (3.173)}$$

Therefore, it is possible to have an “A” moles derivative equation, $\frac{dn_A}{dt}$, depending on the main variables to be found in the global model, L, T, U_t , y, and n_A , which are time dependent variables:

$$\frac{dn_A}{dt} = \sqrt{\frac{4D_{AG} U_t(t)}{\pi L(t)}} (\pi L(t)^2) \left(C_{A,L} - \frac{n_A(t) R C_{tot}}{\frac{\pi}{6} L(t)^3} \frac{T(t)}{P_A(T)^{sat}} \right) \quad \text{Eq. (3.174)}$$

Eq.3.174 will be part of the final first order differential equation system.

3.2.3 Diameter differential equation

This equation gives the final bubble dimension when all the transfer processes being considered are accomplished during the bubble rising through the reactor.

This equation has been developed through the ideal gas equation law,

$$PV_b(t) = (n_A(t) + n_G)RT(t) \quad \text{Eq. (3.175)}$$

where P, is the pressure inside the gas-liquid reactor, R, is the ideal gas constant and “T” is the bubble temperature.

Changing, the bubble volume by its definition with the diameter, L, is obtained,

$$P \frac{\pi}{6} L(t)^3 = (n_A(t) + n_G)RT(t) \quad \text{Eq. (3.176)}$$

and it is possible to isolate the bubble diameter at time t, as

$$L(t)^3 = \frac{6}{\pi P} (n_A(t) + n_G)RT(t) \quad \text{Eq. (3.177)}$$

Eq.3.177 is derived respect to time to obtain,

$$3L(t)^2 \frac{dL}{dt} = \frac{6}{\pi P} R n_A(t) \frac{dT}{dt} + \frac{6}{\pi P} RT(t) \frac{dn_A}{dt} + \frac{6}{\pi P} R n_G \frac{dT}{dt} \quad \text{Eq. (3.178)}$$

Finally, isolating the diameter derivative equation:

$$\frac{dL}{dt} = \frac{2R}{\pi P} \frac{1}{L(t)^2} [(n_A(t) + n_G) \frac{dT}{dt} + T(t) \frac{dn_A}{dt}] \quad \text{Eq. (3.179)}$$

Eq. 3.179 will form part of the final first order differential equation system.

3.1.4 Heat transfer

In this section it will be developed an energy balance, through the First Law of Thermodynamics applied to the bubble at detachment time.

First, the First Law of Thermodynamics will be written in terms of energy fluxes, as

$$\frac{dE_k}{dt} + \frac{dE_p}{dt} + \frac{dU}{dt} = \sum_{streams}^{in} m_j (\hat{U}_j + P_j \hat{V}_j + \frac{u_j^2}{2} + g z_j) - \sum_{streams}^{out} m_j (\hat{U}_j + P_j \hat{V}_j + \frac{u_j^2}{2} + g z_j) + \dot{Q} - \dot{W}_s - P\dot{V} \quad \text{Eq. (3.180)}$$

Eq. 3.180 can be reduced making some assumptions and according the system being study.

First of all, in the system there is no change with of Potential, E_p , and Kinetic Energy, E_k . Then, there is no shaft work because there is no pump or mechanical equipment is performing work. There is not heat flux exiting from the system, while there is an energy flux entering in the system with the evaporation of component “A”.

Then, Eq.3.180 is reduced to

$$\frac{dU}{dt} = \sum_{streams}^{in} \dot{m}_A (\hat{U}_A + P_A \hat{V}_A) + \dot{Q} - P\dot{V} \quad \text{Eq. (3.181)}$$

The last term in the right side of Eq.3.181, representing the work done by the boundary of the system, can be moved to the left side and together with Internal Energy rate is obtained the derivative of Enthalpy of the system, then there will just one enthalpy flux entering to the system identified as, \dot{H}_e , and a conductive flux due to the difference of temperature between the liquid and the bubble, \dot{q} .

After these last modifications, Eq.3.181 can be rewritten as,

$$\frac{dH}{dt} = \dot{H}_e + \dot{q} \quad \text{Eq. (3.182)}$$

Then, each term in Eq.3.182 must be defined according the system.

The system will be constituted by the gas “G” coming from the gas distributor and the vapor of the vaporized liquid which is represented by the component “A”. Taking a reference state as the liquid temperature, the molar enthalpy for component “G” is

$$\hat{H}_G = \hat{H}_G(T_L) + \hat{C}_{p,G}(T(t) - T_L) \quad \text{Eq. (3.183)}$$

where, $\hat{C}_{p,G}$, is the heat capacity at constant pressure of gas “G” and the molar enthalpy for component “A” is

$$\hat{H}_A = \hat{H}_A^{liq}(T_L) + \hat{C}_{p,A}^{vap}(T(t) - T_L) + \Delta\hat{H}_{vap}(T_L) \quad \text{Eq. (3.184)}$$

where, $\hat{C}_{p,A}^{vap}$, is the heat capacity at constant pressure of component “A” inside the bubble as vapor phase and $\Delta\hat{H}_{vap}(T_L)$ is the latent heat of vaporization.

Then, the enthalpy of the system can be defined as summation of the enthalpy of each component,

$$H(t, T) = n_G \hat{H}_G + n_A(t) \hat{H}_A \quad \text{Eq. (3.185)}$$

and its derivative can be calculated as,

$$\frac{dH}{dt} = n_A(t) \frac{d\hat{H}_A}{dt} + \hat{H}_A \frac{dn_A}{dt} + n_G \frac{d\hat{H}_G}{dt} \quad \text{Eq. (3.186)}$$

Replacing each derivative is obtained,

$$\frac{dH}{dt} = (n_A \hat{C}_{p,A}^{vap} + n_G \hat{C}_{p,G}) \frac{dT}{dt} + \frac{dn_A}{dt} (\hat{H}_A^{vap}(T_L) + \hat{C}_{p,A}^{vap}(T(t) - T_L) + \Delta\hat{H}_{vap}(T_L)) \quad \text{Eq. (3.187)}$$

Afterward, the enthalpy flux entering to the system can be defined as,

$$\dot{H}_e = \dot{n}_A \hat{H}_A = \frac{dn_A}{dt} \left\{ \hat{H}_A^{liq}(T_L) + \hat{C}_{p,A}^{liq}(T(t) - T_L) \right\} \quad \text{Eq. (3.188)}$$

And the conductive heat flux can be written as the product of heat transfer coefficient, h_o , a characteristic area for the heat transfer and the temperature difference of the phases:

$$\dot{q} = h_o(\pi L^2)(T_L - T) \quad \text{Eq. (3.189)}$$

The global heat transfer coefficient, h_o can be calculated as,

$$h_o = \frac{1}{\frac{1}{h_G} + \frac{1}{h_L}} \quad \text{Eq. (3.190)}$$

where is $(1/h_G)$ is the gas side heat resistance and $1/h_L$, is the liquid side heat resistance. The liquid side heat transfer coefficient h_L have been determined by means of the Analogy between the Nusselt and Sherwood dimensionless number; Because there is a mass transfer coefficient defined by Higbie for this system it is possible to determine the Sherwood number in function of Reynolds and Schmidt number as:

$$S_h = \frac{k_L L}{D} = \sqrt{\frac{4D}{\pi} \frac{L}{D}} = \sqrt{\frac{\rho U t L}{\mu} \frac{4}{\pi} \frac{\mu}{\rho D}} = \sqrt{\frac{4}{\pi} R_e S_c} \quad \text{Eq. (3.191)}$$

Then by the analogy with Nusselt number,

$$N_u = \frac{h_L L}{k} = \sqrt{\frac{4}{\pi} R_e P_r} \quad \text{Eq. (3.192)}$$

Then, the liquid heat transfer coefficient is calculated as,

$$h_L = \sqrt{\frac{4\rho\hat{c}_p k U t}{\pi L}} \quad \text{Eq. (3.193)}$$

The gas side heat transfer coefficient, h_G , for a rising bubble has been found in literature. However, it was considered equal to the external heat transfer coefficient, that is,

$$h_L = h_G \quad \text{Eq. (3.194)}$$

Then, the global heat transfer coefficient is reduced due to the last consideration, as

$$h_o = \frac{1}{2} h_L = \frac{1}{2} \sqrt{\frac{4\rho\hat{c}_p k U t}{\pi L}} \quad \text{Eq. (3.195)}$$

where \hat{C}_p is liquid heat capacity at constant pressure in (J/Kg K) and k, is the gas thermal conductivity.

Finally, the heat conductive flux can be set as,

$$\dot{q} = \frac{1}{2} \sqrt{\frac{4\rho\hat{c}_p k U t}{\pi L}} (\pi L^2) (T_L - T) \quad \text{Eq. (3.196)}$$

Therefore, the energy balance is reads as follows:

$$\frac{dH}{dt} = \frac{1}{2} \sqrt{\frac{4\rho\hat{c}_p k U t}{\pi L}} (\pi L^2) (T_L - T) + \frac{dn_A}{dt} \left\{ \hat{H}_A^{liq}(T_L) + \hat{C}_{p,A}^{liq}(T(t) - T_L) \right\} \quad \text{Eq. (3.197)}$$

and the derivative of the Enthalpy energy is equal to,

$$\frac{dH}{dt} = (n_A \hat{C}_{p,A}^{vap} + n_G \hat{C}_{p,G}) \frac{dT}{dt} + \frac{dn_A}{dt} (\hat{H}_A^{vap}(T_L) + \hat{C}_{p,A}^{vap}(T(t) - T_L) + \Delta \hat{H}_{vap}(T_L)) \quad \text{Eq. (3.198)}$$

Eq.3.197 and 3.198 can be matched and the derivate of temperature, $\frac{dT}{dt}$, can be isolated as,

$$\frac{dT}{dt} = \frac{1}{(n_A(t) \hat{C}_{p,A}^{vap} + n_G \hat{C}_{p,G})} \left[\sqrt{\frac{4\rho\hat{c}_p k U t(t)}{\pi L(t)}} (\pi L(t)^2) (T_L - T(t)) + \frac{dn_A}{dt} \left\{ (\hat{C}_{p,A}^{liq} - \hat{C}_{p,A}^{vap})(T(t) - T_L) - \Delta \hat{H}_{vap}(T_L) \right\} \right] \quad \text{Eq. (3.199)}$$

Eq.3.199 is the last equation to be obtained for the differential equation system developed in this combined momentum, heat and mass transfer model.

The final differential equation system will be solved in a specific order for the equations but at the same time simultaneously, that is,

First, the derivative of moles of ‘‘A’’

$$\frac{dn_A}{dt} = \sqrt{\frac{4D U_t(t)}{\pi L(t)}} (\pi L(t)^2) \left(C_{A,L} - \frac{n_A(t) R C_{tot}}{\frac{\pi}{6} L(t)^3} \frac{T(t)}{P_A(T)^{sat}} \right) \quad \text{Eq. (3.200)}$$

Second, the derivative of the temperature,

$$\frac{dT}{dt} = \frac{1}{(n_A(t)\hat{C}_{p,A}^{vap} + n_G\hat{C}_{p,G})} \left[\sqrt{\frac{4\rho\hat{C}_p^k}{\pi}} \frac{U_t(t)}{L(t)} (\pi L(t)^2)(T_L - T(t)) + \frac{dn_A}{dt} \left\{ (\hat{C}_{p,A}^{liq} - \hat{C}_{p,A}^{vap})(T(t) - T_L) - \Delta\hat{H}_{vap}(T_L) \right\} \right] \quad \text{Eq. (3.201)}$$

Third, the derivative of the bubble diameter

$$\frac{dL}{dt} = \frac{2R}{P\pi L(t)^2} [(n_A(t) + n_G) \frac{dT}{dt} + T(t) \frac{dn_A}{dt}] \quad \text{Eq. (3.202)}$$

Fourth, the derivative of the position,

$$\frac{dy}{dt} = U_t \quad \text{Eq. (3.203)}$$

And fifth, the derivative of the velocity equation,

$$\frac{dU_t}{dt} = \frac{1}{(m_b + m_v)} \left[\frac{\pi}{6} L^3 \rho_L g - (m_b)g - \frac{dy}{dt} \left[\frac{dn_A}{dt} M_A + \alpha \rho_L \frac{\pi}{2} L^2 \frac{dL}{dt} \right] - \frac{\pi}{4} L^2 C_D \frac{\rho_L}{2} \left(\frac{dy}{dt} \right)^2 \right] \quad \text{Eq. (3.204)}$$

In this way, the solution of the differed equations can be carried out in series, avoiding the solution of a linear system of equation at each time stop.

Chapter 4

Implementation and numerical details

The objective for this chapter will be to show the algorithms in MATLAB and some strategies employed in this thesis project to solve, for different systems, the models described in Chapter 3.

Equations in each model are complex equations in which the unknown variable appears in a nonlinear way in different terms of the equation. So, it is not possible to find an analytical solution. Additionally, there were found several differential equations, first and second order differential equations and some of them were with constant coefficients and other with no constant coefficients.

4.1 MATLAB Algorithms

The results for each model in Chapter 3 were obtained by different mathematical and numerical methods designed to solve these complex equations with the required accuracy. The MATLAB program was the proper tool employed to apply these mathematical and numerical methods.

4.1.1 Bisection Model

It is a numerical method chosen to solve the non-linear equations sometimes called transcendental equations found in the development of the models presented in Chapter 3. Specifically, it will be used in the section 3.1.1 to solve the transcendental equation presented for the First Stage of the bubble formation process, Eq.3.105. Besides, in the Sensitivity Analysis in section 3.1.3, are all non-linear equations solved by this numerical method too.

The bisection method is a set of steps repeated to solve this kind of equations,

$$f(x) = 0 \quad \text{Eq. (4.205)}$$

so, this method is employed to find the roots of an equation but in a certain interval $[a, b]$. It is very useful when the interval is known. The method takes the interval limits and it does an average, the results is identified with the letter, k . Then, the function is evaluated in the average value, $f(k)$. Then, two products are executed $f(k)*f(a)$ and $f(k)*f(b)$ and the sign of these products is evaluated. The product with negative sign is chosen because it contains the root and a new interval will be set by $[a, b=k]$ or $[a=c, b]$ [59].

The error of this method is influenced by the amount of iterations, N , as,

$$e < \frac{|b-a|}{2^N} \quad \text{Eq. (4.206)}$$

Then, the algorithm for the bisection method used in MATLAB solve equations in Chapter 3 mentioned previously will be explained through a flowchart in Fig. 4.11. These equations were written in function of the volume, so the interval to find the root by the bisection method was set as $[0, 1e-4]$ where volume is set in m^3 .

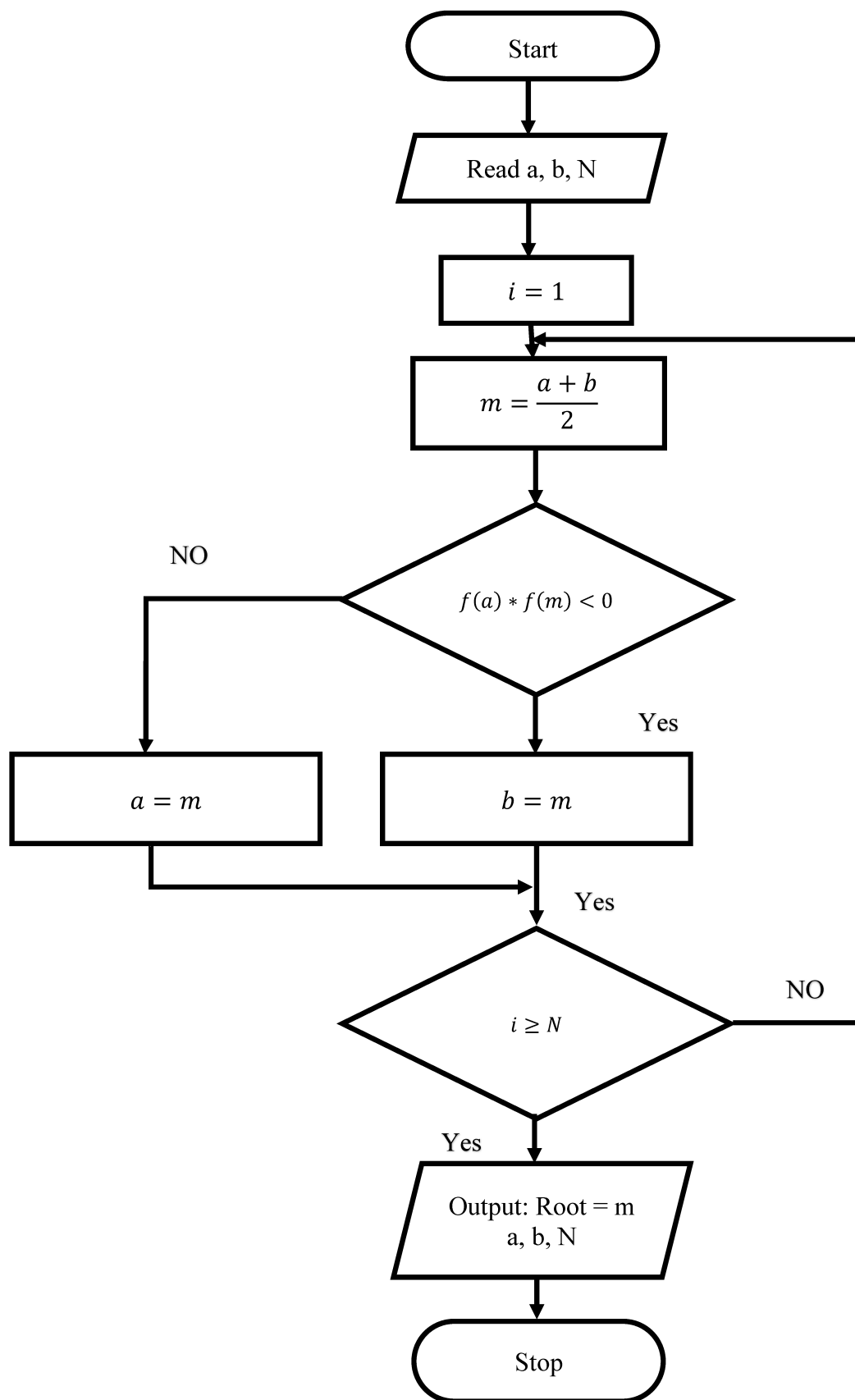


Fig.4.11: Flowchart of MATLAB program for the Bisection Method.

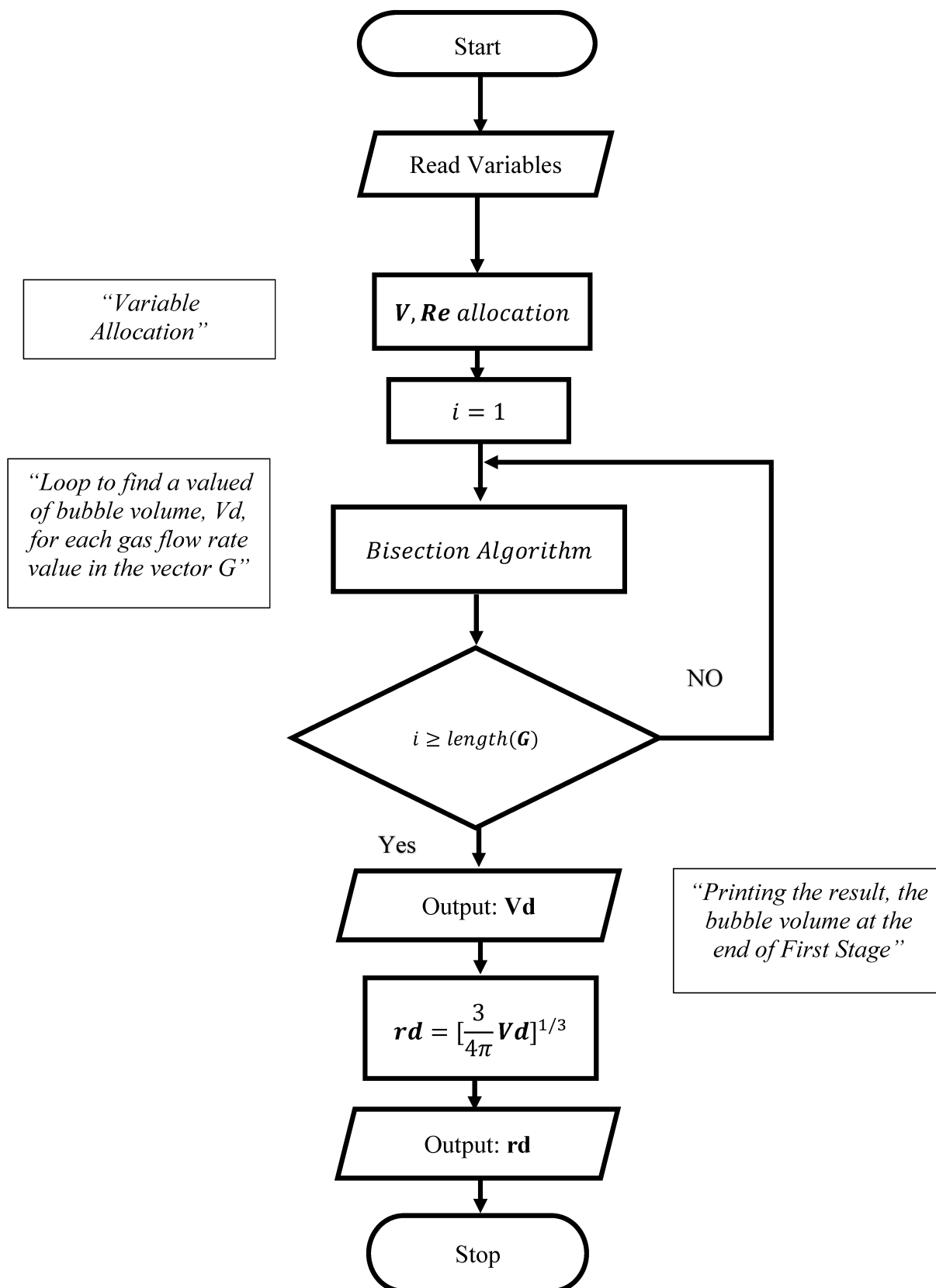


Fig.4.12: Flowchart of MATLAB program to solve the First Stage Model during bubble formation process.

4.1.2 ode45 Solver

The solver from MATLAB employed to solve Ordinary Differential Equations (ODE) or a system of ODEs as shown in equation 4.207 and matrix in Eq.4.208 is the ode45 solver. The solver integrates numerically, that is, through numerical methods, the first order differential equation.

$$\frac{dy}{dt} = y' = f(t, y) \quad \text{Eq. (4.207)}$$

$$M(t, y)y' = f(t, y) \quad \text{Eq. (4.208)}$$

Additionally, it is required to enter an initial condition as input for each differential equation as,

$$y(t_0) = y_0 \quad \text{Eq. (4.209)}$$

This solver employees a Runge-Kutta (4,5) formula. The syntax in MATLAB for ode45 solver is shown in Eq. 4.210. Runge Kutta is a fourth-order method because the total accumulated error has order h^4 and error per step is on the order of h^5 , h is the step size [49].

$$[sol] = \text{ode45}(@\text{myodefun}, t\text{Range}, [\text{initcond}]); \quad \text{Eq. (4.210)}$$

where, “*myodefun*” is the function inside a file.m called “*myodefun.m*”; it is required that the file.m and the function called by ode45 have both the same name. Inside the file.m are written all constants and the first order differential equations to be solved. To solve the model in section 3.1.2, Eq.3.161 and Eq.3.162 will be written in the file.m as the functions and all the constants and calculations needed to evaluate Eq.3.161 and Eq.3.162 must be also written, before solving the differential equations. Then, “*tRange*” denotes the time interval in which the ODE will be assessed as,

$$[t\text{Range}] = [t_0 \ t_f]; \quad \text{Eq. (4.211)}$$

where, t_0 is the lower initial time in the time interval and t_f is the final and higher limit in the time interval. Then “*initcond*” is the vector containing the initial condition values. “*sol*” is the vector containing the variables solution, that is the variable being integrated from each first order differential equation.

The solver computes a solution for each time step using first, the initial time and the initial condition, then, it compares the solution with its error tolerance criteria and if the error tolerance criteria is not satisfied the step size is extensively reduced. Finally, the function “*deval*” is used with a vector time shown in Eq.4.212, inside the time interval, to obtain the solution of the variable integrated with ode45 as shown in Eq. 4.213.

$$x = \text{linspace}(0, t_f, 100); \quad \text{Eq. (4.212)}$$

$$y = \text{deval}(sol, x, 1); \quad \text{Eq. (4.213)}$$

Then, it is possible to plot the result as in Eq.4.200.

$$\text{ploty} = \text{plot}(x, y); \quad \text{Eq. (4.214)}$$

In Fig.4.13 will be presented a flowchart for the Runge-Kutta method, in Fig.4.14 will be shown a flow chart for the calculation process of the second stage during the bubble formation process in section 3.1.2 and finally, in Fig.4.15 will be depicted a flow chart describing the program in MATLAB to solve the differential ODEs system for the model introduced in section 3.2, that is, the combined momentum, heat and mass transfer model for the bubble after detachment time.

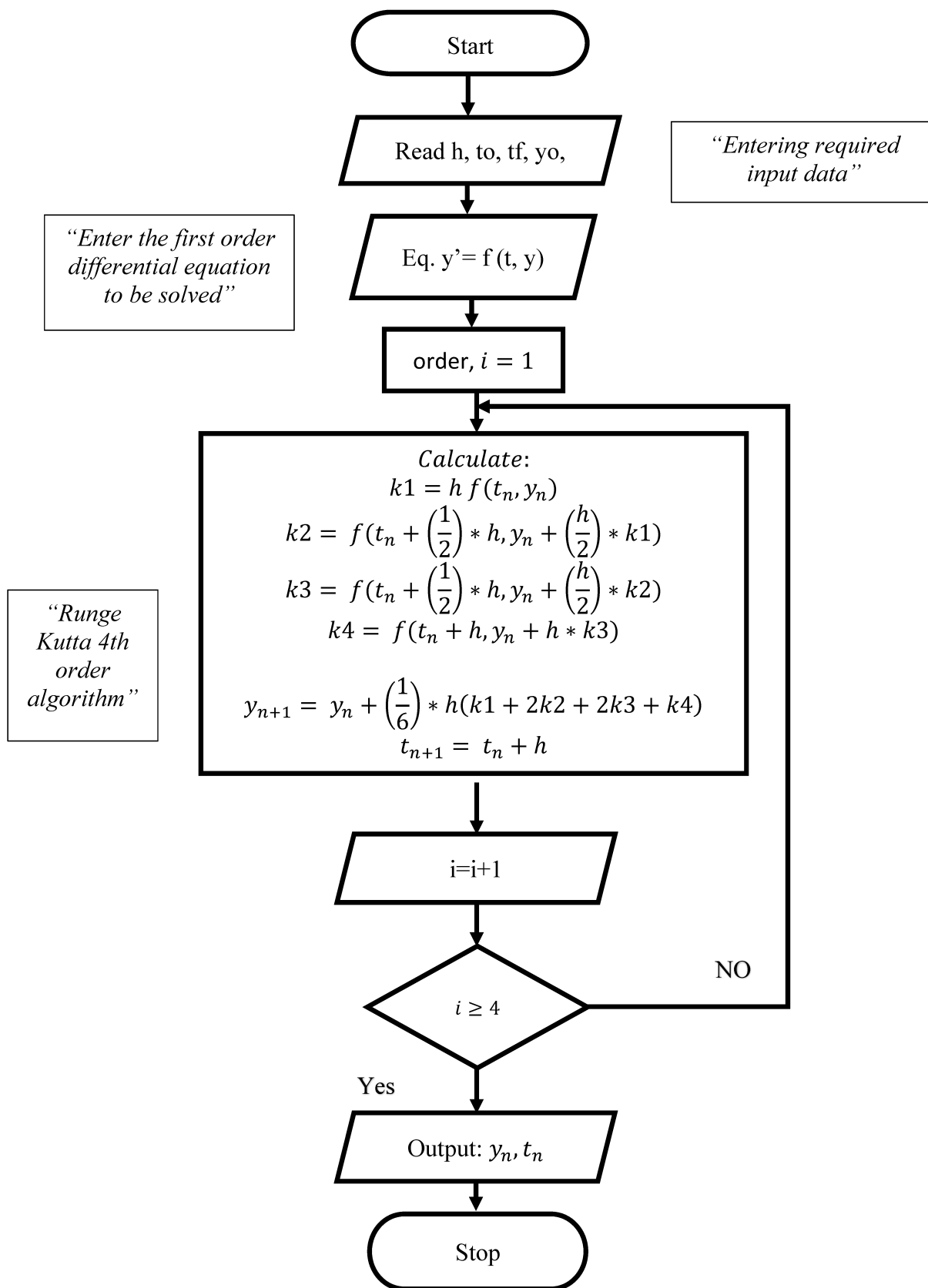


Fig.4.13: Flowchart of Runge-Kutta formula.

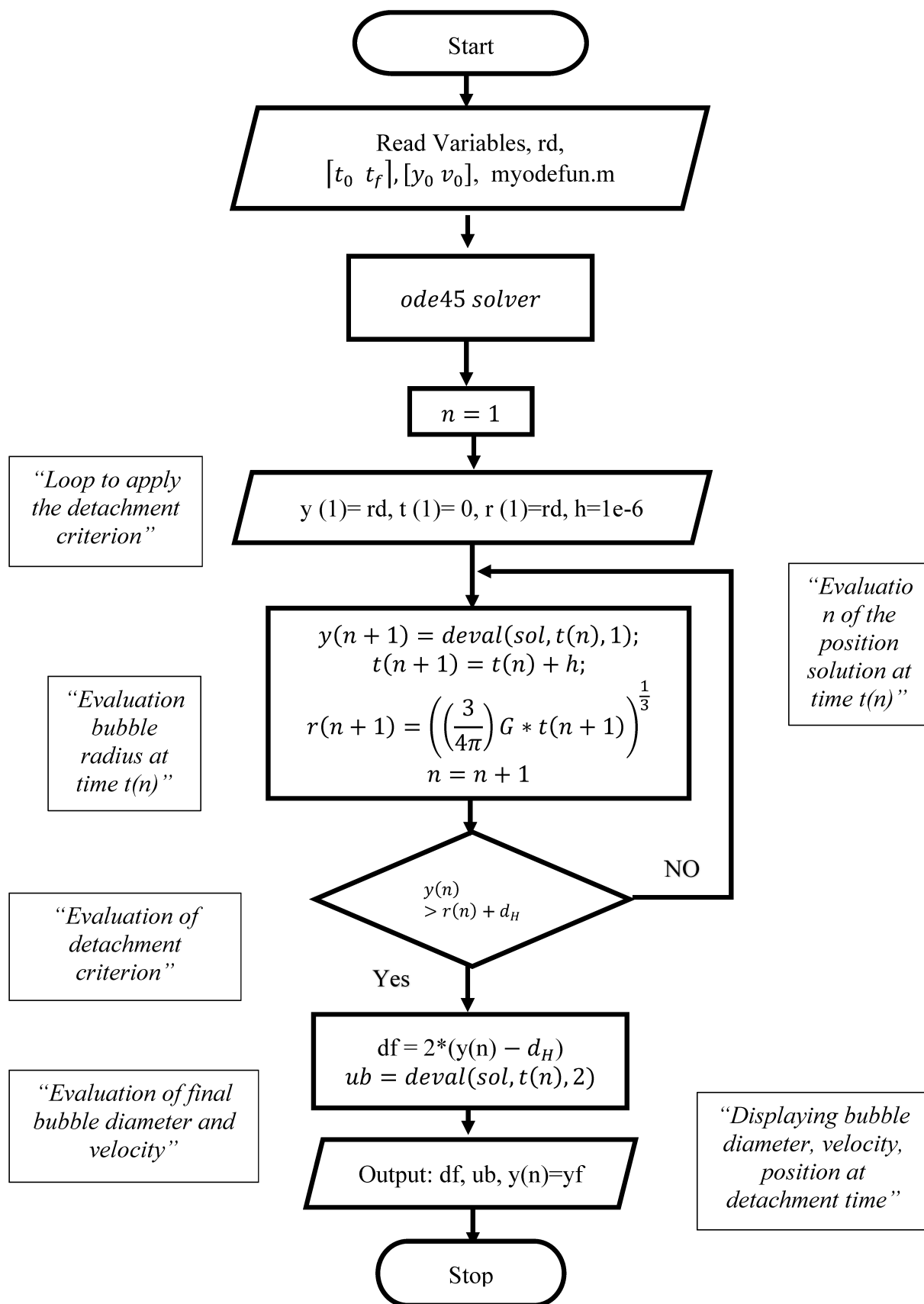


Fig.4.14: MATLAB program for Second Stage in bubble formation process.

4.1.3 System of ODEs

In this subsection will be explained the methodology applied to the combined momentum, heat and mass transfer model result of section 3.2.

The ODEs system will be solved through ode45 solver in MATLAB.

In a file.m will be written all the differential equations to be solved. This file will be called “myodesystem.m” and will be added to an Appendix at the end of this thesis project.

The first order differential equations to be solved are Eq. (4.215), Eq. (4.216), Eq. (4.217), Eq. (4.218) and Eq. (4.219) and their order is important in resolution of the problem. They must be organized in the following order:

First, the derivative of moles of “A”

$$\frac{dn_A}{dt} = \sqrt{\frac{4D U_t(t)}{\pi L(t)}} (\pi L(t)^2) \left(C_{A,L} - \frac{n_A(t) R C_{tot}}{\frac{\pi}{6} L(t)^3} \frac{T(t)}{P_A(T)^{sat}} \right) \quad \text{Eq. (4.215)}$$

Second, the derivative of the temperature

$$\frac{dT}{dt} = \frac{1}{(n_A(t) \hat{c}_{p,A}^{vap} + n_G \hat{c}_{p,G})} \left[\sqrt{\frac{4\rho \hat{c}_p k U_t(t)}{\pi L(t)}} (\pi L(t)^2) (T_L - T(t)) + \frac{dn_A}{dt} \{ (\hat{c}_{p,A}^{liq} - \hat{c}_{p,A}^{vap}) (T(t) - T_L) - \Delta \hat{h}_{vap}(T_L) \} \right] \quad \text{Eq. (4.216)}$$

Third, the derivative of the bubble diameter,

$$\frac{dL}{dt} = \frac{2R}{P\pi} \frac{1}{L(t)^2} [(n_A(t) + n_G) \frac{dT}{dt} + T(t) \frac{dn_A}{dt}] \quad \text{Eq. (4.217)}$$

Fourth, the derivative of the position,

$$\frac{dy}{dt} = U_t \quad \text{Eq. (4.218)}$$

And fifth, the derivative of the velocity equation,

$$\frac{dU_t}{dt} = \frac{1}{(m_b + m_v)} \left[\frac{\pi}{6} L^3 \rho_L g - (m_b) g - \frac{dy}{dt} \left[\frac{dn_A}{dt} M_A + \alpha \rho_L \frac{\pi}{2} L^2 \frac{dL}{dt} \right] - \frac{\pi}{4} L^2 \max \left[\frac{24}{Re_B} \left(1 + 0.15 Re_B^{0.687} \right), \frac{8}{3} \frac{E_o}{E_o + 4} \right] \frac{\rho_L}{2} \left(\frac{dy}{dt} \right)^2 \right] \quad \text{Eq. (4.219)}$$

The ODEs system let to assess the variation of moles of “A” which evaporate, n_A , bubble diameter after detachment time L, Bubble temperature, T, Bubble position, y, and Bubble terminal velocity, U_t with time. At the end it is possible to obtain the graphs of these variables versus time.

A part of the “myodesystem.m” file will be:

```
function dvdt = myodesystem(t,v)
    dvdt = zeros(5,1);
global Lo
% Call of constants and variables.m
Variables
    dvdt(1,1) = Kc*Supscambio*gradconc;
    dvdt(2,1) = (1/(v(1,1)*CpaV+nG*Cpg))* ( ho*superf*gradT + dvdt(1,1)*(-
    (CpaL-CpaV)*gradT-deltavap) );
    dvdt(3,1) =
    ((2*R)/(p*pi*v(3,1)^2))* (dvdt(1,1)*v(2,1)+dvdt(2,1)*(v(1,1)+nG));
    dvdt(4,1) = v(5,1);
    dvdt(5,1) = (1/(mbubble+ mvirt))*(buoy - gravit - inert - Fdrag);
end
```

Then, ode45 will call this function and it will solve the 5 differential equations simultaneously. A flowchart with the MATLAB program for the resolution if this system is shown in Fig.4.15.

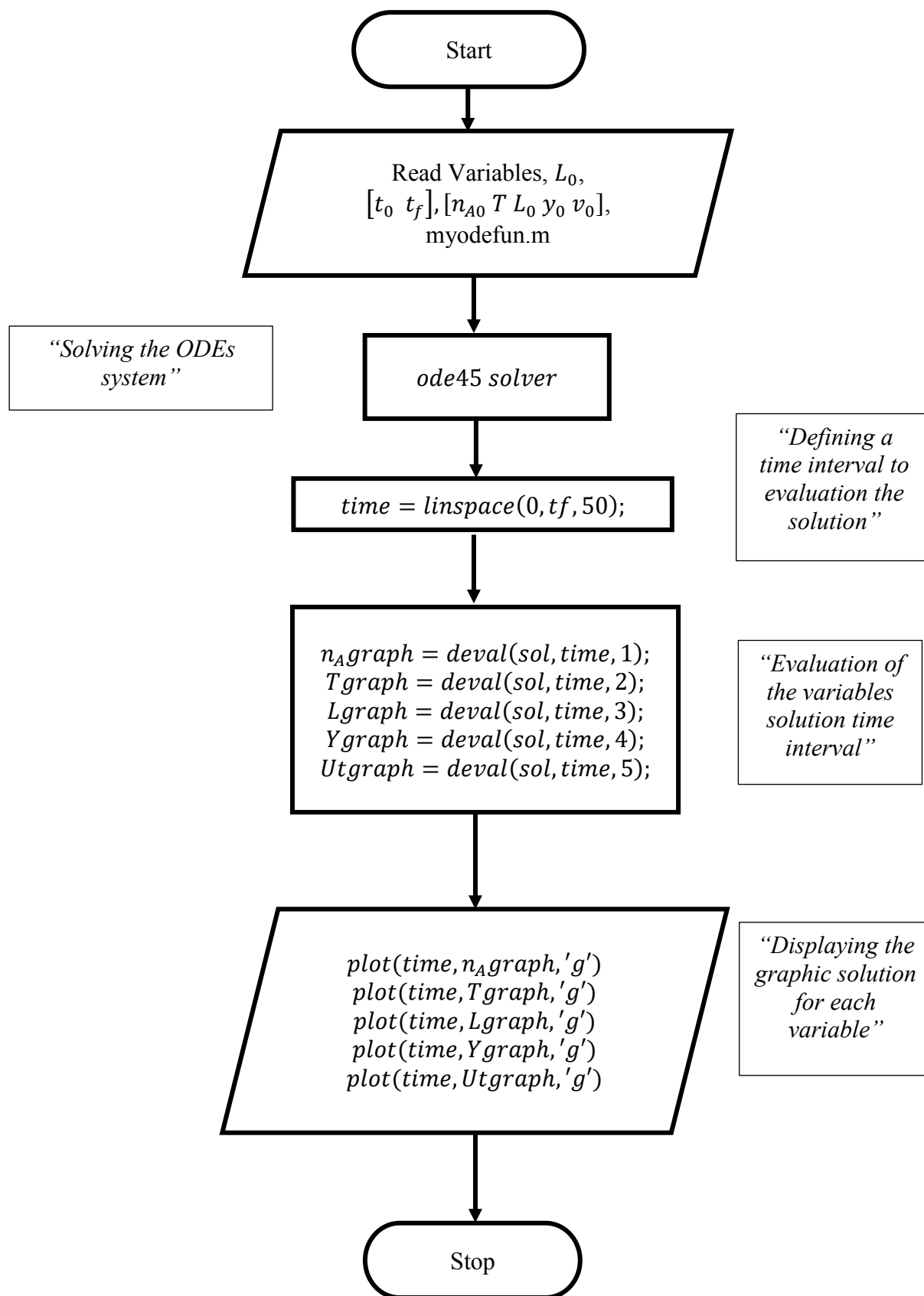


Fig.4.15: MATLAB program for the combined momentum, heat and mass transfer process.

Chapter 5

Results and discussion

5.1 Bubble formation model sensitivity analysis

In the following section both stages for the bubble formation model developed in Chapter 3 will be tested through a sensitivity analysis. The objective of this section will be to understand how models for each stage work and how much they are sensible to fluid properties, operating and geometric parameters. An oily system with fixed properties and operating conditions is presented in Table 5.1 and it will be used for the addition of terms to Original Model 1 in Eq.3.132.

Then, the following table is Table 5.2 and it presents for each property or operating condition the ranges of variation used in the sensitivity analysis.

Furthermore, the analysis is used to assess each stage during the bubble formation process with change of hole gas velocity, U_g .

Table 5.1. Oily-Gas basic system. Data required for First Stage.

Fluid Properties			Operating Conditions		
μ_g	$0.2 \cdot 10^{-4}$	[Pa.s]	U_g	[10-50]	[m/s]
σ	40	[N/m]	P	$8 \cdot 10^6$	[Pa]
ρ_L	800	[Kg/m ³]	TC	25	[°C]
μ	$5 \cdot 10^{-4}$	[Pa.s]	T	298.15	[K]
α	11/16	[-]	Hole Geometry		
ρ_g	20	[Kg/m ³]	r_H	$0.5 \cdot 10^{-3}$	[m]
R	8.314	[Pa m ³ /mol K]	Constants		
%solid	0.05	[-]	g	9.81	[m/s ²]

5.1.1 First Stage

This analysis is required because the bubble formation model exhibited in this work could be simplified in some cases that means that some terms could be negligible in some cases. However, the model was designed to be assessed in extreme conditions, actually, in industrial conditions, that is, higher pressure and temperature. So, it is required to investigate its behavior and the importance of each term inside the balance of forces for these conditions. In Table 5.2 are shown the properties to be varied and their ranges.

Table 5.2. Oily-Gas properties range. Data required for sensitivity analysis.

Fluid			Operating Conditions		
μ_g	$0.2 \cdot 10^{-4}$	[Pa.s]	U_g	[10-50]	[m/s]
σ	[20-70]	[N/m]	P	[2-8]. 10^6	[Pa]
ρ_L	[700-1000]	[Kg/m ³]	TC	25	[°C]
μ_L	[$1 \cdot 10^{-4}$ – $1 \cdot 10^{-3}$]	[Pa.s]	T	298.15	[K]
α	11/16	[-]	Hole Geometry		
ρ_g	[20-100]	[Kg/m ³]	r_H	[0.5 – 2]. 10^{-3}	[m]
R	8.314	[Pa m ³ /mol K]	Constants		
%solid	0.05	[-]	g	9.81	[m/s ²]

5.1.1.1 Adding terms to Original model 1

This subsection will be referred to the Original Model 1, represented by equation 3.132. Original Model 1 contains the most important forces associated to a bubble formation process, neglecting some other that may have an influence on the predictions.

In Fig. 5.16 is possible to perceive the impact on bubble dimension when several terms are added to balance of forces considering the same data exposed in Table 5.1. First at all, was assessed the addition of the bubble weight force and bubble mass into the inertia force through “Rhog Model”. This time it was taken a constant gas density and later it will be varied. So, the change from the terms in Original Model 1 to Rhog Model have produced an increment in bubble dimension about two times bigger than in Original Model 1. This increment on bubble size can be explained with a bubble which remains attached more time to the hole in the sparger due to its weight and the increment on its inertia.

Then, it was added the difference of pressure term to Rhog Model, this new term contemplates the pressure drop through the hole and hole geometry which means its diameter and length through a discharge coefficient, C_o , which also take in account Reynolds number at hole. The discharge coefficient, C_o , for this analysis was considered constant and equal to 0.801. This term has a similar effect of gas momentum term, it makes the bubble to grow but at the same time it triggers its release from the sparger. So, in Fig. 5.16 is possible to notice an important reduction in size at the end of the first stage, which means that the bubble starts to rise quicker than in Rhog Model so its dimension at the end of the first stage is decreased.

The last modification was the change in drag coefficient from Eq.3.90 in the pressure model to Eq.3.89 and this ends in the Drag Model which was chosen as the final model to obtain a reliable result for the bubble dimension at the end of the first stage where bubble just expands. The choice of Drag Model was confirmed assessing also the drag coefficient in Eq. 3.92 for fully contaminated water in the first stage and it results in a very similar radius as in Drag Model. With this modification is obtained the smallest bubble dimension at the end of the first stage as shown in Fig.5.16. A smaller dimension is understood as the result of a reduction in the drag force and the acceleration of the start of bubble rising.

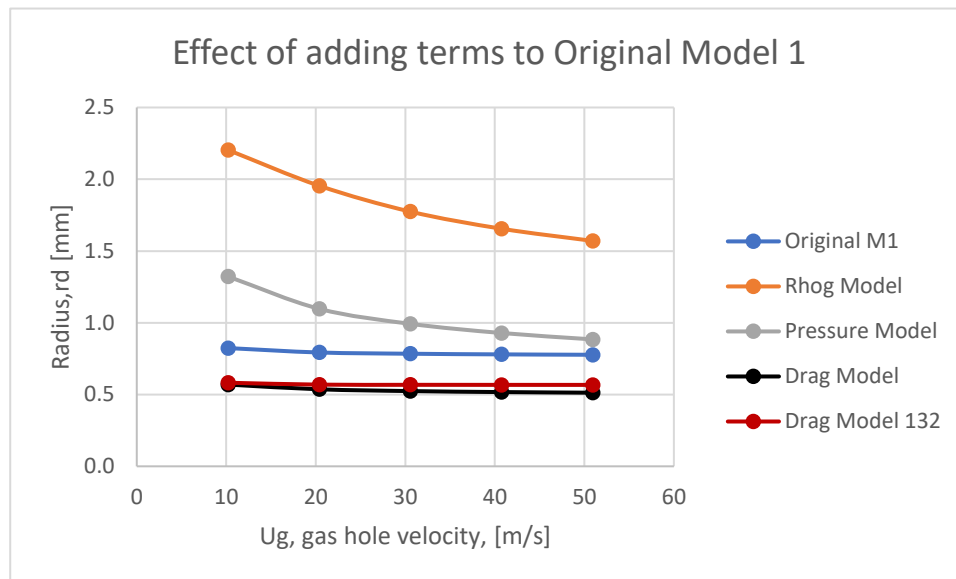


Fig.5.16: Effect of addition of terms to Original Model 1:First Stage.

Doing reference to Fig. 5.16 it is also noted that the addition of the different terms to Original Model 1 causes a reduction on the final bubble radius at the end of the first stage, evidenced with the comparison with the Drag Model 132 line; the difference between Original Model 1 and Drag Model and Drag model 132 is considered negligible. However, the effect of each single force is not negligible. Therefore, the complete model, Drag model will be used in the following.

5.1.1.2 Surface Tension

This force was assessed with different values inside Drag Model, which is considered the most suitable model to obtain a bubble dimension at the end of the first stage. Fig.5.17 highlights the negligible effect of changing the surface tension from a high value, for instance as the one for water up to zero which means that the surface tension term disappears from the balance. A negligible effect of surface tension can be seen for the high gas flow rates values and the instantaneous formation of a bubble in the first stage. Furthermore, increasing the gas flow rate, terms as difference of pressure and gas momentum prevails above surface tension force.

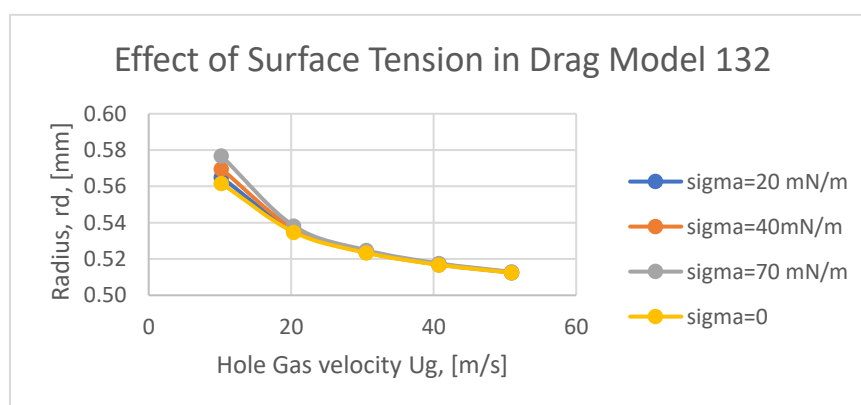


Fig.5.17: Effect of Surface Tension in Drag Model.

5.1.1.3 Gas density

In the evaluation of gas density effect, it must be recalled that it appears in several terms as the gas momentum, difference of pressure, gravity and inertia term and its value is very important for the bubble dimension determination. If gas density is increased, gas momentum and difference of pressure forces are stronger, then, bubble size is reduced because the bubble starts rising in a smaller time. This effect is shown in Fig. 5.18.

Besides, gas density varies with pressure and temperature conditions; increasing pressure gas density increases. Considering air at 25°C with a pressure of 8MPa the gas density through gas ideal equation is about 94 Kg/m³. Another example is to consider the bubble at elevated pressure of 16MPa and elevated temperature as 500°C, as in industrial conditions, in this case, gas density is reduced of about 70 Kg/m³, however, it is still elevated.

In conclusion, it is also important consider the variation of gas density with pressure and temperature because it affects in a considerable way bubble size at the end of the first stage as shown in Fig. 5.18.

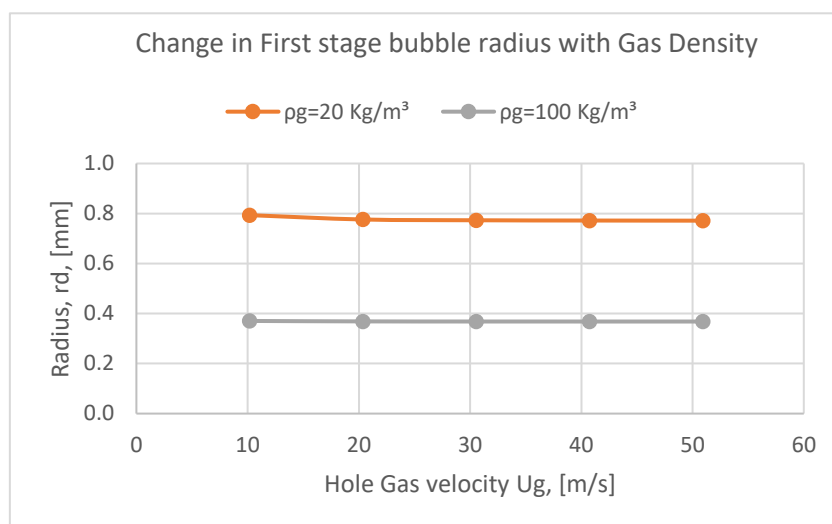


Fig.5.18: Effect of Gas density in the First Stage bubble formation process.

5.1.1.4 Effect of Liquid Density

Through Fig.5.19 is possible to assess bubble size at the end of the first stage with different liquid density values, that is, with different liquid phases. The lower value assessed in this analysis is 700 Kg/m³ and it can be associated with a hydrocarbon liquid mixture and the higher value of liquid density evaluated is 1000 Kg/m³ that can be easily associated to water or an aqueous solution.

The presence of a denser liquid phase inside the reactor causes the higher bubble radius at the end of the first stage of bubble formation process, as shown in Fig.5.19, and it is reasonable because the static pressure at the bottom of the reactor will be higher and the bubble will remain attached to the sparger it will continue to grow for a longer time. Furthermore, with a higher liquid density value drag and inertia force are stronger which enhance the effect of bubble remaining more time attached to the sparger.

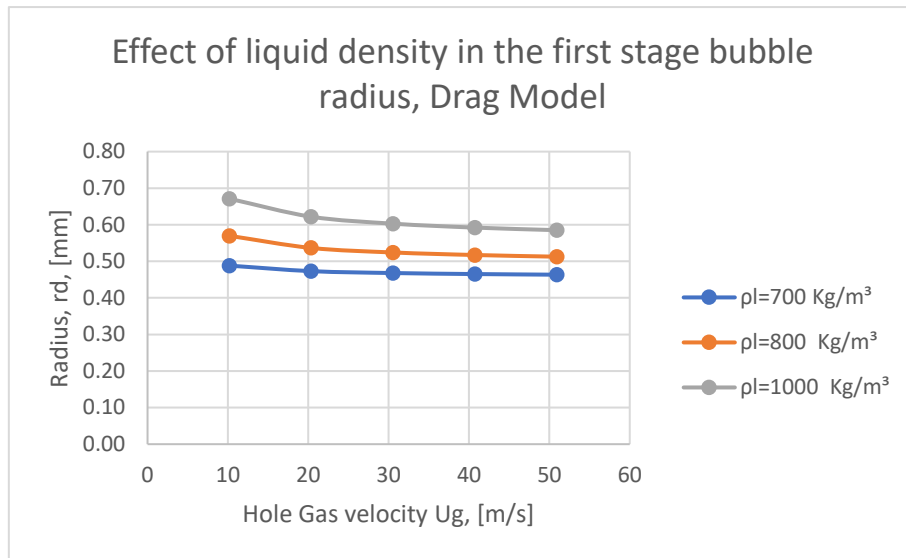


Fig.5.19: Effect of Liquid density in Firs stage bubble formation process.

5.1.1.5 Effect of Hole Diameter

In Fig 5.20 it is possible to appreciate the increment on bubble size at the end of the first stage with a bigger hole which is lighter bigger than the double for a hole diameter increment from 1 mm to 2 mm. Using the Drag Model, bubble radius at the end of the first stage for a hole diameter is 15% bigger than hole dimension; then for a hole diameter of 2 mm the increment on bubble diameter at the end of the first stage is around to 30%, so, it is twice the previous increment. It is evident from Fig. 5.20 that increasing hole diameter the bubble size at the end of the first stage increases. This assessment was done with data from Table 5.1 which has a hole diameter 1 mm and gas density is considered constant; then, the same data was used but changing the hole diameter to the double.

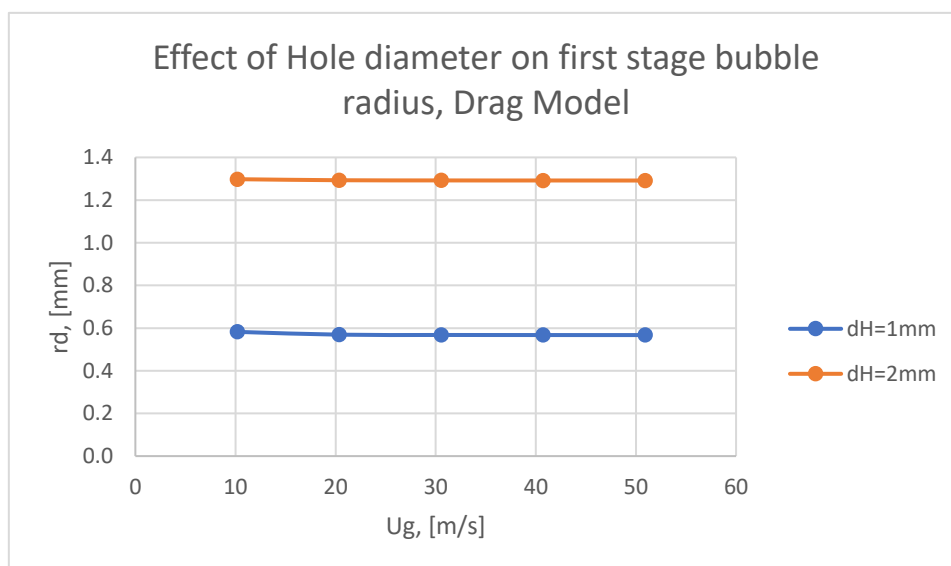


Fig.5.20: Effect of hole diameter on the bubble radius in the first stage, Drag Model.

5.1.2 Second Stage

When the bubble continues to expand and start to rise is the moment in which second stage has begun. During this stage, the bubble base starts to lift, in consequence, a gas neck is formed, and it will be reduced in width until detachment moment arrives. For the first stage, the addition of terms to Original Model 1, for instance, the addition of pressure difference term has demonstrated to have a great impact. As a consequence, is also investigated its effect over the final bubble dimension at detachment.

Fig. 5.16 shows the effect of adding terms to Original Model 1 in the bubble radius at detachment moment when the second stage is over. The results are similar to the addition of terms in the first stage.

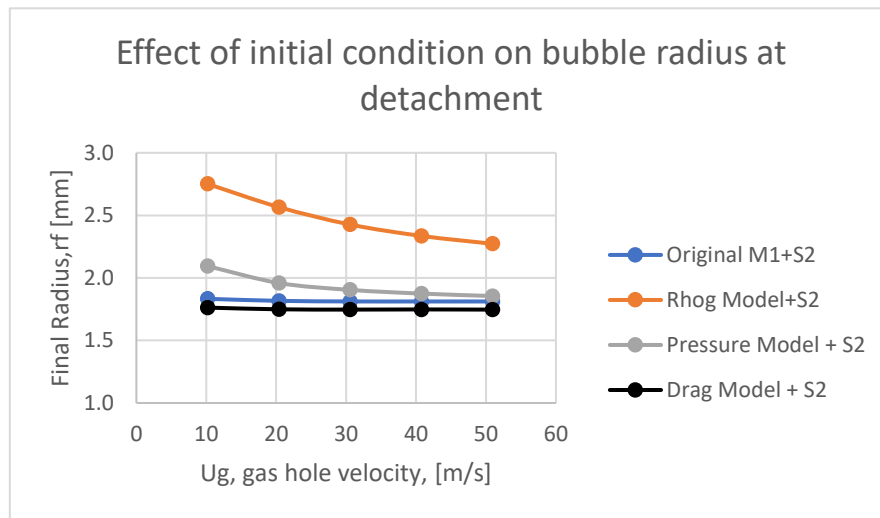


Fig.5.21: Effect of adding terms to Original Model 1 in the final radius at detachment.

However, it is possible to evaluate how much the bubble grows during the second stage until its released. It is important to remember that the radius obtained in the first stage is considered as the initial position of the bubble center of mass for the second stage model. Then, the results are presented in Table 5.3 and the data introduced in each stage comes from Table 5.1 in which the hole diameter, dH , is 1 mm.

Table 5.3. Bubble size results for each stage of bubble formation process.

Ug [m/s]	1 st Stage, rd [mm]	2 nd Stage, rf [mm]	$\Delta r_{12}=rf-rd$ [mm]
10.2	0.570	1.762	1.192
20.4	0.537	1.749	1.212
30.6	0.524	1.747	1.223
40.7	0.517	1.748	1.231

The observations are be done for the Drag Model representing the first stage plus the second stage (S2) represented by the system of differential equation, Eq.3.161 and Eq.3.162 because these 2 models represent together the final bubble formation model for this work. Then, from Table 5.3 is distinguished that about 30% of bubble radius is formed during the first stage

and the final 70% is formed during the second stage. This can be translated as a bubble formed almost instantaneously and then continues to grow in the second stage where it expands and rises at the same time.

5.2 Bubble formation Model validation

In this section some results for the bubble formation model divided in Stage 1 and 2 and explained earlier in Chapter 3 will be presented. It was considered a water-air system for this analysis at different pressure conditions and hole diameters. In table 5.4 are shown the fluid properties, the operating and geometric parameters introduced in the MATLAB program to obtain a bubble dimension for each stage. Besides, the results obtained were compared with experimental data from literature.

Table 5.4. Water-Air system. Data required for First Stage.

Fluid Properties			Operating Conditions		
μ_g	$1.983 \cdot 10^{-5}$	[Pa.s]	G	$[0.1 - 40] \cdot 10^{-6}$	$[m^3/s]$
σ	72	[N/m]	P	$[0.1 - 8.1] 10^6$	[Pa]
ρ_L	1000	$[Kg/m^3]$	T	25	[°C]
μ_L	$1 \cdot 10^{-3}$	[Pa.s]	Hole Geometry		
α	11/16	[-]	C_o	0.801	
MW	$29 \cdot 10^{-3}$	[Kg/mol]	r_H	$[1 - 2] \cdot 10^{-3}$	[m]
R	8.314	$[Pa \cdot m^3 / mol \cdot K]$	Constants		
%solid	0.05	[-]	g	9.81	$[m/s^2]$

The gas density was considered to vary with the ideal gas law and it depends on pressure and temperature system. Then, surface tension is also considered to vary with pressure according a correlation proposed by [22] in Eq. 5.220,

$$\sigma = [\sigma_o - 0.8243P_s + 0.01891P_s^2] * 0.001 \quad \text{Eq. (5.220)}$$

where, σ_o is the surface tension in atmospheric condition in mN/m and P_s is the pressure system in MPa, then, σ is obtained in N/m.

Besides, liquid viscosity must consider the solid suspended inside these reactors. The relationship employed to calculate the liquid viscosity is expressed in Eq. 5.221, and it was called apparent viscosity by [22],

$$\mu_{app} = \mu_L [1 + 2.5\epsilon_S + 10.05\epsilon_S^2 + 0.00273 \exp(16.6\epsilon_S)] \quad \text{Eq. (5.221)}$$

where, μ_L is the liquid viscosity in Pa.s and ϵ_S is the solid particle holdup.

In Fig.5.22 is shown the result from the bubble formation model at two different pressure 1MPa and 6.1MPa, for a hole diameter equal to 1.18mm. The equation used to obtain these results were Eq.3.105 for the first stage bubble formation with a drag coefficient in Eq.3.89 and the differential system of equations constituted by Eq. 3.161 and Eq.3.162 to obtain the bubble dimension at detachment moment with a drag coefficient in Eq. 3.89 and with initial bubble position equal to the radius at the end of the first stage and initial velocity equal to zero. The

data used to obtain these results are in Table 5.4. Then, the outcome of the bubble formation model was compared with literature data in [61].

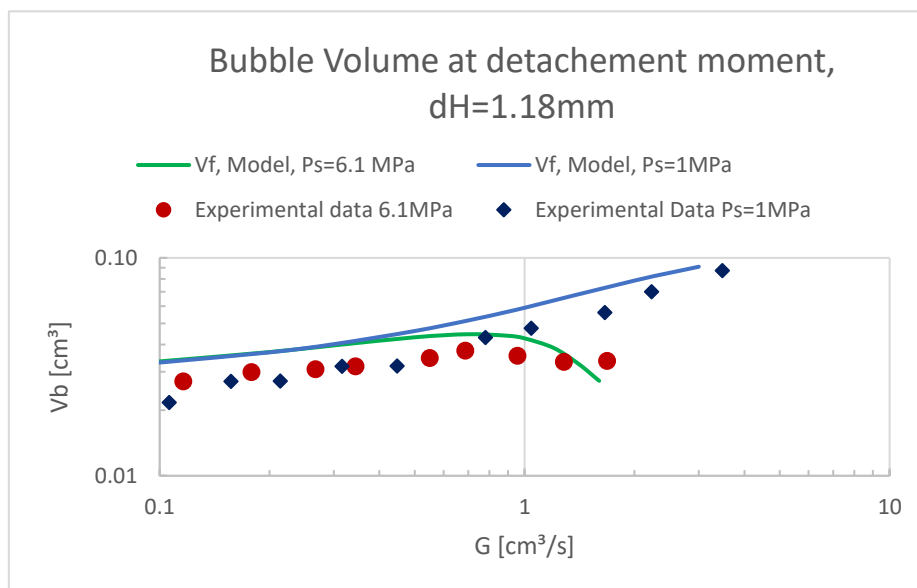


Fig.5.22: Bubble detachment volume with system of different pressure.

It is possible to observe in Fig.5.22 the effect of pressure from the model and from experimental data [61]. First at all, the tendencies for the lines representing the model assessed with different pressure agree the experimental data set shown in Fig.5.22. Then, it is possible to notice a downward trend from the model when the gas flow rate increases at elevated pressure. In contrast, the bubble dimension tends to increase at low pressure when gas flow rate is increased. It is also important to notice that for low gas flow rate the effect of pressure is almost negligible for both experimental and for model results.

The model has been evaluated also for atmospheric pressure and it has been compared with literature data. The results are shown in Fig. 5.23.

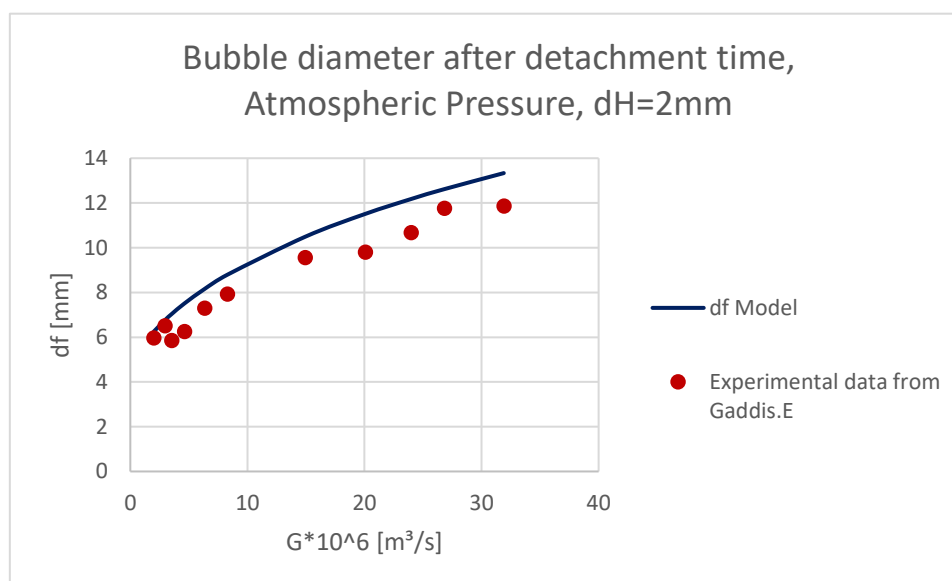


Fig.5.23: Bubble detachment diameter at ambient pressure.

In Fig.5.23 is shown a good agreement between the model result and the experimental data from Gaddis [21]; the model average deviation from the experimental data was about 12%. Then, it is possible to notice again an upward trend in bubble dimension with gas flow rate at low pressure. The discrepancies between the model and the experimental data presented in Fig. 5.22 and 5.23 could be attributed to the assumptions in which the model presented in this work is based on, for instance the shape which is considered spherical and the detachment criterion which is very important in the determination on the bubble dimension.

5.3 Transition to jetting regime

This section is related to the validity of the bubble formation model explained in Chapter 3 and it is restricted to the zone near the sparger where, according the gas flow rate, are recognized different bubble regimes: bubbling regime, chain bubbling regime and jetting regime, as shown in Fig.5.24.

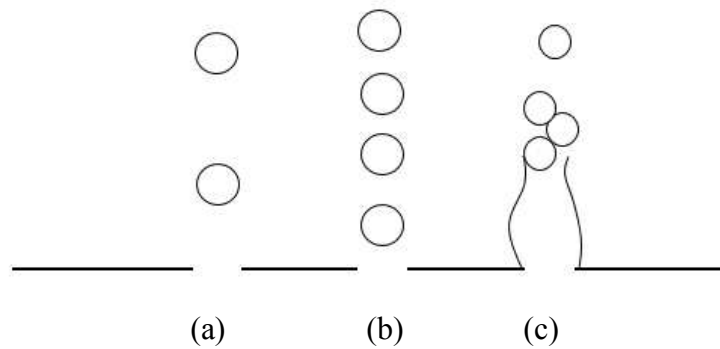


Fig.5.24: Flow regimes near the sparger zone. (a) Bubbling regime, (b) Chain Bubbling regime and (c) Jetting regime.

Several works, [21,36,38], were reviewed to adopt the definition of Weber dimensionless number as the base for the transition to jetting regime criterion. Weber number is defined as in Eq. 5.222.

$$We = \frac{16\rho_g G^2}{\pi^2 d_h^3 \sigma} \quad \text{Eq. (5.222)}$$

where, ρ_g is the gas density, d_h is the hole diameter, G is the gas flow rate at hole and σ is the surface tension. The Weber number criterion is based on the belief that when gas momentum exceeds surface tension force a jet starts developing. In the literature a critical value of Weber number equal to 4 was identified to guarantee the presence of jetting regime. However, the jetting regime is also in systems where the Weber number value is 1-2, [38].

For this reason, it was built some plots to evaluate the critical gas flow rate in function of pressure which are two operating parameters set up normally for bubble columns reactors. The critical gas flow rate representing We equal to 4 is defined in Eq. 5.223,

$$G_{We=4} = \frac{\pi^2 d_h^3 \sigma}{4\rho_g} \quad \text{Eq. (5.223)}$$

Then, a lower boundary to find jetting phenomenon is defined with We equal to 1 as in Eq. 5.224,

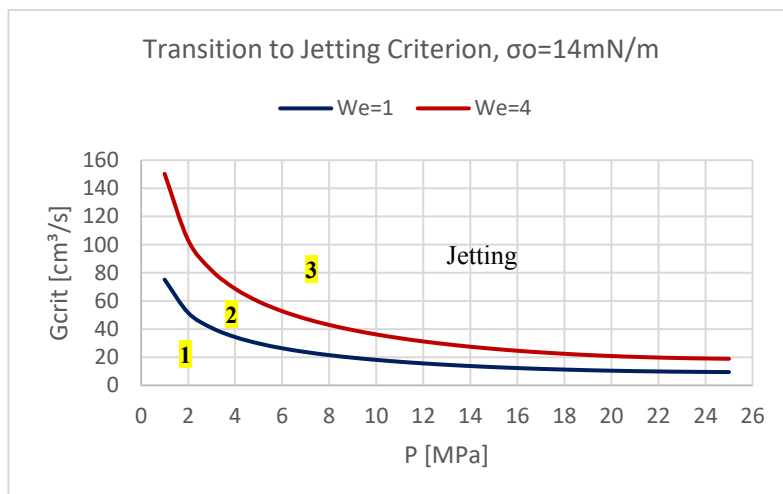
$$G_{We=1} = \frac{\pi^2 d_h^3 \sigma}{16\rho_g} \quad \text{Eq. (5.224)}$$

To evaluate these two boundaries, it was considered that gas density varies with pressure according the ideal gas law and surface tension varies with pressure according Eq.5.225,

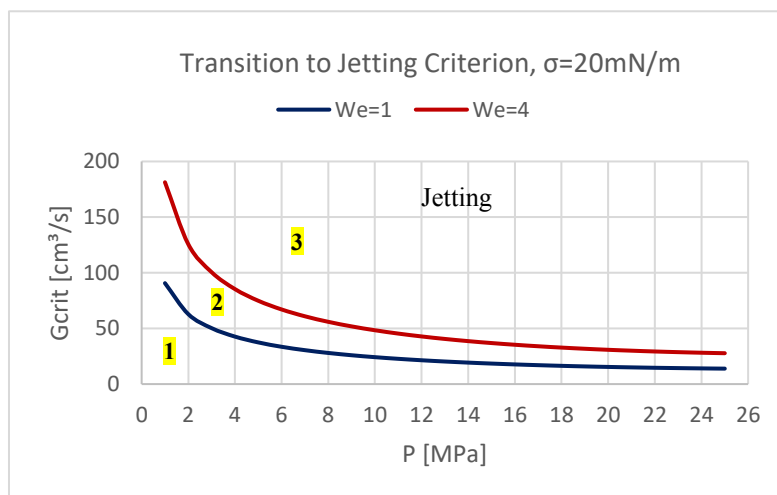
$$\sigma = [\sigma_o - 0.8243P_s + 0.01891P_s^2] * 0.001 \quad \text{Eq. (5.225)}$$

where, σ_o is the surface tension in atmospheric condition in mN/m and P_s is the pressure system in MPa, then, σ is obtained in N/m.

Fig. 5.25 (a) and 5.25 (b) show a critical gas flow rate evaluation with pressure for a hole diameter equal to 6 mm and different surface tension values, 14 and 20 mN/m.



(a)



(b)

Fig.5.25: Critical gas flow rate evaluation, (a) $\sigma_o=14$ mN/m and (b) $\sigma_o=20$ mN/m

These two values of surface tension, 14 mN/m and 20 mN/m were chosen because could represent well the behavior of a hydrocarbon liquid mixture at elevated pressure and temperature.

Then, it is possible to identify 3 zones in Graphs in Fig. 4.25, zone number 1 is limited for the line representing We equal to 1, below this line is found the bubbling zone. Then, zone 2, between line red and blue represents a transition zone where jetting could appear or not. Above the red line representing We equal to 4, jetting occurs in zone 3. Bubble formation model presented in chapter 3 is considered to be valid in zone number 1.

Furthermore, Fig. 5.25 shows 2 graphs for the same conditions but different surface tension values, and it is possible to notice that for a higher value of surface tension the boundaries lines move forward to a higher conditions of critical gas flow rate, then, the bubbling zone grows.

Then, the effect of changing the hole diameter value which influences Weber number is analyzed, taking a constant value for surface tension equal to 20mN/m. Fig. 5.26 and 5.27 show the behavior of the edge lines with the reduction of hole diameter.

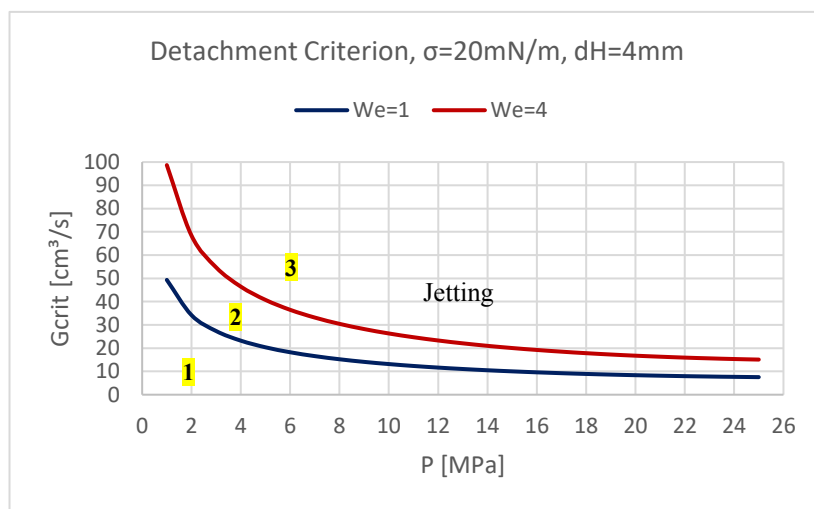


Fig.5.26: Critical gas flow rate evaluation for a hole diameter equal to 4mm.

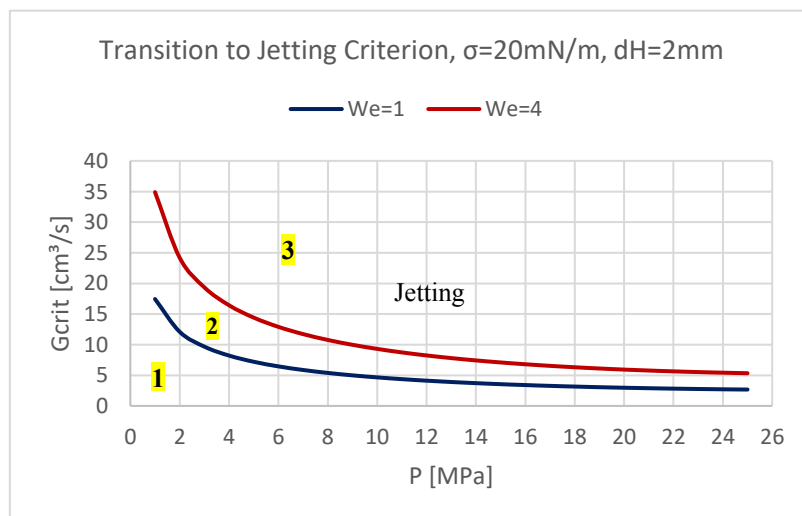


Fig.5.27: Critical gas flow rate evaluation for a hole diameter equal to 2 mm.

The reduction of hole diameter shrunk the bubbling zone, that is, move boundary lines forward a lower values of critical gas flow rate. With a hole diameter of 6 mm in Fig.5.25 (b) and low pressure of 2MPa is possible to reach 50 cm³/s inside the bubbling zone but with a hole diameter equal to 2mm in Fig.5.27 for a low pressure equal to 2 MPa the critical gas flow rate is reduced to 10 cm³/s.

5.4 Combined Momentum, Heat and Mass transfer model

In table 5.5 is presented the input data required to solve the combined momentum, heat and mass transfer model by means of MATLAB.

Table 5.5. Oil Liquid Mixture-Hydrogen system. Data required.

Data for Mass Transfer			Data for Velocity		
Liquid Components			Initial Condition Values		
“A” [Heptane]	C_7H_{16}		n_{Ao}	0	[mol]
“K” [Eicosane]	$C_{20}H_{42}$		T_o	773	[K]
“G” [Hydrogen]	H_2		L_o	<i>These 3 values are result of the second stage of the bubble formation model at detachment.</i>	[m]
M_A	0.114	$\frac{Kg}{mol}$	Y_o		[m]
M_G	$2 \cdot 10^{-3}$	$\frac{Kg}{mol}$	U_{to}		m/s
M_K	$282.56 \cdot 10^{-3}$	$\frac{Kg}{mol}$	Operating Conditions		
\mathcal{D}_{AG}	$7 \cdot 10^{-9}$	$[m/s^2]$	G	$24 \cdot 10^{-6}$	$[m^3/s]$
ρ_A	684	$[Kg/m^3]$	P	$16 \cdot 10^6$	[Pa]
ρ_K	788.6	$[Kg/m^3]$	T	773	[K]
ρ_L	725	$[Kg/m^3]$	T_L	633	[K]
μ_L	$0.4 \cdot 10^{-3}$	$[Pa \cdot s]$	r_H	$3 \cdot 10^{-3}$	[m]
μ_G	$1.618377 \cdot 10^{-5}$	$[Pa \cdot s]$	Constants		
$\Delta H_{vap}(350K)$	35500	$[J/mol]$	Antoine's Parameters		
σ	$14 \cdot 10^{-3}$	$[N/m]$	A	4.02832	[-]
$\hat{C}_{p,G}$	29.6	$\frac{J}{mol \cdot K}$	B	1268.636	[-]
$\hat{C}_{p,A}^{vap}$	317.15	$\frac{J}{mol \cdot K}$	C	-56.199	[-]
$\hat{C}_{p,A}^{liq}$	217	$\frac{J}{mol \cdot K}$	C_o	0.801	[-]
\hat{C}_p^{liq}	1903	$\frac{J}{Kg \cdot K}$	R	8.314	$[Pa \cdot m^3/mol \cdot K]$
k	$392 \cdot 10^{-3}$	$\frac{W}{m \cdot K}$	%solid	0.05	[-]
C_{tot}	4800	$[mol/m^3]$	g	9.81	$[m/s^2]$
X_{AL}	0.5	$[mol/m^3]$	α	11/16	[-]

It will be studied a hydrocarbon liquid mixture with hydrogen gas coming from the gas distributor at real operating conditions in the region near the sparger where bubbles are formed. The aim of this section is to present the results of the first order differential system of equations developed in section 3.2 for the variables, bubble diameter, L , bubble position, y , bubble velocity, U_t , bubble temperature, T and moles of component “A” evaporated and added to the bubble volume after detachment, n_A .

To obtain results for the model exhibited in section 3.2 is required to find the bubble diameter, velocity and position at detachment moment, so, it must be used the 2 stages bubble formation model to obtain the initial conditions for the combined momentum, heat and mass transfer model. The drag coefficient used for the bubble formation model and the combined model is the one exhibited in Eq. 5.227 by [58].

The result for this combined model were five plots exhibited in Fig.5.28, Fig.5.29, Fig.5.30, Fig.5.31 and Fig.5.32. Overall, graphs show an unsteady behavior during the first 4 seconds and then profiles reach a stationary value of the variable being assessed with the exception of Fig.5.26 which represent the bubble center of mass position. In Fig.5.28 is possible to identify the final bubble diameter after the heat and mass transfer processes are carried out; the bubble grows and in Fig.5.30 is possible to see the number of moles of the liquid component “A” which evaporates and have been incorporate to the bubble volume.

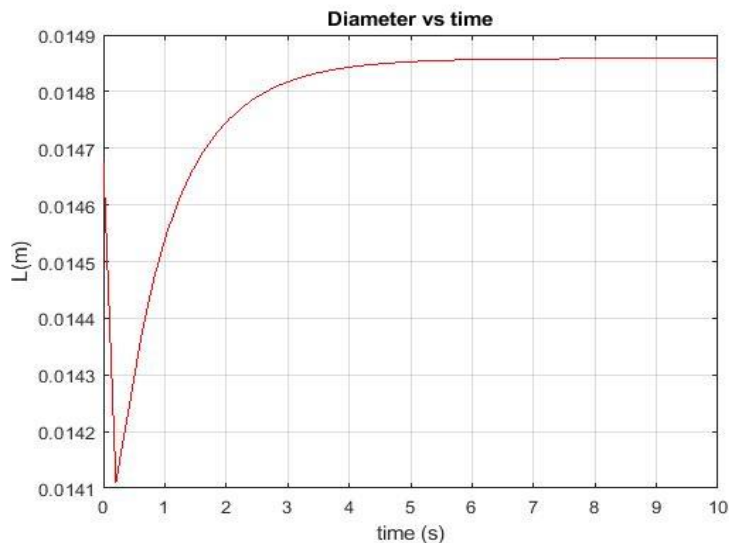


Fig.5.28: Diameter evolution with time after detachment.

In Fig. 5.28 the steady bubble diameter value after detachment was 1.486 cm which is 1.25% bigger than detachment diameter, a difference in diameter which is not considered significant. Then, is possible to notice sudden decrease of the diameter during the first milliseconds and this is associated to the important decrease in temperature of the bubble shown in Fig.5.29, that is, the bubble cooled because the difference of temperature with the liquid around and because the evaporation of an amount of liquid around.

Then, it is possible to see in Fig. 5.29 that the temperature increases until the liquid temperature, the bubble is heated because the mass transfer process continues for a few seconds more as shown in Fig.5.30.

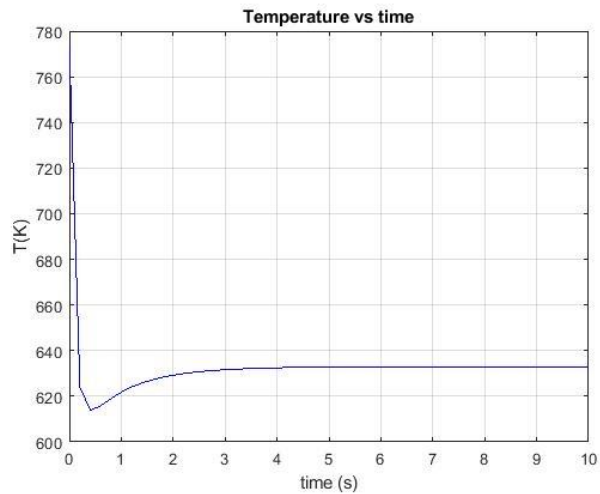


Fig.5.29: Bubble temperature profile after detachment.

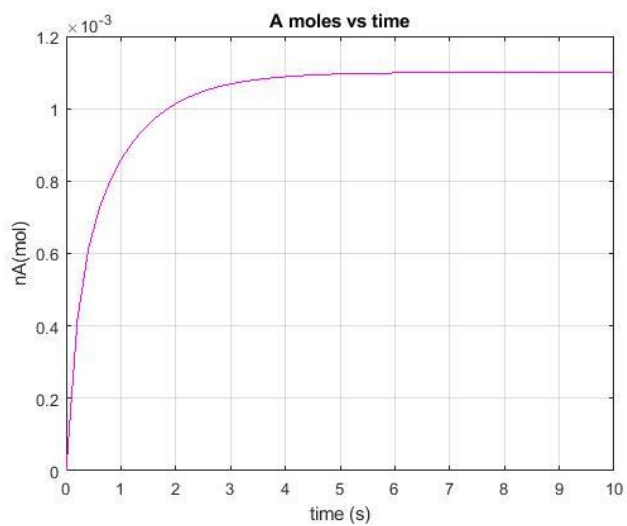


Fig.5.30: Moles of A variation with time.

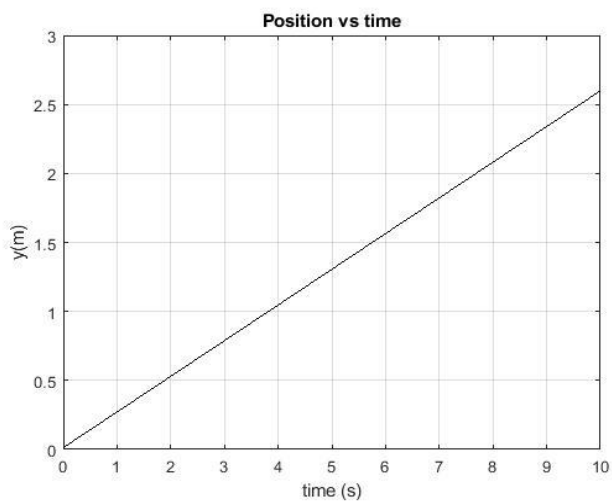


Fig.5.31: Bubble center of mass position with time.

In Fig.5.23 it is possible to appreciate the bubble velocity profile and that a terminal velocity is reached in some milliseconds after detachment; the increment on velocity respect the bubble velocity at detachment is around to 15%.

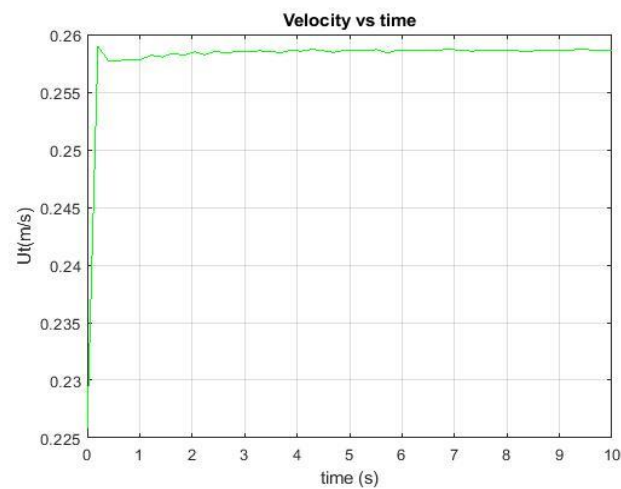


Fig.5.32: Bubble velocity profile with time.

5.4.1 Effect of hole diameter

The results above, that is, graphs in Fig.5.28, Fig.5.29, Fig.5.30, Fig.5.31 and Fig.5.32 were obtained with data in Table 5.5. The hole diameter specified in table 5.5 was 6 mm and because the hole diameter is an important geometric parameter which influence the bubble dimension during its formation it will be assessed its influence on the bubble dimension after the bubble is detached.

For this analysis will be used just the first graph presented in the previous section, section 5.4, the graph for the bubble diameter evolution with time after detachment for different sparger hole dimension.

Fig.5.33, Fig.5.34, Fig.5.35 and Fig.5.36 show the bubble diameter evolution with time for different sparger orifice dimension, 1mm, 2mm, 4mm and 6mm.

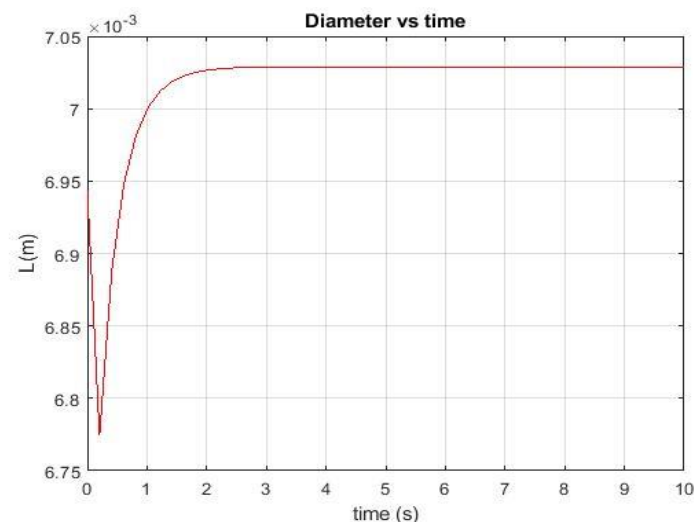


Fig.5.33: Bubble diameter evolution after detachment. $d_H=1\text{mm}$.

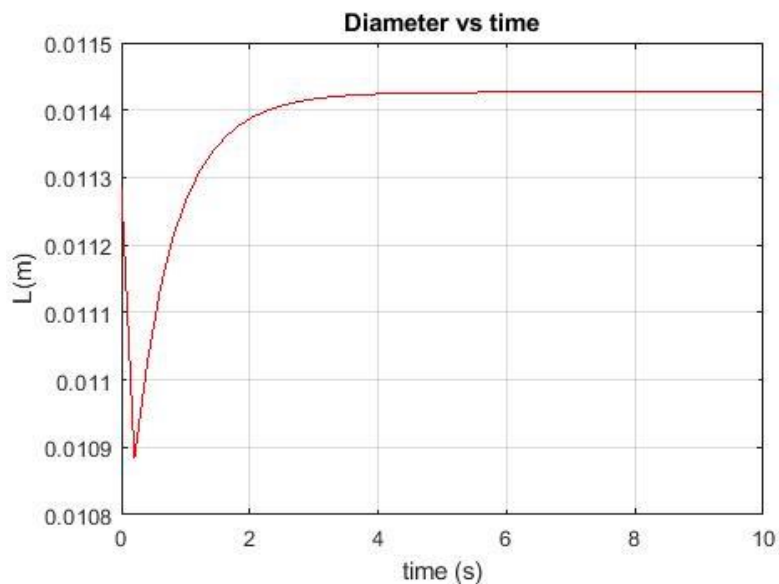


Fig.5.34: Bubble diameter evolution after detachment. $dH=2\text{mm}$.

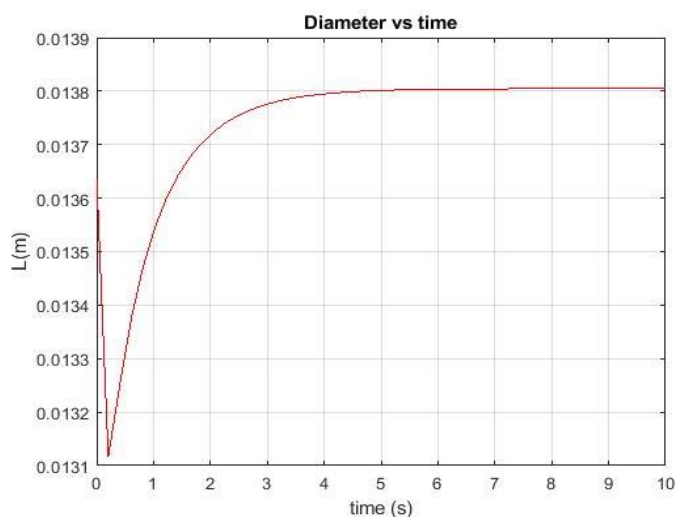


Fig.5.35: Bubble diameter evolution after detachment. $dH=4\text{mm}$.

The results of this analysis are summarized in Table 5.6 presented below.

Table 5.6.Effect of hole diameter on bubble dimension after detachment.

dH [mm]	1st Stage, rd [mm]	2nd Stage, Lo [cm]	Vo, 2nd Stage[cm³]	Combined Model Final size, Lf,[cm]	Vf, After detachment [cm³]	$\Delta V= Vf-V_0$, [cm³]
1	1.2680	0.6943	0.17524	0.7025	0.1815	6.26×10^{-3}
2	2.5151	1.1287	0.7529	1.142	0.7798	0.0269
4	3.3404	1.3636	1.3276	1.38	1.3761	0.0485
6	3.5291	1.4677	1.6554	1.486	1.7181	0.0627

The examination of hole diameter impact on the final bubble dimension after detachment reveals that the increment in the hole diameter on the gas distributor produce and increment on the bubble final dimension after detachment. In general, the increment on bubble volume with respect to the bubble volume at detachment due the process of mass and heat transfer after detachment was on average 3.6% with properties established in table 5.5 and for the different hole diameter assessed in section 5.4.1.

5.4.2 Effect of Vapor pressure

Vapor pressure of the component “A” in the liquid mixture is an important property related to how much the bubble will grow after detachment because when the vapor pressure is larger the liquid is more volatile, that is, it tends to evaporate easier.

The component “A” assessed in section 5.4 is heptane and it is supposed to evaporate and make the bubble grow, nevertheless, its vapor pressure is not high enough to obtain an important increment of bubble volume after detachment.

The aim of this section will be assessed the effect of increasing vapor pressure on the final bubble dimension after detachment. A bigger vapor pressure could be obtained changing the component “A” in the liquid mixture by a more volatile hydrocarbon, for instance, hexane or pentane. However, instead of changing the component “A” which require the change of all properties set up in Table 5.5, the vapor pressure of component “A”, heptane, will be enlarged with a coefficient, k_1 , during the calculations to achieve the aim of this section.

Fig. 5.36, Fig. 5.37, Fig.5.38, Fig.5.39 and Fig.5.40 shows the diameter evolution with time after detachment for different coefficient, k_1 .

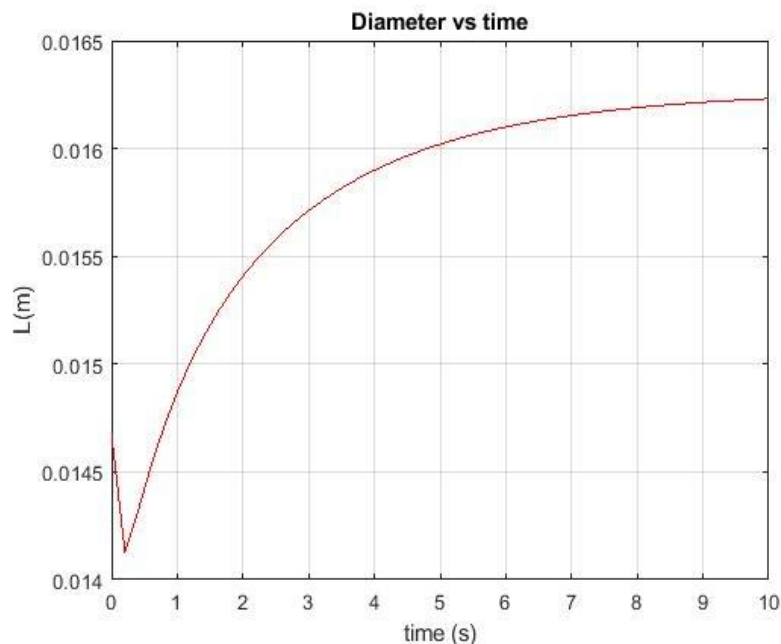


Fig.5.36: Bubble diameter evolution after detachment. data from Table 5.5, $k_1=1.892$.

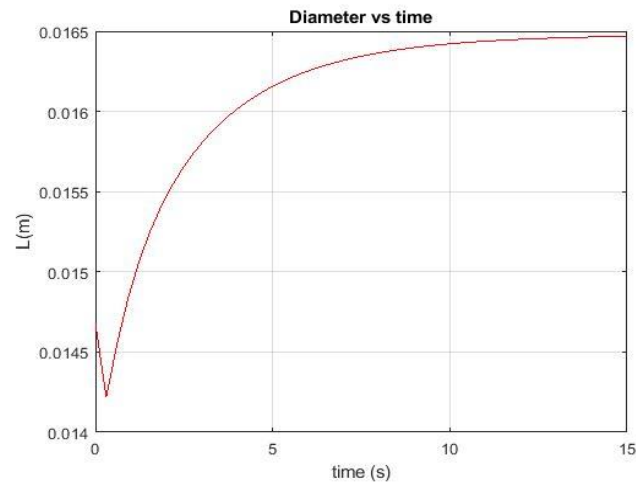


Fig.5.37: Bubble diameter evolution after detachment. data from Table 5.5, $k_1=2$.

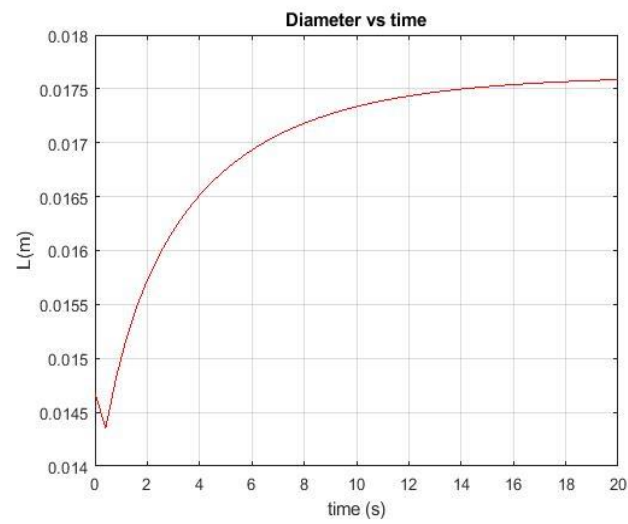


Fig.5.38: Bubble diameter evolution after detachment. data from Table 5.5, $k_1=2.37$.

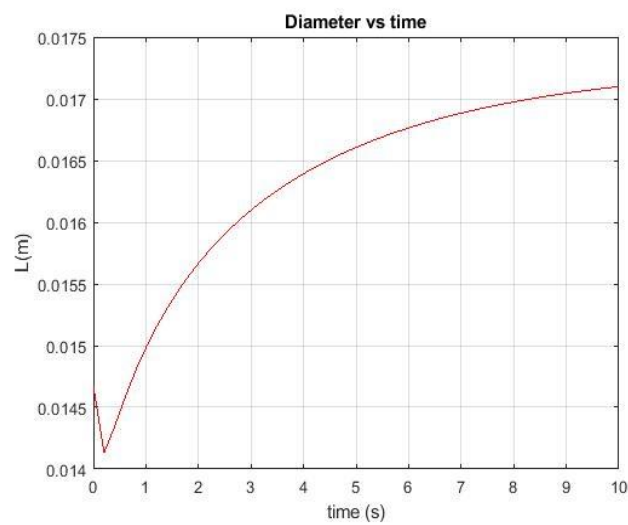


Fig.5.39: Bubble diameter evolution after detachment. data from Table 5.5, $k_1=2.5$.

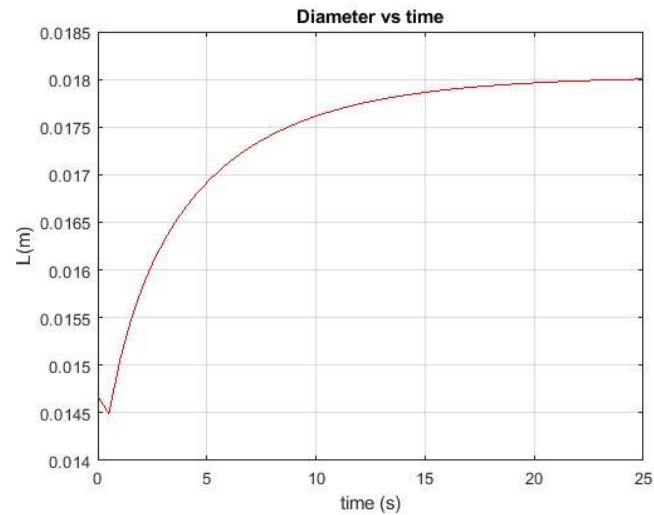


Fig.5.40: Bubble diameter evolution after detachment. data from Table 5.5, $k_1=2.65$.

Table 5.7 presents the results of this analysis in terms of change of bubble diameter after detachment and Table 5.8 presents results in terms of change of bubble volume after detachment.

Table 5.7.Effect of vapor pressure on bubble diameter after detachment.

T[K]	Psat(T) C7H16[MPa]	$k_1 \cdot \text{Psat(T)}$ C7H16[MPa]	Lo 2 nd Stage [cm]	Lf [cm]	$\Delta d = L_f - L_o$ [cm]
660	8.4574	$1.892 \cdot \text{Psat(T)}$	1.4677	1.62	0.1523
654	8.056	$2 \cdot \text{Psat(T)}$	1.4677	1.65	0.1823
633	6.7435	$2.37 \cdot \text{Psat(T)}$	1.4677	1.71	0.2423
628	6.4514	$2.5 \cdot \text{Psat(T)}$	1.4677	1.751	0.2833
624	6.0377	$2.65 \cdot \text{Psat(T)}$	1.4677	1.8	0.3323

Table 5.8.Effect of vapor pressure on bubble volume after detachment.

T[K]	Psat(T) C7H16[MPa]	$k_1 \cdot \text{Psat(T)}$ C7H16[MPa]	Vo 2 nd Stage, [cm ³]	Vf, combined Model, [cm ³]	$\Delta V = V_f - V_o$ [cm ³]
660	8.4574	$1.892 \cdot \text{Psat(T)}$	1.6554	2.226	0.571
654	8.056	$2 \cdot \text{Psat(T)}$	1.6554	2.352	0.697
633	6.7435	$2.37 \cdot \text{Psat(T)}$	1.6554	2.618	0.9626
628	6.4514	$2.5 \cdot \text{Psat(T)}$	1.6554	2.811	1.1556
624	6.0377	$2.65 \cdot \text{Psat(T)}$	1.6554	3.054	1.3986

The objective of include k_1 was increase the vapor pressure of the liquid mixture to simulate a more volatile compound and to enhance the evaporation of liquid around the bubble.

Table 5.8 shows that the increment on vapor pressure results in an increment on the bubble volume after detachment due the evaporation of more liquid around the bubble; the bigger is the coefficient k_1 , bigger is the stationary bubble diameter after detachment. With the highest coefficient, k_1 equal to 2.65 the increment in volume was about 84% respect the bubble volume at detachment. Even with the lowest coefficient, k_1 equal to 1.892, the increment in volume was about 34% respect the bubble volume at detachment. Comparing these results with the result obtained with a k_1 equal to 1, specified in the last line of table 5.6 where the increment in volume was about 4% respect the detachment volume, it is possible to demonstrate that the effect of increment on bubble volume after detachment due to the liquid evaporation around the bubble is more pronounced when the vapor pressure is higher, so, when a more volatile liquid hydrocarbon is present in the liquid phase.

5.4.3 Effect of drag coefficient

During the modeling of bubble velocity and position different drag coefficient expressions were evaluated to obtain the most reasonable result of the bubble position and velocity through its rising inside the reactor.

The equation to be evaluated in this analysis will be, Eq.5.226 and Eq.5.227 which were considered the most accurate for the process of bubble formation and bubble ascension after detachment.

$$C_D = \frac{18.5}{Re_B^{0.6}} \quad \text{for } 2 \leq Re_B \leq 500, \text{ according [23]} \quad \text{Eq. 5.226}$$

$$C_D = \max\left[\frac{24}{Re_B} (1 + 0.15Re_B^{0.687}), \frac{8}{3} \frac{Eo}{Eo+4}\right] \quad \text{according to [58]} \quad \text{Eq. 5.227}$$

Using data from Table 5.5 will be shown in Fig.5.41 the position and the velocity obtained with drag coefficient exhibited in Eq. 5.226; first, it will be used in the balance of forces for each stage inside the bubble formation process until detachment and then, for the combined momentum, heat and mass transfer associated to the bubble after detachment.

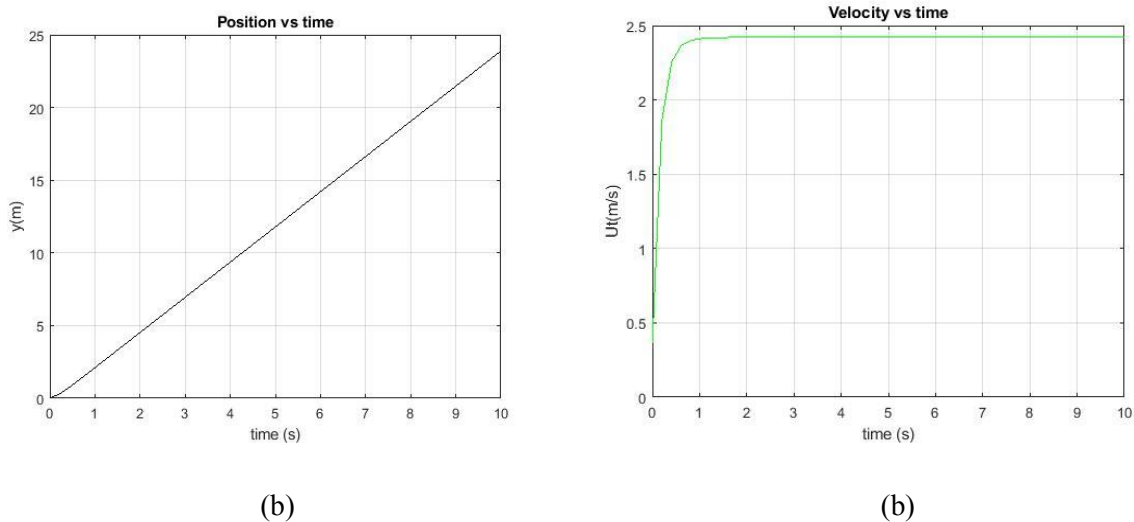


Fig.5.41: Bubble position (a) and bubble velocity (b) after detachment, drag coefficient expression Eq.5.226.

Using the same data from Table 5.5 will be shown in Fig.5.42 the position and the velocity obtained with a different drag coefficient expressed in Eq.5.227 and designed for contaminated water by [58]. Eq.5.227 has been employed in the bubble formation process exhibited in Chapter 3 and then, inside the equations for the combined momentum, heat and mass transfer model associated to the bubble after detachment to obtain the final results in section 5.4.

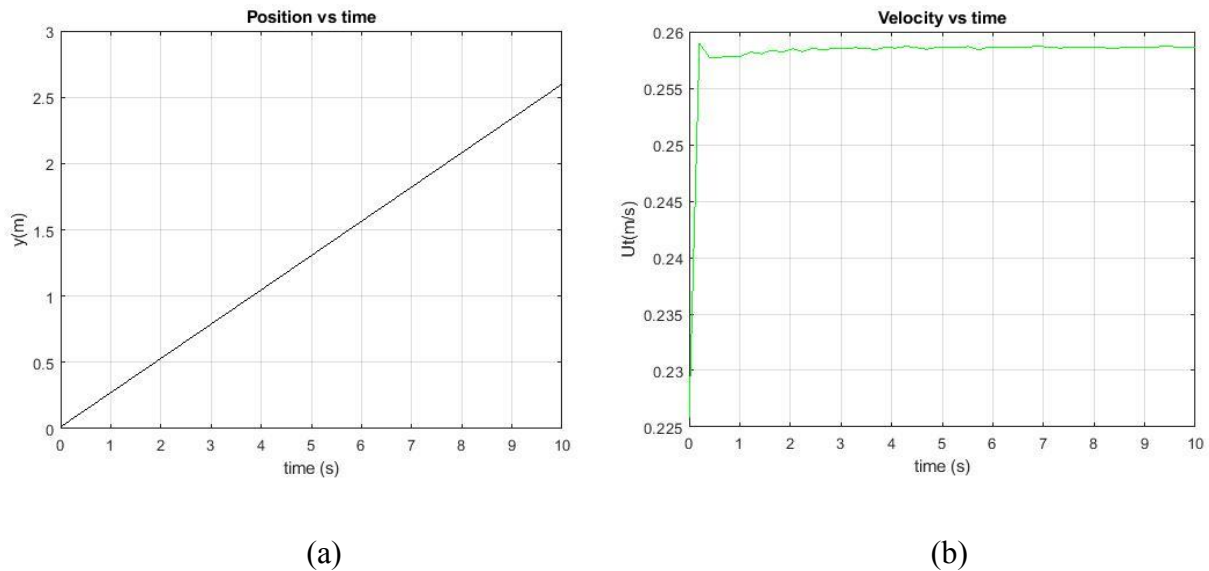


Fig.5.43: Bubble position (a) and bubble velocity (b) after detachment, drag coefficient expression Eq.5.227.

The results in section 5.4, which are 5 graphs for the different variable being studied after detachment, shown that in a time of 4 seconds the variables, diameter, temperature, moles of component “A” evaporated, and velocity reach a steady value. Then, Fig.5.41 which represent the bubble center of mass shown that in 4 seconds the bubble has ascended around 9 meters and it has reached a steady velocity of 2.4 m/s; these 2 values of position and velocity obtained with Eq.5.226 were compared with bubble terminal velocities in experimental data from [51] and those are extremely large and not physical.

In contrast, the results obtained for drag coefficient in Eq.5.227 show a more realistic representation of what is happening inside the reactor regarding to the bubble ascension; the values of position and velocity found in Fig.5.43 and Fig. 5.44 in 4 seconds were 1 meter of bubble ascension and a terminal velocity about 0.26 m/s which is more coherent with experimental data from [62].

As consequence of this analysis the final drag coefficient recommended for the bubble formation process until detachment and a posterior analysis after detachment is the one in Eq.5.227 proposed by Tomiyama et.al. [58].

Chapter 6

Conclusions

The main objective of this thesis project was to determine the bubble dimension near the sparger region in a slurry gas-liquid reactor at detachment moment and after detachment when a process of heat and mass transfer processes take place during the bubbling motion inside the reactor. To reach this objective there were developed different tasks to present now the final conclusions:

1. The two stages bubble formation model proposed in this thesis project was assessed with a water-air system for different pressure conditions and hole diameters and it was found to agree properly with the tendencies in the experimental data. However, the model overestimate in 20% average the bubble volume at detachment at elevated pressure. Then, at low pressure the average deviation of the model was found 12% respect experimental data found in literature. This error can be associated with model assumptions as the spherical shape and the bubble detachment criterion.
2. From the sensitivity analysis carried out for the first stage of the bubble formation model it was found that terms as the difference of pressure between gas and liquid at the orifice is very important when the bubble is completely connected to the hole of the gas distributor and when elevated pressure and gas flow rate occur. In contrast, surface tension force is not significant for the determination of the bubble dimension in the conditions mentioned before. Besides, at elevated pressure of the system the gas density is considerably larger, and it results in a smaller bubble dimension because it is proportional to terms inside the model which push the bubble to rise, such as the gas momentum and pressure difference forces. Regarding to the liquid density it was found that with a denser liquid, the bubble increases because the bubble remains attached more time to the hole sparger.
3. Through the sensitivity analysis for both stages of the bubble formation model it was possible to set the final equations for the bubble formation model and for which the validation mentioned above was done.
4. It was established the range of validity for the bubble formation model exhibited in this work through the definition of Weber dimensionless number. The model is considered to be valid for a system where the Weber number is lower than one, meaning that the system is characterized by the bubbling regime. The increment of surface tension and hole dimension have an effect on the Weber number, allowing to have bubbling regime for higher gas flow rate.
5. The bubble dimension after the detachment was assessed for a hydrocarbon liquid mixture and hydrogen gas coming from the gas distributor. The superheated bubble was supposed to increase in volume due the evaporation of the liquid around the bubble and due to the difference on pressure. However, this increment was determined to be negligible, around 3.5%, for a system in which the heptane is the evaporating chemical component due to the low vapor pressure at 16MPa and 500°C. This effect could be

significant increased for more volatile liquids (such as hexane and pentane) for which vapor pressure is higher at this condition of pressure and temperature. The increase of final bubble volume for a liquid compound with a vapor pressure equal to the double of vapor pressure of heptane is around 42% compared to the bubble volume at detachment time for the same conditions of pressure and temperature mentioned before.

6. Drag coefficient expression have been found to influence in a significant way the bubble position and velocity during the bubble formation until detachment and the bubble position and terminal velocity after detachment. It was chosen the drag coefficient expression presented in the work of Tomiyama [58] for contaminated water as the most accurate for the bubble formation model and the bubble rising after detachment according to experimental data found in the literature.

Recommendations

After the development of this work some improvements and more detail investigations are suggested to be done as:

1. An experimentation with the hydrocarbon system proposed at relevant conditions for chemical industry because experimental data found in literature is mostly related to water-air system.
2. Perform more comparison analysis with experimental data of different authors and different system to the one presented in this work.
3. Investigate the influence of the different sparger configurations, for instance, the sparger located at the top of the reactor and produce bubble downwards.
4. Investigate mass and heat transfer models for variable interface position.

Bibliography

- [1] Jakobsen H. 2014. *Chemical Reactor Modeling*, chap. 8 pp. 883, Springer Cham Heidelberg., New York, USA.
- [2] Deckwer W., 1985, *Bubble Column Reactors*, chap. 1, 11, pp. 1-9, 379-383. John Wiley & Sons, New York, USA.
- [3] Joelianingsih, Hitoshi Maeda, Shoji Hagiwara, Hiroshi Nabetani, Yasuyuki Sagara, Tatang H. Soerawidjaya, Armansyah H. Tambunan, Kamaruddin Abdullah. "Biodiesel fuels from palm oil via the non-catalytic transesterification in a bubble column reactor at atmospheric pressure: A kinetic study". *Renewable Energy* **33** ELSEVIER 24 October 2007: 1629–1636.
- [4] E.M. Matos and R. Guirardello. "Modeling and simulation of a pseudotwo-phase gas-liquid column reactor for thermal hydrocracking of petroleum heavy fractions". *Brazilian Journal of Chemical Engineering* **19** July - September 2002: 319-334.
- [5] Montserrat Motas Carbonell and Reginaldo Guirardello. "Modelling of a slurry bubble column reactor applied to the hydroconversion of heavy oils". *Chemical Engineering Science* **52** ELSEVIER 1 July 1997: 4179-4185.
- [6] Lasa H. Dogu G. and Ravella A. 1992. *Chemical Reactor Technology for environmentally safe reactor and products*, pp. 353-377, Springer Science+Business Media, B.V., Canada.
- [7] Zhenyu Liu, Shidong Shi, Yongwang Li. "Coal liquefaction technologies—Development in China and challenges in chemical reaction engineering". *Chemical Engineering Science* **65** ELSEVIER 18 May 2009: 12-17.
- [8] L. Peeva, S. Ben-zvi Yona, J.C. Merchuk. "Mass transfer coefficients of decane to emulsions in a bubble column reactor". *Chemical Engineering Science* **56** ELSEVIER May 2001: 5201-5206.
- [9] R. Krishna, J. M. van Baten, M. I. Urseanu, J. Ellenberger. "Design and scale up of a bubble column slurry reactor for Fischer–Tropsch synthesis". *Chemical Engineering Science* **56** ELSEVIER 2001: 537-545.
- [10] Dimitri Gidaspow, Yuting He, Vishak Chandra. "A new slurry bubble column reactor for diesel fuel". *Chemical Engineering Science* **134** ELSEVIER 12 June 2015: 784-799.
- [11] M. Plevan, T. Geißler, A. Abánades, K. Mehravaran, R.K. Rathnam, C. Rubbia, D. Salmieri, L. Stoppel, S. Stückrad, Th. Wetzel. "Thermal cracking of methane in a liquid metal bubble column reactor: Experiments and kinetic analysis". *International Journal of Hydrogen Energy* **40** ELSEVIER 8 May 2015: 8020-8033.
- [12] Deckwer W., 1985, *Bubble Column Reactors*, chap. 1, 11, pp. 1-9, 379-383. John Wiley & Sons, New York, USA.

- [13] Tomasz Olewski, Branislav Todić, Lech Nowicki, Nikola Nikacević, Dragomir B. Bukur. “Hydrocarbon selectivity models for iron-based Fischer–Tropsch catalyst”. *Chemical Engineering Research and Design* **95** ELSEVIER 13 January 2015: 1-11.
- [14] H. da Silva Almeida, O.A. Corrêa, C.C. Ferreira, H.J. Ribeiro, D.A.R. de Castro, M.S. Pereira, A. de Andrade Mâncio, M.C. Santos, S.A.P. da Mota, J.A. da Silva Souza, Luiz E.P. Borges, N.M. Mendonça, N.T. Machado. “Diesel-like hydrocarbon fuels by catalytic cracking of fat, oils, and grease (FOG) from grease traps”. *Journal of the Energy Institute* **90** ELSEVIER 4 June 2016: 337-354.
- [15] Roberto Galiasso Tailleur, Gustavo Andrei Salva, Geormayl Garcia. “Hydrotreated-LCO oxidation in a transported slurry reactor-hydrocyclon system reactor for a low emission fuel oil production: I Kinetic of reactions”. *Fuel* **88** 24 November 2008: 744–755.
- [16] C.O. Okieimen, F.E. Okieimen. “Effect of natural rubber processing sludge on the degradation of crude oil hydrocarbons in soil”. *Bio Resource Technology* **82** 31 August 2001: 95-97.
- [17] M. Plevan, T. Geißler, A. Abánades, K. Mehravaran, R.K. Rathnam, C. Rubbia, D. Salmieri, L. Stoppel, S. Stückrad, Th. Wetzel. “Thermal cracking of methane in a liquid metal bubble column reactor: Experiments and kinetic analysis”. *International Journal of Hydrogen Energy* **40** 8 May 2015: 8020-8033.
- [18] Besagni. G., Inzoli F., “The effect of liquid phase properties on bubble column fluid dynamics: Gas holdup, flow regime transition, bubble size distribution and shapes, interfacial areas and foaming phenomena”. *Chemical Engineering Science*: **170** (2017) 270-296.
- [19] Hyndman C., Faical L., Christophe G. “Understanding gas-phase hydrodynamics in bubble columns: a convective model based on kinetic theory”. *Chemical Engineering Science* **52** 1: 63-77.
- [20] Romain Lemoine, Arsam Behkish, and Badie I. Morsi. “Hydrodynamic and Mass-Transfer Characteristics in Organic Liquid Mixtures in a Large-Scale Bubble Column Reactor for the Toluene Oxidation Process”. *Ind. Eng. Chem. Res* **43** 2004: 6195-6212.
- [21] Gaddis E. and Vogelpohl A. “Bubble formation in quiescent liquids under constant flow conditions”. *Chemical Engineering Science* **41** 21 March 1985: 97-105.
- [22] D.-H. Yoo, H. Tsuge, K. Terasaka and K. Mizutani. “Behavior of bubble formation in suspended solution for an elevated pressure system”. *Chemical Engineering Science* **52** ELSEVIER 4 July 1997: 3701-3707.
- [23] Liu Changjun, Liang Bin, Tang Shengwei, Zhang Haiguang and Min Enze. “A Theoretical Model for the Size Prediction of Single Bubbles Formed under Liquid Cross-flow”. *Chinese Journal of Chemical Engineering* **18** 21 May 2010: 770-776.

- [24] Stoyan Nedeltchev. "Theoretical prediction of mass transfer coefficients in both gas–liquid and slurry bubble columns". *Chemical Engineering Science* **157** ELSEVIER 21 June 2016: 169-181.
- [25] Jaewon Lee, Muhammad Yasin, Shinyoung Park, In Seop Chang, Kyoung-Su Ha, Eun Yeol Lee, Jinwon Lee and Choongik Kim. "Gas-liquid mass transfer coefficient of methane in bubble column reactor". *Korean J. Chem. Eng.* **32** 20 November 2014: 1060-1063.
- [26] Geary N. and Rice R., "Bubble size prediction for rigid and flexible spargers". *AIChE Journal* **37** 8 April 1991: 161-168.
- [27] Changjun L, Bin L, Shengwei T, and Enze M., "Effects of orifice orientation and gas-liquid flow pattern on initial bubble size". *Chinese Journal of Chemical Engineering* **21** 18 October 2012: 1206-1215.
- [28] Krishnamurthi S., Kumar R., and Kuloor N.R., "Bubble Formation in viscous Liquids under constant Flow Conditions". *I&EC Fundamentals* **7**, 4 November 1968: 549-553.
- [29] Zhang L., and Shoji M. "Aperiodic bubble formation from a submerged orifice". *Chemical Engineering Science* **56**, 28 Mayo 2001: 5371-5381.
- [30] Luo X., G. Yang, Lee D.J., and Fan L. "Single bubble formation in high pressure liquid-solid suspensions". *Powder Technology* **100** 2 June 1998:103-112.
- [31] Lin T., and Fan L., "Heat transfer and bubble characteristics from a nozzle in high-pressure bubble columns". *Chemical Engineering Science* **54**, 1999:4853-4859.
- [32] Soong Y., Harke F.W., Gamwo I.K., Schehl R.R and Zaroachak M.F. "Hydrodynamic study in a slurry-bubble-column reactor" *Catalyst Today* **35**, 1997:427-434.
- [33] Camarasa E., Vial C., Pochin S., Wild G., Midoux N. and Bouillard J. "Influences of coalesce behavior of the liquid and of gas sparging on hydrodynamics and bubble characteristics in a bubble column". *Chemical Engineering and Processing* **38**, 1999:329-344.
- [34] Chaumat H., Billet A. M. and Delmas H. "Hydrodynamics and mass transfer in bubble column: Influence of liquid phase surface tension" *Chemical Engineering Science* **62**, **24**, December 2007: 7378-7390.
- [35] Zhao Y.F and Irons G.A.s "The Breakup of Bubbles into Jets during Submerged Gas Injection". *Metal Trans B* **21(6)**, 1990: 997–1003.
- [36] Qu C., Yu Y., and Zhang J. "Experimental study of bubbling regimes on submerged micro-orifices" *International Journal of Heat and Mass Transfer* **111**, 2017:17-28.
- [37] Sundar R. and Tan R.N.H. "A model for bubble-to-jet transition at a submerged orifice" *Chemical Engineering Science* **54**, 9 March 1999: 4052-4060.

- [38] Yang G.Q., Bing Du and Fan L.S. "Bubble formation and dynamics in gas-liquid-solid fluidization-A review" *Chemical Engineering Science* **62**, 25 August 2006: 2-27.
- [39] Pradeep, Ahuja. *Chemical Engineering Thermodynamics*. New Delhi: PHI Learning Pvt. Ltd, 2008.
- [40] Avison, John. *English Alive!*. Second Edition. Cheltenham: Nelson Thornes, 2014.
- [41] Barry Azzopardi, Donglin Zhao, Y. Yan, H. Morvan, R. F. Mudde, Simon Lo. *Hydrodynamics of Gas-Liquid Reactors: Normal operations and Upset conditions*. Chichester: John Wiley & Son, 2011.
- [42] Avison, John. *The World of Physics*. Second Edition. Cheltenham: Nelson Thornes, 2014.
- [43] Marshall, Stephen Henry. "Air bubble formation from an orifice with liquid cross-flow". *Department of Chemical Engineering, University of Sydney* December 1990.
- [44] Lichtarowicz A. Duggins R. and Marhland E., 1965, "Discharge coefficients for incompressible non cavitating flow through long orifices". *Journal of mechanical eng. Science*. Vol.7. 210-219.32
- [45] Byron Bird R. Stewart W. and Lightfoot E., 2002, *Transport Phenomena*, chap. 10, 14, 17, 18., John Wiley & Sons, Inc., New York, USA.
- [46] Pickover, Clifford. *Archimedes to Hawking: Law of Science and the Great Minds Behind Them*. Oxford: Oxford University Press, 2008.
- [47] Joint initiative of IITs and IISc. Mass Transfer Operation 1. Module 3: Mass Transfer Coefficients, Lecture NO. 6. Pp. 1-5.
- [48] Smith J. and Van Ness H., 1987, *Introduction to chemical engineering thermodynamics*, chap. 2, 3, 4, 10 pp. 21-26, 29-30, 63, 105-114, 304. McGraw-Hill, Inc, Singapore.
- [49] David C. Cassidy, Gerald Holton, F. James Rutherford, Harvard Project Physics. *Understanding Physics*. New York: Springer Science & University Media, 2002.
- [50] Mackay, Donald. *Handbook of Property Estimation Methods for Chemicals: Environmental Health Sciences*, p. 57, Boca Raton: CRC Press, 2000.
- [51] McKetta Jr, John J. *Encyclopedia of Chemical Processing and Design: Volume 61 – Vacuum System Design to Velocity: Terminal Setting: Estimation*, p. 362, New York: CRC Press, 1997.
- [52] Lide, David R. *CRC Handbook of Chemistry and Physics: A Ready-reference Book of Chemical and Physical Data*. 84th Edition, pp. 15-19, Boca Raton: CRC Press, 2005.

- [53] Ten Berge, Wil F. *Mathematical Models for Estimating Occupational Exposure to Chemicals*, p. 90, Fairfax: AIHA, 2000.
- [54] Albright L., 2009. *Albright's Chemical Engineering Handbook*. Taylor & Francis Group. USA.
- [55] Ucko, David A. *Basics for Chemistry*, p. 323, New York: ELSEVIER, 2013.
- [56] Byung C. and Mazen A., 2010, *Chemical thermodynamics with examples for nonequilibrium processes*, chap. 3 pp. 31-41. World Scientific Publishing Co. Pte. Ltd, ISBN-10 981-4295-11-6. Singapore.
- [57] Lichtarowicz A. Duggins R. and Marhland E., "Discharge coefficients for incompressible non cavitating flow through long orifices". *Journal of Mechanical Eng. Science* **7** 1965: 210-219.
- [58] Tomiyama, A., Kataoka, I., Zun, I., Sakaguchi, T. 1998. "Drag Coefficients of Single Air bubbles under normal and micro gravity conditions". *JSME Int. J. Series B*,**41**,472–479.
- [59] "Bisection Method." *Indian Institute of Technology Madras*. 10 Oct. 2018. <http://mat.iitm.ac.in/home/sryedida/public_html/caimna/transcendental/bracketing%20methods/bisection/bisection.html>.
- [60] Christodoulou, Nikolaos S. "An Algorithm using Runge-Kutta Methods of Orders 4 and 5 for Systems of ODEs". *International Journal of Numerical Methods and Applications* **2** 2009: 47-57.
- [61] Tsuge H, Nakajima Y., Terasaka, K. "Behavior of bubbles formed from submerged orifice under high system pressure". *Chemical Engineering Science* **47**, 13/14, 1992: 3273-3280.
- [62] Clift, R., Grace, J.R., Weber, M.E., 1978. *Bubbles, Drops and Particles*. Academic Press, New York.

Appendix

A

Nomenclature

Symbol	Meaning	Unit of measure	Symbol	Meaning	Unit of measure
a_b	Bubble acceleration	[m/s ²]	M_K	Molecular weight of liquid component "K"	[Kg/mol]
α	Added Mass coefficient	[-]	m_G	Mass of gas component "G"	[Kg]
\mathcal{D}_{AG}	Binary diffusivity coefficient	[m/ s ²]	\hat{H}_A	Molar enthalpy of component "A"	[J/mol]
A_b	Bubble Area	[m ²]	\hat{H}_G	Molar enthalpy of component "G"	[J/mol]
F_b	Buoyancy Force	[N]	C_{tot}	Liquid total concentration	[mol/ m ³]
θ	Contact Angle	[rad]	n_G	Moles of gas component "G"	[mol]
d=L	Bubble diameter	[m]	M_G	Molecular weight of gas component "G"	[Kg/mol]
d_H	Hole diameter	[m]	N_u	Nusselt dimensionless number	[-]
C_0	Discharge Coefficient	[-]	$P_A(T)^{sat}$	Vapor pressure of "A". Antoine's Eq.	[Pa]
F_D	Drag Force	[N]	P_A	Partial Pressure of component "A"	[Pa]
C_D	Drag Coefficient	[-]	P_r	Prandtl dimensionless number	[-]
ρ_g	Gas density	[Kg/ m ³]	L_f	Length neck	[m]
ρ_A	Density of liquid component "A"	[Kg/ m ³]	p_L	Liquid Pressure	[Pa]
ρ_K	Density of liquid component "K"	[Kg/ m ³]	p_g	Gas Pressure	[Pa]
H	Enthalpy	[J]	y_f	Final Bubble position	[m]
t_e	Exposure time from Higbie's Theory	[s]	$P_{A,i}$	Partial pressure of "A" at the interface	[Pa]
EO	Eötvös number	[-]	E_p	Potential Energy	[J]
G	Gas Flow Rate at hole	[m ³ /s]	F_p	Pressure Force	[N]

F_m	Gas Momentum Force	[N]	P	Pressure System	[Pa]
ho	Global heat transfer coefficient	[W/m ² K]	r	Bubble radius	[m]
h_G	Gas side heat transfer coefficient	[W/m ² K]	n_A	“A” moles rate	[mol/s]
h_L	Liquid side heat transfer coefficient	[W/m ² K]	r_d	First stage bubble radius	[m]
g	Gravity Acceleration	[m/s ²]	r_f	Bubble detachment radius	[m]
F_g	Gravity Force	[N]	r_H	Hole radius	[m]
R	Gas Constant	[m ³ Pa/mol K]	Re_B	Bubble Reynolds number	[m]
\dot{Q}	Heat Flux	[J/s]	Re	Reynolds Number	[-]
\dot{q}	Conductive Heat Flux	[J/s]	σ	Surface/Interfacial Tension	[N/m]
$\hat{C}_{p,G}$	Molar Heat capacity at constant pressure of “G”	[J/mol K]	σ_o	Surface tension in atmospheric condition	[mN/m]
\hat{C}_p	Liquid Heat capacity at constant pressure	[J/Kg K]	T	Bubble temperature	[K]
$\hat{C}_{p,A}^{vap}$	Molar Heat capacity at constant pressure of vapor “A”	[J/mol K]	TC	Bubble temperature in Centigrade	[°C]
$\hat{C}_{p,A}^{liq}$	Molar Heat capacity at constant pressure of liquid “A”	[J/mol K]	T_L	Liquid Temperature	[K]
d_h	Hole Diameter	[m]	k	Thermal Conductivity	[W/m K]
U	Internal Energy	[J]	F_s	Surface Tension Force	[N]
\widehat{U}_A	Internal Energy per unit mass of A	[J/Kg]	S_h	Sherwood dimensionless number	[-]
F_i	Inertia Force	[N]	ϵS	Solid particle holdup	[-]
$\Delta\hat{H}_{vap}(T)$	Latent heat of vaporization	[J/mol]	U_b	Bubble Velocity	[m/s]
ρ_L	Liquid Density	[Kg/ m ³]	U_t	Bubble terminal velocity	[m/s]
ρ_K	Density of liquid component K	[Kg/ m ³]	U_g	Hole Gas velocity	[m/s]
E_k	Kinetic Energy	[J]	μ_{app}	Apparent Viscosity	[Pa.s]
$C_{AL,i}$	“A” gas-liquid interface molar concentration	[mol/ m ³]	μ_g	Gas Viscosity	[Pa.s]

$C_{A,L}$	“A” Liquid molar concentration	[mol/ m ³]	m_v	Virtual mass	[Kg]
$X_{A,i}$	molar fraction of “A” at the vapor-liquid interface	[-]	$\mu_L = \mu$	Liquid Viscosity	[Pa.s]
k_L	Mass transfer coefficient	[m/s]	V_b	Bubble Volume	[m ³]
m_b	Bubble mass	[Kg]	V_d	First Stage Bubble Volume	[m ³]
m_A	Mass of gas component “A”	[Kg]	\dot{V}	Volume rate	[m ³ /s]
n_A	Moles of gas component “A”	[mol]	\hat{V}_A	Specific volume of “A”	[m ³ /Kg]
n_G	Moles of gas component “G”	[mol]	W_e	Weber dimensionless number	[-]
M_A	Molecular weight of gas component “A”	[Kg/mol]	\dot{W}_S	Shaft Work	[J/s]

B

First Stage Model MATLAB

```

clearvars;

%Model 1_H2_Heat and mass transfer model
%Stage 1
%HYDROGEN-C20H42

% Call the constants and variables from "Variables.m"
Variables

% Results arrays allocation

V = zeros(1,length(G));
RE = zeros(1,length(G));

% Bisection method for the evaluation of bubble volume

for i=1:length(G)

    Gi=G(i);      % Gas low rate of the i-th element of G

    % Definition of the first search interval

    vn = 0;          % Left limit (m^3)
    vp = 1E-4;      % Right limit (m^3)
    vmp = (vp+vn)/2; % Average volume (m^3)
    dmp = (6/pi*vmp)^(1/3); % Average diameter (m)

    % Evaluation of drag coefficient

    velb = Gi/(pi*dmp^2); % Bubble velocity (m/s)
    Reb = rho1*dmp*velb/miulapp; % Bubble Reynolds number (-)
    Eo = dmp^2*g*(rho1-rhog)/sigm; % Bubble Eotvos number (-)
    Cd = max(24/Reb*(1+0.15*Reb^0.687),8/3*Eo/(Eo+4)); % Drag coefficient
    according to Tomiyama et al. 1998 correlation (fully contaminated) (-)

    % Evaluation of different forces acting during bubble formation

    bugr = vmp*(rho1-rhog)*g; % Buoyancy and gravity (N)
    momPr = Gi^2*rhog/(pi*rH^2)*(1+1/Co^2); % Momentum and pressure
    difference forces (N)
    surTe = 2*pi*sigm*rH; % Surface tension force
    (N)
    drag = 1/2*pi/4*dmp^2*rho1*Cd*velb^2; % Drag force (N)
    iner = (rhog+alfa*rho1)*Gi^2/(12*pi*(dmp/2)^2); % Inertia term (N)

    Re = 4*rhog*Gi/(pi*dH*miug);

    zmp = bugr + momPr - surTe - drag - iner;

    for j = 1:1000
        if zmp > 0

```

```

        % ymp is less than zero
        vp=vmp;
    else
        % ymp is greater than zero
        vn=vmp;
    end
    vmp = (vn + vp) / 2;
    dmp = (6/pi*vmp)^(1/3); % Average diameter (m)

    % Evaluation of drag coefficient

    velb = Gi/(pi*dmp^2); % Bubble velocity (m/s)
    Reb = rho1*dmp*velb/miulapp; % Bubble Reynolds number (-)
    Eo = dmp^2*g*(rho1-rhog)/sigm; % Bubble Eotvos number (-)
    Cd = max(24/Reb*(1+0.15*Reb^0.687), 8/3*Eo/(Eo+4)); % Drag
    coefficient according to Tomiyama et al. 1998 correlation (fully
    contaminated) (-)

    % Evaluation of different forces acting during bubble formation

    bugr = vmp*(rho1-rhog)*g; % Buoyancy and gravity (N)
    momPr = Gi^2*rhog/(pi*rH^2)*(1+1/Co^2); % Momentum and pressure
    difference forces (N)
    surTe = 2*pi*sigm*rH; % Surface tension force
    (N)
    drag = 1/2*pi/4*dmp^2*rho1*Cd*velb^2; % Drag force (N)
    iner = (rhog+alfa*rho1)*Gi^2/(12*pi*(dmp/2)^2); % Inertia term (N)

    zmp = bugr + momPr - surTe - drag - iner;
end

V(i) = vmp;
RE(i) = Re;

end

% Results post processing

Vd=V*1e6; %cm3
Vd=real(Vd)
V = real(V);
rd = (3/(4*pi))^(1/3)*V.^(1/3); %m, y(0)
rd
rdmm=rd*1000 %rd in mm
Ref=Re

```

C

Second Stage Model MATLAB

Function.m: “myodefun.m”

```

function dvdt = myodefun(t,v)
dvdt = zeros(2,1);

global rd

% Call of constants and variables
Variables;

% Evaluation of bubble velocity, volume, diameter and bubble mass+virtual
at time t

velb = v(2,1); % Bubble velocity (m/s)
Vb = (G*t+4/3*pi*rd^3); % Bubble volume (m^3)
db = (6/pi*Vb)^(1/3); % Bubble diameter (m)
mass = (rhog+alfa*rhol)*Vb; % Bubble+Virtual mass (kg)

% Evaluation of drag coefficient

Reb = rhol*db*velb/miulapp; % Bubble Reynolds number (-)
Eo = db^2*g*(rhol-rhog)/sigm; % Bubble Eotvos number (-)
Cd = max(24/Reb*(1+0.15*Reb^0.687),8/3*Eo/(Eo+4)); % Drag coefficient
according to Tomiyama et al. 1998 correlation (fully contaminated) (-)

% Evaluation of different forces acting on the moving bubble during
% formation

bugr = Vb*(rhol-rhog)*g; % Buoyancy and gravity (N)
momPr = G^2*rhog/(pi*rH^2)*(1+1/Co^2); % Momentum and pressure difference forces (N)
surTe = 2*pi*sigm*rH; % Surface tension force (N)
drag = 1/2*pi/4*db^2*rhol*Cd*velb^2; % Drag force (N)
iner = (rhog+alfa*rhol)*G*velb; % Inertia term (N)

% Evaluation of source terms for ode solver

dvdt(1,1) = v(2,1); % Position
derivative (m/s)
dvdt(2,1) = 1/mass*(bugr + momPr - surTe - drag - iner); % Velocity
derivative (m/s^2)

end

clearvars;
%MODEL 2, SOLVING MYODEFUN
%Initial condition rd, Drag force last one varying Re with velocity
%Smaller values of Qg than 0.9 give imaginary numbers

global rd;

Variables

```

```

rd = 3.5291e-03; % Initial condition - Bubble radius from first stage (m)

Ug = (G/aH);      % Gas hole velocity (m/s)
disp(Ug)          % Print on screen Ug (m/s)
disp(G)           % Print on screen G (m^3/s)
disp(dH*1000)     % Print on screen dH (mm)

% Initialization of ode45 routine

tRange = [0 1]; % Time integration range
y0      = rd;   % Initial condition for position (bubble center of mass)
(m)
v0      = 1E-9; % Initial condition for velocity (m/s)

% Call of ode45 routine
[sol] = ode45(@myodefun,tRange,[y0 v0]);

% Results post-processing
% loop to find the value of y at detachment moment

n=1;
t(1)=0;
y(1)=rd;
r(1)=rd;
h=1e-6;

while y(n) < r(n) + dH
    y(n+1) = deval(sol,t(n),1);
    t(n+1) = t(n)+h;
    r(n+1) = ( (3/(4*pi))*G*t(n+1) + rd^3 )^(1/3);

    n=n+1;
end
%Results

yfcm=real(y(n))*100; %cm
yfcm
rfscm=yfcm-(dH*1e2) %cm
dfscm=rfscm*2;
dfscm
tfn = t(n);
ub = deval(sol,t(n),2); %Bubble velocity at detachment
ub

```

D

FILE Variables.m

```

% Constants

rH = 3e-3;           % Hole radius (m)
dH = 2*rH;          % Hole diameter (m)
p = 16e6;           % Pressure (Pa)
P = p*1e-6;         % Pressure (MPa)
TC = 500;           % Temperature (°C)
T = TC+273.15;      % Temperature (K)
R = 8.3145;         % Gas constant (m^3 Pa/mol K)
G = 24e-6;          % Gas flow rate (m^3/s)
miug = 1.618377E-5; % Gas viscosity (Pa s) [HYDROGEN]
Co = 0.801;         % Orifice discharge coefficient (-), [in theory change
with G and Re]
rhol = 725;         % Liquid density (Kg/m^3)
MG = 2e-3;          % Gas Molecular weight (Kg/mol) [HYDROGEN]
rhoA = 684;         % A liquid component density (Kg/m^3) [HEPTANE]
MA = 100.21e-3;     % Liquid component which evaporate (Kg/mol) [HEPTANE]
MK = 282.556e-3;   % K Molecular weight (Kg/mol) [EICOSANE]
rhok = 788.6;       % K liquid component density (Kg/m^3) [EICOSANE]
g = 9.81;           % Gravity acceleration (m/s^2)
alfa = 11/16;       % Virtual mass coefficient (-)
miul = 0.4e-3;      % Liquid viscosity (Pa s) [heptane-C20H42]
es = 0.05;          % Volume fraction of solid particles in liquid (-)
CA = rhoA/MA;       % Molar concentration of liquid component
A, (mol/m^3) [HEPTANE]
CK = rhok/MK;       % Molar concentration of liquid component
K, (mol/m^3) [EICOSANE]
Ctot = (CA+CK)/2;   % Total molar concentration, mol/m^3
XAL = 0.7;          % Molar fraction of component A in the liquid mixture,
(-)
CAL = XAL*Ctot;    % Molar concentration of component A in the liquid,
(mol/m^3)

% Constants inside the temperature derivative equation dT/dt

Cpg = 29.6;         % Molar gas heat capacity at constant pressure
(J/mol K)
CpaL = 217;         % Molar liquid heat capacity at constant pressure
of component A: Heptane (J/mol K) @303K
CpL = CpaL/MA;      % Mass liquid heat capacity at constant pressure
of component A: Heptane (J/Kg K) @303K
CpaV = 317.15;      % Molar vapor heat capacity at constant pressure
of component A: Heptane (J/mol K) @700K
k = 392e-3;         % Gas Thermal Conductivity (W/m K) [HYDROGEN]
Dag = 1.27e-7;      % Diffusivity coefficiente (m^2/s)
TL = 360;           % Liquid temperature (°C)
TLK = TL+273;      % Liquid temperature (K)
deltavap = 35500;   % Liquid Vaporization enthalpy of component
A(J/mol) [Heptane]

%Antoine's empirical parameters to Evaluate Saturation Pressure Psat(T):

A = 4.02832;
B = 1268.636;
C = -56.199;

```

```
% Evaluation of gas and liquid properties, hole geometry and velocities

rhog    = p*MG/(R*T);           % Gas Density (ideal gas)
(Kg/m3) [HYDROGEN]
sigm    = (14 - 0.8243*P + 0.01891*P^2)*1E-3; % Surface tension (evaluated
through correlation Yoo et al. CES 1997) (N/m)
miulapp = miul/(1-(es/0.68))^2; % Liquid apparent viscosity
(after the presence of particles: correlation of Yoo et al. CES 1997) (Pa
s)
aH      = pi*rH^2;             % Hole area (m^2)
```

E

COMBINED MOMENTUM, HEAT AND MASS TRANSFER CODE MATLAB

Function file: "myodesystem"

```
function dvdt = myodesystem(t,v)
dvdt = zeros(5,1);
global Lo

% Call of constants and variables
Variables

% Variables allocation

nA = v(1,1); % Number of moles of [HEPTANE] into the bubbles at time t
(mol)
Tb = v(2,1); % Temperature of the bubble at time t (K)
Lb = v(3,1); % Size of the bubble at time t (m)
pos = v(4,1); % Position of the bubble at time t (m)
velb = v(5,1); % Velocity of the bubble at time t (m/s)

% Evaluation of Bubble volume, amount of moles at detachment stage

VG = (pi/6)*Lo^3; % Bubble volume at detachment (m^3)
nG = (rhog*VG)/MG; % Amount of gas moles at detachmet (mol)
[G, HYDROGEN]

% Evaluation of drag coefficient

rhogv = (nA*MA + nG*MG)/(pi/6*Lb^3); % Bubble density
after detachment (Kg/m^3)
Reb = rhol*Lb*velb/miulapp; % Bubble Reynolds
number (-)
Eo = Lb^2*g*(rhol-rhogv)/sigm; % Bubble Eotvos
number (-)
Cd = max(24/Reb*(1+0.15*Reb^0.687), 8/3*Eo/(Eo+4)); % Drag coefficient
according to Tomiyama et al. 1998 correlation (fully contaminated) (-)

% Evaluation of terms inside mass transfer equation, dnA/dt

Kc = (4*Dag*velb/(pi*Lb))^(1/2); % Mass transfer
coefficient according to Higbie penetration theory (m/s)
surfarea = pi*Lb^2; % Mass transfer area
(m^2)
PA = (nA*R*Tb)/(pi/6*Lb^3); % Partial Pressure of
componet A according to ideal gas law assumption, [HEPTANE] (Pa)
Pasat = 10^(A-(B/(Tb+C)))*1e5; % Vapor Pressure,
Antoine's equation (Pa)
```

```

    XAi = PA/Pasat; % Molar fraction of
component A at the interface (-)
    CALi = XAi*Ctot; % Molar concentration of
component A at the liquid-gas interface (mol/m3)
    gradconc = CAL-CALi; % Mass transfer driving
force, gradient concentration (mol/m^3)
    dvdt(1,1) = Kc*surfarea*gradconc; % dnA/dt calculation
    dnAdt = dvdt(1,1); % dnA/dt variable
allocation

% Evaluation of terms inside the heat transfer equation dT/dt

    hext = ((4*rhol*CpL*k*velb)/(pi*Lb) )^(1/2); % Liquid Heat transfer
coefficient derived by Analogy of Nusselt and Sherwood numbers (W/m^2 K)
    hint = hext; % Gas side Heat
transfer coefficient, (W/m^2 K)
    ho = 1/((1/hint)+(1/hext)); % Global Heat transfer
coefficient, (W/m^2 K)
    gradT = TLK-Tb; % Heat transfer driving
force, Difference of Temperature (K)
    dvdt(2,1) = (1/(nA*CpaV+nG*Cpg))*( ho*surfarea*gradT + dnAdt*(-(CpaL-
CpaV)*gradT-deltavap)); % dT/dt calculation
    dTdt = dvdt(2,1);
% dT/dt variable allocation

% Evaluation of dL/dt

dvdt(3,1) = ((2*R)/(p*pi*Lb^2))*(dnAdt*Tb+dTdt*(nA+nG)); % dL/dt
calculation
dLdt = dvdt(3,1); % dL/dt variable
allocation

% Evaluation of bubble and virtual mass and forces in the velocity
derivative Equation dUt/dt

mbubble = nA*MA + nG*MG; % Bubble mass (Kg)
mvirt = pi/6*alfa*rhol*Lb^3; % Virtual mass (Kg)
buoy = pi/6*rhol*g*Lb^3; % Buoyancy Force (N)
gravit = mbubble*g; % Gravity Force (N)
inert = velb*(MA*dnAdt+pi/2*alfa*rhol*Lb^2*dLdt); % Part of inertia
Force (N)
Fdrag = pi/8*rhol*Cd*Lb^2*velb^2; % Drag Force (N)

% Evaluation of position and velocity derivatives

    dvdt(4,1) = velb; % dy/dt
Position derivative equation
    dvdt(5,1) = (1/(mbubble+ mvirt))*(buoy - gravit - inert - Fdrag); %
dUt/dt, Velocity derivative equation

end

```

ode45Solver for Combined Momentum, Heat and Mass Transfer Model

```

clearvars;
%Integral MODEL, SOLVING MYODEFUNSYSTEM
%Initial condition nAo,To,Lo,yo, vo

global Lo

% Call of constants and variables
Variables

Lo = 1.4677e-2; %Initial bubble diameter from detachment stage(m)

% Initialization of ode45 routine

    tRange = [0 10];      % Time integration range

        nAo = 0;          % Initial condition for moles of component A
(mol) Heptane
        To = 773;         % Initial condition for bubble temperature (K)
        Loo = Lo;         % Initial condition for bubble diameter (m)
        yo = 1.3338e-2;   % Initial condition for position (bubble center
of mass) (m)
        vo = 0.2258;     % Initial condition for velocity (m/s)

% Call of ode45 routine

[sol] = ode45(@myodesystem,tRange,[nAo To Loo yo vo]);

% Results post-processing

    time = linspace(0,10,50); % Time range evaluation for graphic results
nAgraph = deval(sol,time,1); % Position Evaluation in the time interval
    Tgraph = deval(sol,time,2); % A Moles Evaluation in the time interval
    Lgraph = deval(sol,time,3); % Temperature Evaluation in the time interval
    ygraph = deval(sol,time,4); % Diameter Evaluation in the time interval
    utgraph = deval(sol,time,5); % Velocity Evaluation in the time interval

% Graphic Results

% Velocity Plot
figure(1)
subplot(3,2,1)
plot(time,utgraph,'g')
title('Velocity vs time') % Plot tittle
xlabel('time (s)') % X name axes
ylabel('Ut(m/s)') % Y name axes
grid on
% Diameter Plot
subplot(3,2,2)
plot(time,Lgraph,'r')
title('Diameter vs time') % Plot tittle
xlabel('time (s)') % X name axes
ylabel('L(m)') % Y name axes
grid on
% A Moles Plot
subplot(3,2,3)
plot(time,nAgraph,'m')

```

```
title('A moles vs time') % Plot tittle
xlabel('time (s)') % X name axes
ylabel('nA(mol)') % Y name axes
grid on
% Position Plot
subplot(3,2,4)
plot(time,ygraph,'k')
title('Position vs time') % Plot tittle
xlabel('time (s)') % X name axes
ylabel('y(m)') % Y name axes
grid on
% Temperature Plot
subplot(3,2,5)
plot(time,Tgraph,'b')
title('Temperature vs time') % Plot tittle
xlabel('time (s)') % X name axes
ylabel('T(K)') % Y name axes
grid on
```